RUSSIAN ACADEMY OF SCIENCES
INSTITUTE OF CHEMICAL PHYSICS SEMENOV N.N.

SHEMETOV YEVGENY Vasilevich.

STUDIES OF PHASE TRANSITIONS IN THE UNITED A_2BX_4 STRUCTURE b-K_2SO_4 METHOD NUCLEAR QUADRUPOLE RESONANCE AT ATMOSPHERIC AND HIGH PRESSURE.

MOSCOW 1995

CONTENTS

INTRODUCTION

Studies of the structure of the crystal structures, the nature of phase transitions recently reached a qualitatively new level. By theoretical and experimental work has been formulated a universal approach to the description of phase state on the basis of solving discrete field theory models. In the language of the theory of interacting nodes on harmonic lattice spins have been found and studied nonlinear solutions in the form of fermions. At the same time, as it turned out, the system can be represented by the normal fermion modes. The theory of the soft mode condensation Goldstounovskogo boson is just a special case of solutions in the form of single-particle fermion states - for example, the spin-wave or soliton.

Theoretical and experimental studies carried out for the external magnetic field and take into account only the spin-spin interaction in the framework of models with different dimensionality, showed that the behavior of the system depends not only on the spin and spatial dimension of the system, but. must be considered a significant radius interspin interaction. It has been found that in this case there are classes of solutions to form the long-period structure, and observed experimentally.

In recent years, were discovered and studied compounds with charge density waves, quasi-one organic semiconductors and dielectrics, in which it was found ordering various elements of the structure similar to the long-period form of magnets.

Unlike magnetic systems in dielectric crystals at the forefront of the dipole-dipole interaction and the dimension of the spin variable gives way pseudospin ordering chemical bonds. In crystalline dielectrics with a structure of β-K_2SO_4 were first detected with an incommensurate phase, compared with the original sample intervals. From X-ray data indicated that the emerging superstructure reflections can be characterized by a temperature dependent parameter disparity.

Change the local environment of the structural units in phases with such features more optimal way to observe change of the electric field, or its constituents. Therefore, the method of nuclear quadrupole resonance (NQR) observed in the nucleus with the quadrupole moment and depends on the electric field gradient at the nucleus under study, is optimal for the study of incommensurate structures. Nucleus Cl, Br, J in crystals of the family A_2BX_4 occupy a convenient structural position and allow to obtain information about the origin of the primary structural disproportion, the type of phase transition, modulation features.

With the participation of the author have been made one of the first such studies, including those under the influence of high hydrostatic pressure. Involvement of the latter, as an additional parameter allows you to get a new non-trivial information about the incommensurate phase.

The objectives of this thesis include studies by nuclear quadrupole resonance of halogens (Cl, Br, J), and other methods, crystals family β-K_2SO_4 with structural disproportion. Elucidation of changes in the spectral features of the resonance parameters in phase transitions and symmetry transformations, the analysis of the local environment and the nucleus of its transformation into different compounds of this series with temperature and high hydrostatic pressure. Investigation of the processes of the spin dynamics. In combination with other methods of analysis of changes in the crystal symmetry at structural phase transitions.

Chapter 1. Disproportionately modulated phases in dielectrics with structure type β-K_2SO_4.

§ 1.1.Theory of phase transitions and incommensurate phases.

Phase transition is called structural when changes-crystallographic structure of matter. Symmetry of the crystal lattice, as it is known, in the general case described simorfnymi 230 space groups. Change in the symmetry of the crystal at the phase transition seemed, until recently, in the framework of the Landau-Devonshire, as a change of some function, called the order parameter, by the loss of the symmetry elements and decreasing the initial symmetry G_o to a certain subgroup of the symmetry group G_1 G_o.

From the point of view of the atomic structure of the crystal, this means that the asymmetric atoms in the G_1 phase, shifted relative to the equilibrium positions which they occupy at the high phase. The structure of the new phase G_1 is a superposition of the displacements corresponding frozen soft mode and structure of G_0 phase. Hence the structure of the new phase is uniquely determined by the structure of the initial phase and the vector of the soft mode (the symmetry of the soft mode).

According to Anderson's theory [1], phase transitions caused by the instability of the crystal relative to some of its normal modes in the high-temperature phase. The frequency of this mode decreases when approaching the critical temperature $T_{i,}$ and the restoring force for displacements corresponding to such a fashion tends to zero as long as the phonon does not condense on the stability boundary. Consequently, the static displacements of atoms at the transition from phase G_0 to G_1 phase are frozen vibrational displacement codes corresponding to the soft phonon ($q_{s)}$.

However, this concept is applicable when the displacements of atoms from the high-small positions (phase transitions of bias) and becomes less useful for large displacements (phase transitions of the order-disorder).

In the latter case, structural changes are usually described in the framework of the Ising model, which deals with large-scale motions and entered the (pseudo) spin variables describing the position of atoms or groups. The results of this approach generally boil down to the fact that the phase transition occurs at the wave vector $q_{s,}$ which corresponds to a maximum of interactions J(q) between objects Ising nodes.

Parallel - the development of theory undertaken considerable experimental efforts to study the microscopic nature structure phase transitions. Most known results of the classical study of the temperature dependences of q_s in β-K_2SO_4 [2]. Neytron - diffraction method on this crystal were shot dispersion curves q(ω) at different temperatures Figure 1.1. Temperature dependence of q for S_2 fashion shows that the wave rector q_s can have values between zero and the wave vector at the Brillouin zone boundary. In this case, the value , corresponding to a minimum the dispersion curve, the symmetry is not fixed and typically depends on the temperature.

Changes in the structure of the crystal in this case determined by the symmetry of high-G_0 phase, followed by some pretransitional area corresponding mitigation fashion responsible for the phase transition at $T_{i.}$ Below T_i there is a phase where the minimum of the soft mode varies near the symmetrical point of reciprocal space G*, and when they correspond exactly q_s G*, at T_c transition occurs in the low-symmetry structure. The phase between T_i and T_c is called, incommensurat because values of the wave vector q_s, when it is a continuous change can take irrational values, which corresponds to an infinitely large unit cell of the crystal. In this case the crystal is represented three-dimensionally periodic structure, where any inside – crystalline function in one or more directions superimposed long-wavelength spatial modulation period is generally not a multiple of the period of the unit cell of high-symmetry phase. Displacement of nucleus of symmetric function of the order parameter in this

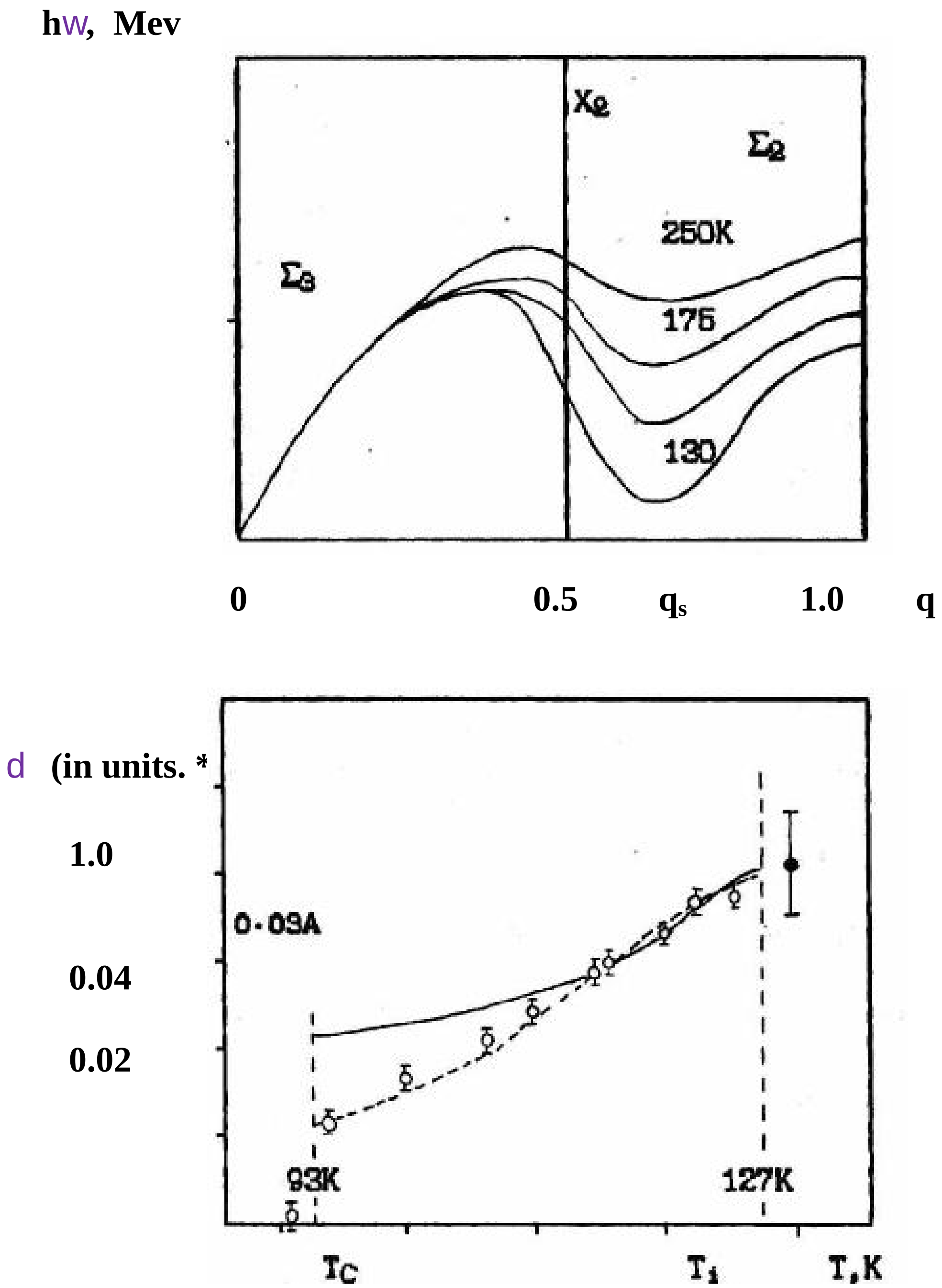

Figure 1.1. Dispersion curves for the soft mode in K_2SeO_4 at different temperatures and the dependence $q_S=1/3(1-\delta)\times 2\pi/a$.

case, can be represented by an expansion in the eigenvectors of the soft mode [2,3]:

$$u_{lkp}=\Big\{\underset{\lambda}{\mathring{a}}\, A\grave{}_{\lambda}\, \times \overset{uu}{e}{}_k^{l}+\underset{\lambda}{\mathring{a}}\, A_{\lambda}\, \times[\overset{r}{e}\times\overset{ur}{X}(lk)]\Big\}\ \times \exp 2\pi i(qx_{l} + \varphi).. \quad (1.1.)$$

where e_k^l - eigen vectors irreducible representation G*; $A\grave{}_{\lambda}$, A_{λ} - amplitude eigenvectors; X (lk) – l-st position of the atom, the center of mass of k-th group in the p-th unit cell; j -wave phase modulation.

Analysis of the interaction of atoms in an external periodic potential shown [4,5] that the period of the structure is fixed on the true meaning and proportioned incommensurate phase is not realized. The resulting wave vector, depending on the "pressure", varies continuously, but Nonanalytic. For this strange behavior, mathematicians devised a very original name - "Devil's Staircase" (devil or Satan staircase) [5]. However, initially there was no hope to explore different types of non-analytic behavior numerically, and even more so by experiment.

In addition to the theory of Aubrey [5,6], in [7,8,9], to describe the transition from incommensurate (Jc) to the commensurate phase were introduced "domain" wall or soliton theory and developed the idea as part of Macmillan Ising models with solitons, phasons and "devil's staircase".

Results McMillan, reduced to the fact that the transition from J_C in the commensurate phase can be represented by a picture of soliton-like structure of the atomic displacements described by the soliton (domain) wall :

$$\mathbf{u = A\ cosj\ (x);\ j\ (x) - k/p\ arctg(exp(-ax/p\ ))} \qquad (1.2)$$

j (x)2p/p; p = 1,2,...k. These walls separate regions with different values of the phase shifts of atoms j (x) = 2p/p; p = 1,2,...k.. Shape of the phase function in the incommensurate (incommensurate) phase is given by:

$$j\ (\mathbf{x}) = j_{o} + \frac{2\pi m}{p}\ j\ (x-mb) \qquad (1.3)$$

where j_o - the phase shift; distance between the walls, m = 1,2,3, ... p.

When the temperature decreases, the width of the soliton wall and a^{-1} is a continuous transition to the commensurate state. Order parameter in this case is the number of solitons.

In real crystals, if the width of the soliton is a few lattice periods, the center of the soliton is energetically advantageous to have at some point in the unit cell [10]. In this case, the transition to the final as symmetrical, the system will experience a sequence of phase transitions of the first kind, until you reach the main phase with p = k. In addition, there are often a few stars of the wave vectors that lead to the existence of incommensurate walls of various types, and can be carried out transitions between different configurations of the soliton structure.

There are other types of non-linear numerical solutions (kinks, wobblers, etc.), describing the shape of the atomic displacements in the incommensurate phase. Such as

$NaNO_{2,}$ the structure seems almost plane waves, and up to T_C no harmonics incommensurate wave vector [11].

McMillan ideas were developed Janson[8] Aubrey [12]and Buck [13] These authors studied the behavior of soliton solutions of the discrete problem in Ising-like systems with the interaction up to three neighbors (ANNNI - model). In this case, the deviation of the wave vector q_d = (1-)*/3 proportioned values can be represented by a rational number x = M/N, and the structure of solutions (steps "devil's staircase") may be associated with symmetry interconnected sublattices with symmetry restrictions on the values of the numbers N and M. Then the transition from the high-G_0 in the low-symmetry phase $G_{i,}$ between the phase diagram there is a region where the structure is represented by a cascade of intermediate or long-period incommensurate states with discrete or continuous variation of the wave vector q_d (Fig.4.38 and 4.39). The regions of these states are very sensitive to external (theoretical) effects.

By this time the state of the theory of symmetry was enough to make its results for the classification of all possible types of theoretical incommensurate structures [15] and classify them into different classes incommensurate space groups in the theory of supersymmetry [16].

Supersymmetry transformation rules allow you to specify the direction of the transformation and permissible types of symmetry of incommensurate structures that can realistically be implemented in each class Fedorovskoye crystal structure.

As an illustration, we give an outline of possible directions changes in lattice symmetry Brillouin highly symmetric group D_{2h}^{16} (Pnma), Figure 1.2. In the circles of indexed figures experimentally realized soft modes for crystals 1) $Tb_2(Mo0_4)_{3,}$ k_m = p (110) 2) $RbD_3(Se0_3)_{2,}$ k_z = p (001) 3) K_2SeO_4 , k = 2p (m00) m»1/3 In [18] is a diagram indicating the possible ways of symmetry transformations structure Pnma (D_{2h}^{16}).

From the experimental data revealed that the sequence of phase transitions in crystals with high-symmetry group symmetry Pnma structure β-K_2SO_4 defines mitigation dispersion curve along the S line. There are four irreducible representations of S_1, S_2, S_3, S_4 of this group. In $K_2SeO_{4,}$ for example, the soft mode associated with the representation of S_2:

E-line E-line
D_{2h}^{16} (Pnma) ---------® Jc modulation --------® C_{2v}^{9} (Pna2_1)
m»1/3 along the x-axis m»1/3

Later in other compounds of the family A_2BX_4 type structure β-$K_2SO_{4,}$ installed other possible sequences of symmetry transformations, which are determined by another basis of irreducible representations of D_{2h}^{16} (Table 1.1).

Given the possibility of experimental observation of the behavior of "devil's staircase" or to account for the influence of concomitant and secondary order parameters, the analysis of experimental structural data necessary to know the various ways allowed symmetry transformations of the structure, taking into account the parity ratio x= N/M in the case of long-period structures . The analysis performed in Refs [17, 18], which indicates all possible subgroups generated representations S_i, L_i, G_1

The above theory of solids based on the adiabatic or Born-Oppenheimer approximation, where the kinetic energy of the nucleus T (R_{n}) is actually neglected. However, as the last experimental studies [23], the characteristic times of nuclear motions can be compared with the electronic. Arise in this case, the vibronic interaction, even in the case of mixed singlet states, lead to Jahn-Teller distortions, which crystal system can be a source of instability and dipole explain the nature of ferroelectricity [22]. From the standpoint of the vibronic theory postulates soft mode are consequences of the cooperative pseudo-Jahn-Teller effect. In the framework of this theory can be explained and the disproportionate nature of the state in dielectric crystals. Interaction of the electron or nuclear state leads to interaction pseudo-soft phonon modes of different symmetry, localized near a variety of provisions of the reciprocal lattice symmetry [8, 94]. In the high-temperature phase G_{0}, these modes do not interact, but below the temperature will determine the resonant interaction of the two components of the structure, phase-shifted. From

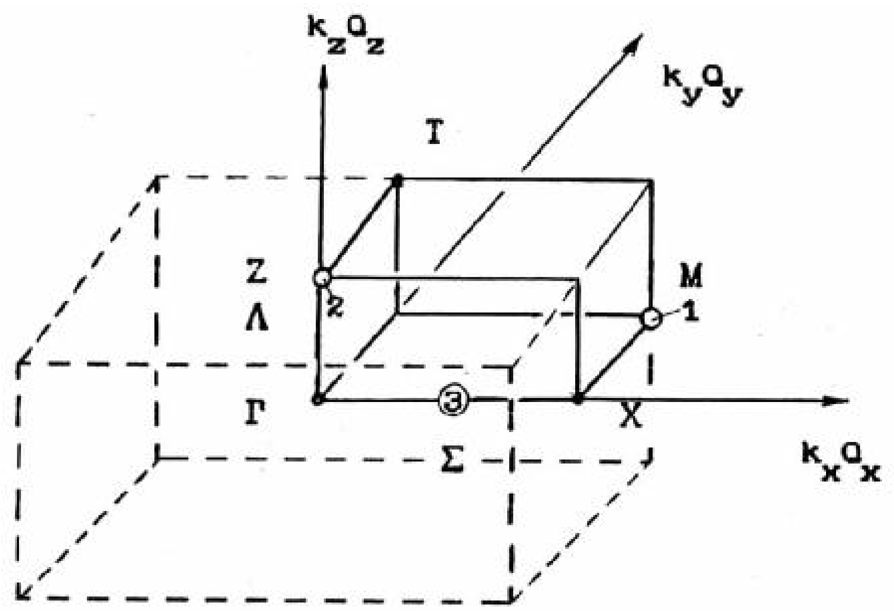

Figure 1.2. Symmetric points and directions of the lattice Brillouin grupy D_{2h}^{16} (Pnma).

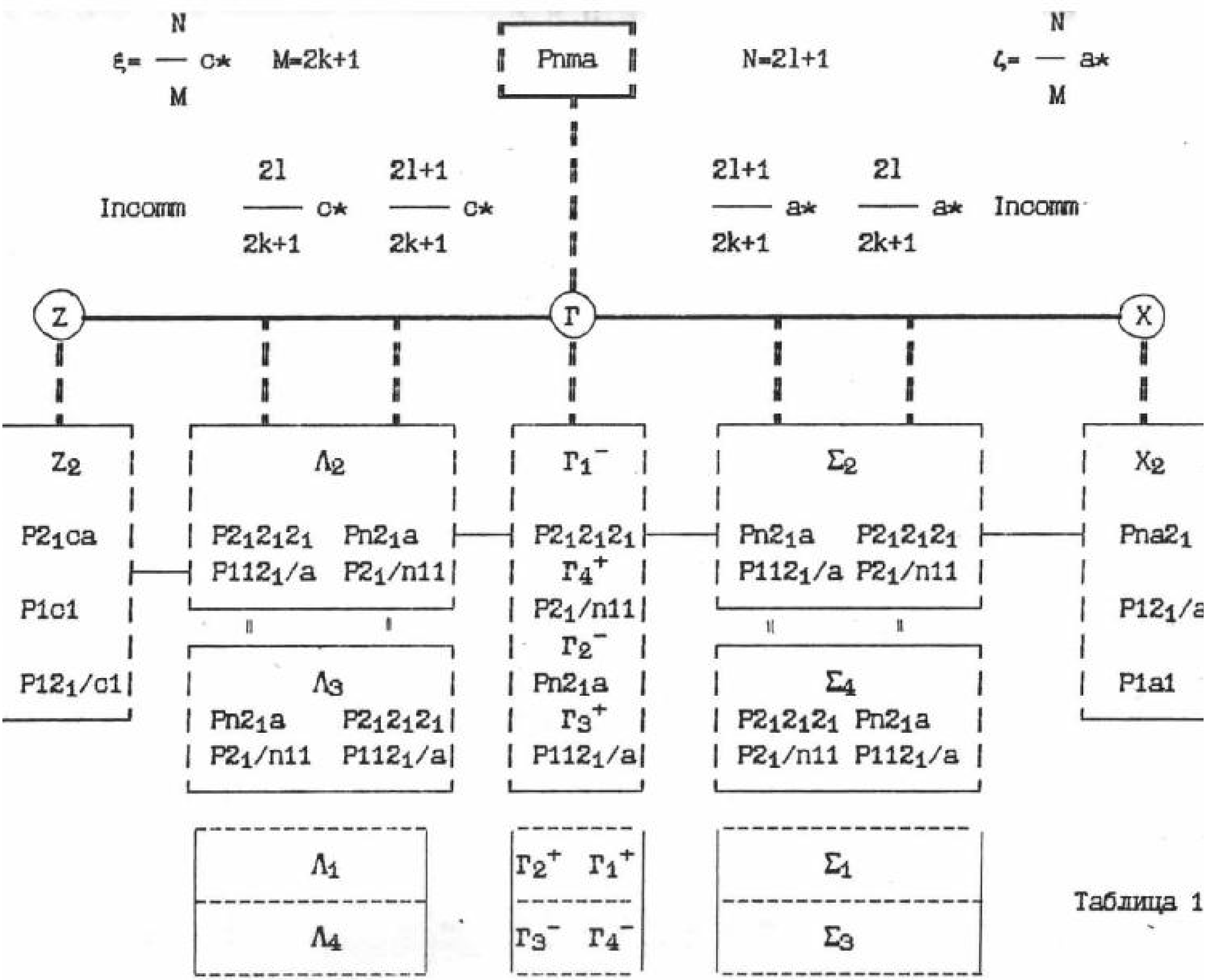
$\xi = \frac{N}{M} c^*$
$M=2k+1$
Pnma
$N=2l+1$
$\zeta = \frac{N}{M} a^*$
Incomm
$\frac{2l}{2k+1} c^*$
$\frac{2l+1}{2k+1} c^*$
$\frac{2l+1}{2k+1} a^*$
$\frac{2l}{2k+1} a^*$
Incomm
Z
Γ
X
Z_2
$P2_1ca$
$P1c1$
$P12_1/c1$
Λ_2
$P2_12_12_1$
$Pn2_1a$
$P112_1/a$
$P2_1/n11$
Λ_3
$Pn2_1a$
$P2_12_12_1$
$P2_1/n11$
$P112_1/a$
Γ_1^-
$P2_12_12_1$
Γ_4^+
$P2_1/n11$
Γ_2^-
$Pn2_1a$
Γ_3^+
$P112_1/a$
Σ_2
$Pn2_1a$
$P2_12_12_1$
$P112_1/a$
$P2_1/n11$
Σ_4
$P2_12_12_1$
$Pn2_1a$
$P2_1/n11$
$P112_1/a$
X_2
$Pna2_1$
$P12_1/a$
$P1a1$
Λ_1
Λ_4
Γ_2^+
Γ_1^+
Γ_3^-
Γ_4^-
Σ_1
Σ_3

Таблица 1

the standpoint of the atomic arrangement of this will lead to cooperation between the two sublattices of the crystal with different periods and realized a disproportionate or mosaic-cluster state.

Recently, efforts have been made to combine the universality hypothesis and cluster theory of phase transitions. In this way on the basis of experimental data for the theoretical foundations of association phase transitions of receiving and order-disorder [19,20]. There are reasonable grounds to believe that these transitions differ only in magnitude of the contribution from the phonon modes and pseudospin. This theory considers the equilibrium configurations of atoms in direct space:

$$H=\sum_{l}\left\{\frac{1}{2}u^{2}(l)+V_{S}\left\langle u(l)\right\rangle\right\}+\frac{c}{2}\sum_{l}[u(l)-u(l^{/})]^{2} \quad (1.4)$$

with single-particle potential:

$$V_{s}(u)=\frac{A}{2}u^{2}+\frac{B}{4}u^{4}+\ldots$$

In contrast to the models discussed above is introduced varying degrees of anharmonicity motion near double-well potential. In the case where the value of *g* = $V^{\circ}_{s}/K_{S}T_{C}$ (ratio of the depth of the pit to the local thermal energy) is small, the offset describes weakly damped mode, otherwise the soft mode is strongly overdamped, and there is strong anharmonicity of the atomic motion in the potential V_s (g>l). In the latter case, at low temperatures (below $T_{C)}$ one of the holes has a large population. As numerical calculations before T_C there Pretransitional area where there are buds (clusters), whose structure is similar to the structure of the low-temperature phase. Finite lifetime and size correlated moving clusters form different from that of the matrix, a dynamic structure, which is manifested in the spectral response function of the system. Molecular dynamics method were obtained solving the equations of motion with the Hamiltonian (4) as a nonlinear soliton solutions. In case of submission of solitons in the form of pseudo-ideal gas particles, the spectral function of the system is described as a phonon spectrum plus scattering due to slower movement of clusters (Gallo, diffuse bands on radiographs). When the speed of the cluster (or its borders) greater than the change in its size, there is a critical narrowing of the spectral components (central peak). Or, in the case of bias, if the fluctuations around quasi offset provisions are large compared with the quasi-equilibrium by the local displacements.

Even for small fluctuations in the presence of correlated moving regions should lead to redistribution contribution to the spectral response function between the quasi-harmonic frequencies and part responsible for the cluster scale movement.

Thus, even if the bias (g « 1), the spectral function of the coordinate ordering Q completely changed at $T_i > T_C$ with decreasing T. For $T < T_i$ soft phonon spectrum into the growth of the central peak. In systems offset soft mode has a resonant nature, although it may be a bit muted (Re and Im parts different from zero). In systems of order-disorder imaginary part of the soft mode is always different from zero, a Re part only if the quantum mechanical ground state splitting (tunneling, H-bonds). Cluster pattern in the transition of the displacement type allows crossover from mode to mode bias order-disorder at $T > T_{c,}$ as a result of the coherence of atomic motions.

Temporal and spatial correlation functions of clusters, also have considerable scale range. Maximum size and lifetime limited correlation length and time, and the minimum value - the size of embryos and their lifetime indevelopment threshold temperature fluctuations. If the system causes an increase in the size of preventing germs time structural redistribution could increase significantly and experimentally observed complete or partial freezing of non-equilibrium state of the system (windows). In the thermodynamic sense, the surface free energy of the system in the microscopic space of external parameters is represented by many local minimums separated by high energy barriers which may exist for a long time long-lived metastable *phases* overlapped with the topological structure (quasi-ergodic behavior) [21].

The problem of implementation of some elements of the crystal structure in a state such as glass, under quasiergodic assumptions led to the development of new approaches in the thermodynamic description of phase transitions. Quasiergodic system under certain conditions can evolve different structural time-dependent pathways in megascopic (cluster) and the macroscopic sense. In this case also, there is certain temperature $T_к$, the separating region with various types of thermodynamic behavior.

§ 1.2 Radiospec research methods disproportionately modulated structures.

Radiospectroscopic research methods substances based on excitation of transitions between energy levels of nuclear spins by the RF field. In the case of crystalline solids RF interaction with nuclear or electron spins in a crystal field representation atoms in the form of:

$$H = H_0 + H_1 + ... \qquad (1.6)$$

where **Ho** is **about -** the interaction Hamiltonian of the spin of an electron-nuclear environment of crystal atoms, **H$_1$** - interaction of the RF field.

In general terms, in connection with the usual symmetry of the nuclear wave functions, crystal-field Hamiltonian **H** atoms can be represented by a series expansion in even powers of the spin moments [19,24]:

$$(1.7) \qquad H_0 = \sum_{-2}^{2} V_2^m Q_2^m + \sum_{-2}^{2} V_4^m Q_4^m + ...$$

where Q_i - operators associated with the projection of the spin operators; $V_i^{m,}$ - coefficients, expressed in terms of parameters inside and interatomic interactions. Symmetry of these factors, in particular, depends on the symmetry of the crystal lattice and the phase transition is mainly determined by the symmetry of the soft mode.

In the case of nuclear quadrupole resonance (NQR) the interaction of spherically asymmetric nucleus of an atom with an inhomogeneous electric field electron environment. Coulomb energy of this interaction is given by [25]:

$$H_0 = \int\int \frac{\rho_e \rho_n dV_e dV_n}{|r_n - r_e|} \qquad (1.8)$$

where ρ_e and ρ_n - density of electron and nuclear weapons; **r$_n$-r$_e$** - distance between the interacting charge volume **dV$_e$ dV$_n$**. Using the decomposition

$$\frac{1}{|r_n - r_e|} \sum_{l=0} \sum_{m=-1} \frac{4\pi r_n^l}{(2l+1) r^{l+1}} Y_l^m(\theta_n \varphi_n) Y_l^{-m}(\theta_l \varphi_l) \qquad (1.9)$$

in spherical and radial functions and introducing the notation V_i for the l-th term in the expansion potential of the dipole moments of the electron nucleus

$$V_l^m = \sqrt{4\pi/(2l+1)} \int \frac{\rho_e}{r_l^{l+1}} Y_l^m(\theta_e \varphi_e) dv_e \qquad (1.10)$$

$$Q_l^m = \sqrt{4\pi/(4l+1)} \int \rho_n r_n \frac{\rho_e}{r_l^{l+1}} Y(\theta_n \varphi_n) dv_n$$

and passing to the operators, we obtain the interaction Hamiltonian nuclear electric moment with the atomic electrons in the form (1.7). Nuclear quadrupole interaction is described by the term

$$H_Q = \sum_{-2}^{2} V_2^m Q_2^m \qquad (1.11)$$

where, as is well known [24], the operators Q_2^m expressed in terms of the operators of the nuclear spin I, I_z, I_-, I_+, and the components of V_2^m through komponty EFG tensor q_{ab}:

$$v_2^{-m} = \sum_{\alpha,\beta=x,y,z} a_2^{-m} q_{\alpha\beta} \delta_{\alpha\beta}^{-m}; \quad \text{, где} \quad q_{ab} = \frac{d^2}{dX_\alpha dX_\beta} \int \frac{\rho_{ei}}{r_i} dv_e \qquad (1.12)$$

In the simplest approximation is considered point-charge model, oscillating near the sites of the crystal lattice r_i.

$$q_{\alpha\beta} = \sum \frac{\partial^2}{\partial X_\alpha \partial X_\beta} \frac{e_i}{r_i} = -\sum_{\alpha\beta} \frac{e_i(3X_\alpha X_\beta - \delta_{\alpha\beta} r_i^2)}{r_i^5} \qquad (1.13)$$

Returned to the expression (1.7), we see that the coefficients of $V_2^m{}_{,4}$ are determined, in particular the nature of the atomic displacements in the crystal and in the general case can be presented through static and dynamic displacements of these

$$V_{2,4}^m = \left\langle V_{2,4}^m \right\rangle + V_{2,4}^m(t) \qquad (1.14)$$

In highly phase most of $V_2^{m,}{}_4$ is zero. In the distorted phase one (or more) of the coefficients Perfect Branch becomes zero and can be expanded in powers of order parameter Q =u

$$V = V_C + A_1 Q + A_2 Q^2 + . \qquad (1.15)$$

Taking into account the fluctuations of Q, above T_i

$$V = V_C + \sum_k A_1(k) Q(k) + \sum_k A_2(k_1,k_2) Q(k_1) Q(k_2) + \ldots \qquad (1.16)$$

For the EFG tensor tensor this expansion into more formal recording renaming symbols represented in the form [19,27]: at T> T_i

$$\left\langle V_{i,j} \right\rangle = V_{ij}^0(0) + A_{k2} \left\langle Q^c(k,t) \right\rangle + \ldots\ldots \qquad (1.17)$$

$$\langle V_{ij}\rangle=V_{ij}(0)+S A_k 2\langle Q^c(k,t)\rangle+\ldots \qquad (1.17)$$

$$\left\langle V_{i,j}\right\rangle=\sum_{k} A_1(k)\delta Q(k,t)+\sum_{k1,k2} A_2^{/}\{\delta Q(k_1)\delta Q(k_2)-\left\langle \delta Q(k_1)\delta Q(k_2)\right\rangle\}+\ldots..$$

$> T_i$ at $T> T_i$

$$\left\langle V_{i,j}\right\rangle=V_{ij}^{0}(0)+\sum_{k} A_1^{/}(k)\left\langle Q\ (k,t)\right\rangle+\sum_{k1} A_2^{/}\left\langle Q(k_1,t)\right\rangle^2+\sum_{k1} A_2\left\langle \delta Q(k_1)\delta Q(k_2)\right\rangle+\ldots\ldots\ldots$$

$$\left\langle V_{i,j}\right\rangle=\sum_{k} A_1(k)\delta Q(k,t)+\sum_{k1,k2} A_2^{/}\{\delta Q(k_1)\delta Q(k_2)-\left\langle \delta Q(k_1)\delta Q(k_2)\right\rangle\}+\ldots..$$

where **$Q(q_s-k,t)=\langle Q(q_s-k,t\ )\rangle+\delta Q(q_s-k,t\ )$ -** static and the fluctuation of the order parameter near the dew point of the soft mode $q_{s.}$ The spectral function of a critical variable Q (k, t) has the form [19]:

$$G(k,\omega)=\int\left\langle V\ (k,0)V\ (k,t)\right\rangle \exp\{-i\omega t\}dt \qquad (1.18)$$

under decomposition and V_{ij} (k, t) may be represented as

$$G(k,\omega)=\int\left\langle |V^{/}(k,t)|^2\right\rangle v(k,t)\exp\{-i\omega t\}dt \qquad (1.19)$$

where V (k, O) V (k, t) is divided into static and temporal parts. If the time-dependent part of v (k, t) is a slowly varying function of time, for the wave vector q_s component of the spectral response function

$$\int G(q_S,\omega)d\omega=\left\langle |V\ (q_S,t)|^2\right\rangle : \left\langle |Q(q_S,t)|^2\right\rangle \qquad (l.20)$$

with contributions by close to $q_{s,}$ the line shape will be (taking into account the first term of the expansion)

$$\Gamma(\omega)=\sum_{k}\left\langle |Q(k,t)|^2\right\rangle g(k,\omega) \qquad (1.21)$$

thus the line shape reflects the shape of the distribution function of the atomic configuration of distortion caused by movement in slow-time radio. Linewidth characterizes while the rms value of the contributions to the distortion caused by the Fourier components of the displacement field with frequencies small compared to the reciprocal of the time threshold permits radio ($1/T^*_{Q.}$). If the low-temperature phase is observed any preferential swings from a position displaced by an amount ± Q_0(T)from the position of a highly, the line will consist of two components.

When $T\to T_i$ $Q_0\to 0$ and splitting becomes small in comparison with (slow) fluctuations subtransient ordering. In the case of atom spectral line narrows to a minimum when the upper limit of the transition ordering. When a Q linear terms are comparable in magnitude with quadratic, it is necessary to take into account the contribution of the relaxation processes in the Raman linewidth. Finally it should be noted that the lineshape Γ(w) is determined by all phonon wave vectors k . In view of this, it is necessary to analyze the results to have any model representation for g(k, w).

Expression (1.17) for the transformation of the EFG tensor near the phase transition indicates that studies of radiospectroscopic can extract information about the behavior of the order parameter Q (Qs-k, t).

Already at T> Ti measurements enable us to estimate <Q(t)> temporarily averaged square of the criticalcoordinates, which in the pre-transition region is associated with the critical dynamics. In particular, this refers to the crystals, where the phase transition is associated with an increase in the amplitude of the fluctuations caused by lattice vibrations or librational modes. Time-dependent part of the GEF determined by the speed and the type of processes with which the spin-lattice system can exchange energy.

Therefore, as follows from (1.17), can be studied microscopic dynamics of critical fluctuations amount of change in the fluctuations of the order parameter near $T_{i.}$

From the standpoint of radiospectroscopy question is how to properly excite the spin system and measure the spin-lattice relaxation time, to separate the various contributions and then link the measured values with the dynamics of critical fluctuations. In the case of nuclear NQR excitation system is an alternating magnetic field $H_{1.}$Hamiltonian describing the RF exposure to the system of nuclear spins in the case of continuous sensing has the form:

$$\overrightarrow{H}_1 = 2\gamma hI\, H_1\cos 2\pi\nu t \qquad (1.22)$$

where n - frequency of the RF field, g - gyromagnetic ratio.

The transition probability per unit time between the states c and c_1 in this case is given by [30,135]:

$$W_{kl} = \eta^{-2}\omega_{k1}Q(\nu) = \eta^{-2}|\langle\chi_k|I^*H_1|\chi_l\rangle|^2 G(\nu) \qquad (1.23)$$

W_{k1} –relative transition probabilities, G(n) - a function of the spectral distribution of the resonance line. Absorption intensity under resonant excitation depends on the difference in population levels and, in the absence of saturation, the expression [26,29]:

$$P_{kl} = \frac{N\nu^3}{\pi(2I+1)\Delta\nu kT} W_{kl} = \frac{n_0\eta\nu\gamma^2H_1^2T}{1+2\gamma^3H_1^3T_{Q1}T_{Q2}} = \eta\nu n_0\gamma^2G(\nu)S_1 \qquad (1.24)$$

N-number of nucleus , Dn - half-width of the absorption line.

Under pulsed excitation quantum spin system operators depend on time and to calculate the amplitude of transient signals commonly used density-matrix method [30]. In this case the change of the static density operator s is described by Neumann

$$\frac{ds}{dt} = \frac{1}{h}[s, H];\ H(t) = H_0(t) + H_1(t) + \qquad (1.25)$$

$\boldsymbol{H_0}$(t) - the operator of the quadrupole interaction,

$\boldsymbol{H_1}$(t) - operator interaction with the RF field H_1 cosnt. The last operator is zero between pulses. Equation is represented as [31,135] $s = \mathbf{R}^{-1}s_0\mathbf{R}$ where $\mathbf{R=R_IR_tR_{II}R_{t+t}}$. $\mathbf{R_I}$ **and** $\mathbf{R_{II}}$

solving the Schrodinger equation for the period action pulses (intervals nutation); $\mathbf{R}_t$ and $\mathbf{R}_{tt}$ -for free precession intervals between pulses

Developed methods for the solution of equation (1.25) allow us to calculate the amplitude of the signal induction $\mathbf{A}_t$, $\mathbf{A}_{t+t}$ and spin echo $\mathbf{A}_{t+t}$ with a two-pulse excitation of nucleus with spin 3/2 [32]. Spin echo envelope, as shown, may be represented by two terms - term proportional to the magnitude of the constant component and a corresponding member of the induction signal, which is small if $\mathbf{T}^*_{Q2} < t < \mathbf{T}_{Q2}$ ($\mathbf{T}_{Q2} \ll \mathbf{T}^*_{Q2}$). Study of spectral functions transient signals are not known. However, under certain spectral conditions, and in particular cases, referring to the direct comparison, it is reasonable to select those conditions of pulsed excitation, when the spectral shape of the resonant response is comparable to form a continuous sounding excited.

Referring to the description of known femenological model static and dynamic characteristics incommensurate phases [33,34].In the adiabatic approximation of the resonance line shape is described by the expression [27]

$$\Gamma(\nu)=\int_{-\infty}^{\infty} g(t)\exp(-i\nu t)dt \qquad (1.26)$$

where
$$g(t)=\left\langle \exp\{\int_0^t \nu(t')\,dt'\}\right\rangle$$

that looks like a static redistribution

$$G(\nu)=\int^{\infty}\langle V(t)\,V(0)\rangle\exp(i\nu t)\,dt=\int g(\nu-\nu_C)\,A(\nu_C)\,d\nu_C \qquad (1.27)$$

If we assume that at the phase transition, the frequency of the resonance absorption of the nucleus can be expanded in powers of the displacements

$$\nu_i=\nu_{0i}+A_{ij}u_i+A_{2i}u_i^2+A_{3i}u_i^3+\ldots\ldots \qquad (1.28)$$

where u_i can be represented as an expansion in the eigenvectors of the soft mode (1.1), for each atom **p** varieties can write (nonlocal description) [35]:

$$u_{ip}=u_{0p}^C\cos((x_i))+u_{op}^S\sin((x_i)) \qquad (1.29)$$

where the plane-wave approximation modulation (PWA), the phase changes of the atomic displacements *as:*

$$\varphi(\mathbf{x})=\mathbf{q}_s\mathbf{x}_p+\varphi_{op}(\mathbf{x}); \qquad (1.30)$$

and in the soliton approximation:

$$\varphi(x)=\varphi_{op}+\frac{2\pi m}{p}+\frac{m}{p}\text{arctg}\{\exp(-\alpha(x-mb)\sqrt{p})\} \qquad (1.31)$$

If the modulation long periodic then

$$q_S=(1-\delta)a^*/p=q_C-\frac{N}{M}q_C$$

After substituting (29) into (28) we obtain

$$\nu(X)=\nu_0+\nu_1\cos(\psi(x)+\varphi)+\nu_2^{/}+\nu_2\cos^2\psi(x)+\ldots \qquad (1.32)$$

The density of the spectral function **f(n)** according to [33] will be determined by the expression:

$$f(\nu)=\frac{N}{|¶n/¶j\ |}=\frac{N}{(¶n/¶j\ )(¶y\ /¶x)} \qquad (1.33)$$

where are N - the number of nucleus per unit length in the direction of the incommensurate modulation. In the case of long-period of modulation **f(n)** represents the sum of the discrete frequency components of each unit cell unit .

The specific form of the expansion is determined by the local crystal symmetry and lattice site for which the expansion is made, namely, the symmetry of the electronic environment and the symmetry of the eigenvectors of the soft mode. This imposes restrictions on the type of decomposition (1.28), and some of the coefficients $\mathbf{A}_{\mathbf{ki}}$ may be zero (**$\mathbf{A}_1$**0, **$\mathbf{A}_2$**=0 - linear expansion, **$\mathbf{A}_1$**=0, **$\mathbf{A}_2$**0 - quadratic expansion, etc.).

Analysis of the function **f(n)** was carried out for all sorts of occasions decomposition n(x). First results were obtained under the assumption that the resonance frequency $n_{\mathbf{o1}}$ working nucleus depends only on the in-phase shifting him atoms (local description) [34]. For illustration, Figure 1.3 shows a view of functions **f(n)** and thermal splitting of boundary singularities on the situation for high-symmetry phase in the case of a quadratic approximation PVM.

Later, it was considered femenologicheski impact on GEO Dunn nucleus atomic displacements of the nearby environment associated with other eigenvectors of the soft mode (nonlocal description) [35]. In this case it was possible to achieve greater agreement with experiment. From a theoretical point of view and questions analyzed the spin-lattice relaxation of nucleus in incommensurate systems [33,35].

Thus there is a theoretical basis for the description of the resonance spectra in neoorazmerennyh systems, both static and dynamic aspects. Experimental research objective is to obtain data for comparison.

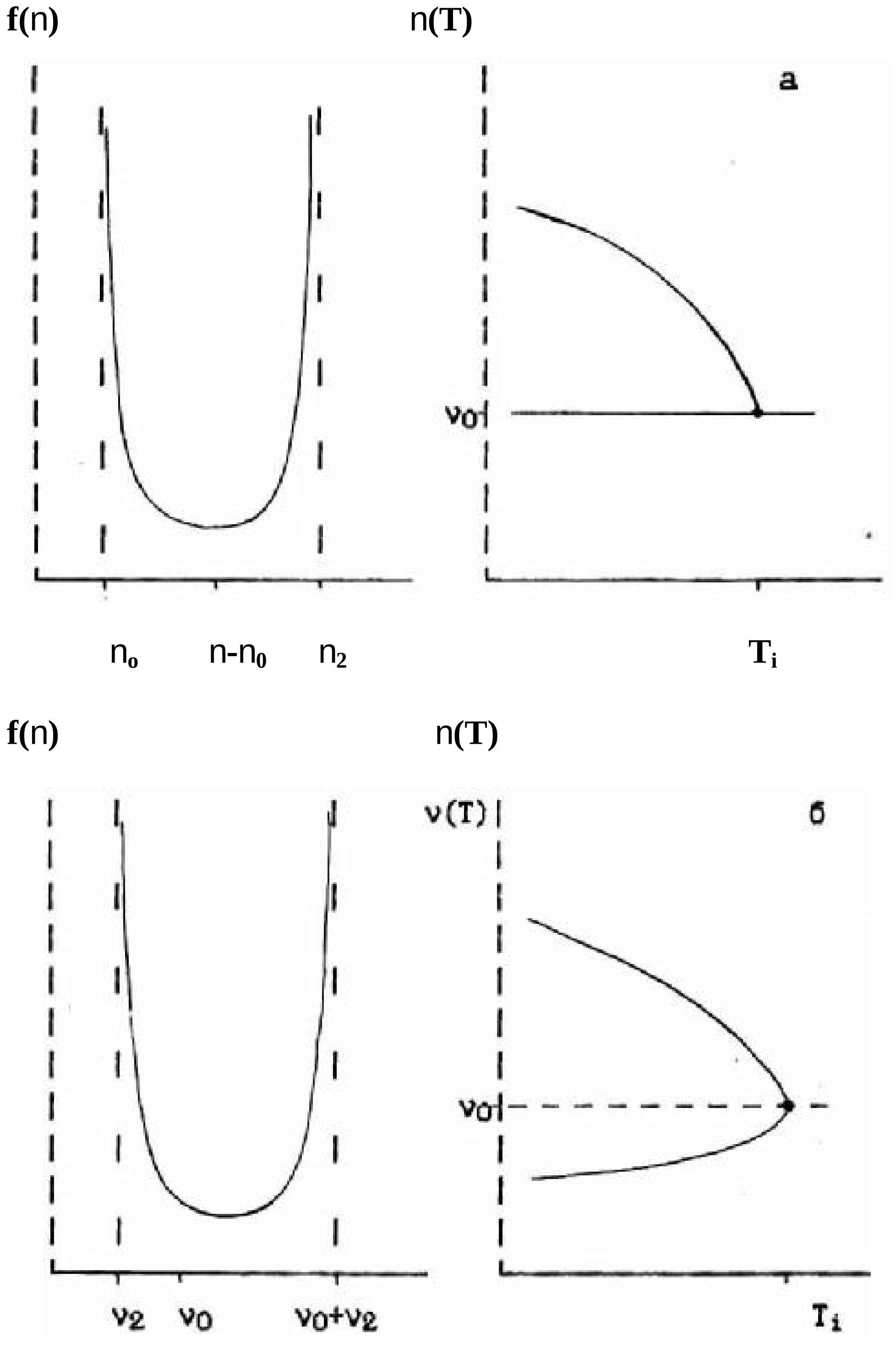

Figure 1.3. Type function **f(n)** and when disconnection of frequencies in T_i a) local and b) nonlocal cases.

§ 1.3 Experimental studies of families of compounds A_2BX_4 structure type β-K_2S0_4.

By now, several hundred compounds of the chemical composition A_2BX_4 (A = K, Na, Rb, Cs, NH_4 ...; B = Zn, S, Co, Mn, Cd, Mg, Se; X = F, Cl, Br, J. ..) with an octahedral, tetrahedral, and planar coordinations distorted anion X, relative to the atoms of type A 170 from various structures such composition is one of the most interesting type structure β-K_2SO_4, wherein the coordinating anion is close to the tetrahedral . In recent years, representatives of this structural type attract attention due to the discovery disproportionately modulated phases in compounds β-K_2SO_4 [2], Rb_2ZnCl_4 [39], K_2ZnCl_4 [37], Rb_2ZnBr_4 [38], $(NH_4)_2ZnCl_4$ [39], Cs_2HgBr_4 [46] and others.

High-temperature phase β-K_2SO_4 is orthorhombic and space group D_{2h}^{16}(Pnma) (b>a>c) [40]. It is also assumed that this structure is praphase nonpolar structure with space group symmetry D_{6h}^{4}($P6_3/mm_6$). This structure was observed above T = 745K in K_2SeO_4 [58].

On the basis of structural studies in the literature formed the view that the diversity of family structures in the A_2SBHal_4, due to the high porosity of the core nucleus halogens and volatile cations A relatively small perturbation of the electron configuration of anions The connection A-A' in some cases resembled relation H-H'with two minimumnym potential [128].

Crystal-structure analysis of stability β-K_2SO_4 [4] made based on a comparison of anionic and cationic radii in the problem of dense packing gives the forecast for the region of stability of the structure (Figure 1.4). Experimental data indicate that the most structurally diverse compounds properties are located on the border of stability of structure β-K_2SO_4. Such compounds with various external effects exhibit, as a rule, a tendency to a sequence of phase transitions in less symmetrical, manner in the structural hierarchy, phase. In this sequence and implemented disproportionately modulated structure. In addition, the analysis of the crystal-chemical and experimental data indicates the possibility of the existence of another type of instability ion frame associated with symmetry-unrelated transformation structure.

Modulated phases owe their existence delicate balance intracrystalline interactions, which, as experience shows, can be easily broken. Preliminary theoretical studies of these interactions indicate that itself modulated structure can be represented by a sequence of higher level of symmetry. On the basis of these results, the physics can expect the discovery of new principles describe the crystalline state and the detection of previously unknown properties of dielectric solids.

Currently, research efforts are focused on the one hand to find and codify different structures in the incommensurate phase and a generalized phase diagram of these compounds and, on the other hand, figuring out the new features and capabilities to manage these structures.

Until the moment of this writing the most studied compounds were presented in Table 4.4. They all have high-temperature phase with the space group symmetry D_{2h}^{16} (Rnma) and with decreasing temperature test sequence of phase transitions. Presented in Table compounds can be divided into three groups according to the position of the symmetry in the Brillouin cell dew point of the soft mode: near the S-line, L-line and **X**-line.

Incommensurate phases observed in these compounds have one-dimensional modulation, characterized by displacement of the atoms along the **a, b** or **c** directions "direct" lattice. As the temperature decreases observed sequence of phase transitions between phases with space group symmetry, which are sufficiently consistent scheme developed in [18]. The experimental data presented in the table 4.1 were obtained with the assistance of various macroscopic and structural measurements. All of these compounds were investigated radiospectroscopic methods. In most of the compounds detected the presence of

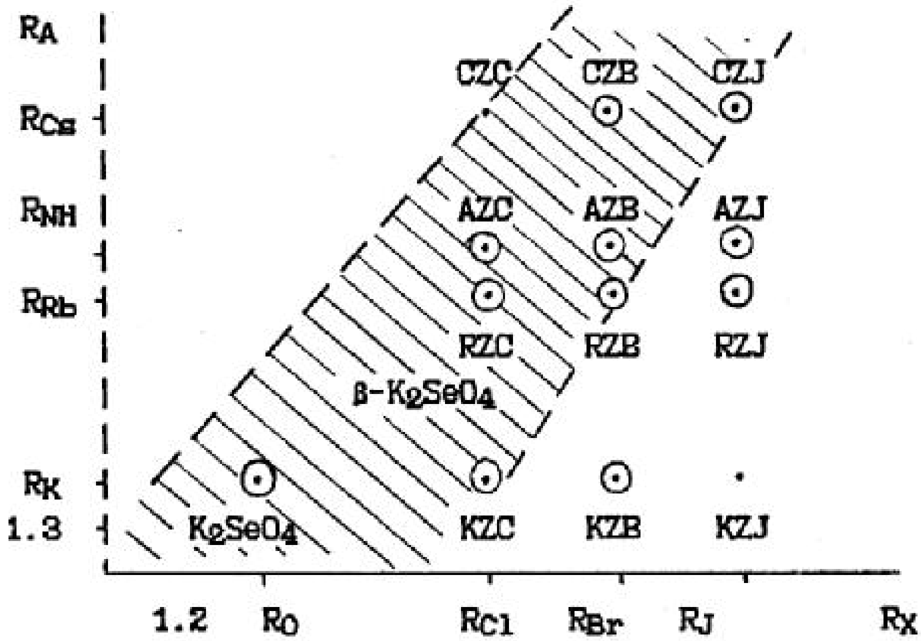

Figure 1.4. Stability domain structure β-K_2SO_4 for compounds A_2ZnX_4. (See the notation in Table. 3.1)

an incommensurate phase NQR, NMR and EPR. Below we will focus mainly on the NQR studies, and the results of other resonance techniques will attract only as needed As seen from Table 4.1, most of the nucleus of atoms of compounds have a nonzero quadrupole moment. However, from a practical point of view, are the most suitable halogen isotopes: J, Br and Cl. The nucleus of the lasttwo have spin 3/2, and according to theory NQR can be in two doubly degenerate energy states [43]:

$$E_{12} = \frac{eQq_{zz}}{4}\rho\,;\ \rho = \left(1 + \frac{\eta^2}{3}\right)^{1/2} \qquad (1.33)$$

where Q - quadrupole moment; h - the asymmetry parameter; q_{zz} - EFG component along the main axes of the tensor $q_{ab.}$ In the absence of disturbances, for there is one observation of the NQR frequency

$$\nu_{1/2\text{-}3/2} = \frac{1}{2}eQq_{zz}\rho\,, \qquad (1.34)$$

change that is required to change the EFG at work at the core of the structural phase transformations. On the measurement of the NQR frequencies of non-equivalent structural positions of the nucleus based simplest methods NQR.

For quantum transitions between levels of quadrupole nucleus with spin different from 3/2 with more than two non-degenerate transitions, which is possible to observe the effect of "pure" NQR [24]. The most common methods of NQR are stationary when the spin system affects continuous RF field and unsteady - recorded when the system response to impulse action.

First NQR data in compounds A_2BX_4 (X-halogen) have been presented in [44,45]. For a large group of compounds bysuper-regenerative spectrometer were measured NQR frequencies at room temperature and the boiling point of nitrogen. It was noted that in some compounds the signals are not observed or observed only partially and incontradiction with the diffraction structural data The pioneering research NQR incommensurate phases were performed in in IF SB AN USSR A.K.Moskalev and et al. [36] and IN&OCh AS USSR G.K.Semin [46]. In these papers to study incommensurate phases was applied pulse NQR method. In the first of the cited work was to study the evolution of the NQR spectra in the crystal Cs_2ZnCl_4 and built the temperature dependence of the frequency dependences of nucleus ^{35}C1 (Figure 1.5). [46] studied the compounds $Cs_2HgBr_{4,}$ where the authors observed NQR spectra in the incommensurate phase. Following work was performed at the junction of Rb_2ZnBr_4 [38], where the NQR spectra were studied in the incommensurate phase and frequency dependence is built in a wide temperature range (Figure.1.5b).

Given the experimental data of [36,33,38] on the basis that existed at that time, theoretical ideas about the disproportionate state model was proposed femenologicheskaya cancellation resonance line shape evolution in the incommensurate phase [33]. The frequency distribution of NQR spectra have been analyzed in the framework of the plane-wave approximation and the soliton. On the basis of the calculated line shape fit to the experimental qualitative agreement was reached with the description of the proposed model of the incommensurate phase in the framework of the plane wave approximation [34]. However near T_C agreement was unsatisfactoryIn this area, there was an attempt to describe the theory of Dzyaloshinskii-Landau, through the concept of identifying the density of solitons with the order parameter of the phase transition to the ferroelectric phase.

Another attempt to study the incommensurate phase was undertaken in K_2ZnCl_4 stationary NQR method [37]. At room temperature, as in [44], with the resonance lines 6 $^{35}C1$. However, in the incommensurate phase NQR signals were observed only near $T_{i,}$ the position (I) $C1^{35}$ nucleus in the structure Pnma. The absence of signals from other nucleus $^{35}C1$ explained significant reorientation of the $ZnCl_4$ tetrahedra around its axis passing through the position of the nucleus Cl(1) and coincides with the axis symmetry structure.

In 1980 he was made a comprehensive study of the compounds Cs_2HgBr_4 and Cs_2CdBr_4 [48] and the observed sequence of phase transitions shown in Table 4.1. Using pulse technology NQR was tracked the temperature dependence of the frequency, while in the incommensurate phase NQR signals were observed only on the position. I core structure Rnma ^{81}Br. Line shape in the Jc-phase had continual distribution and attempted to describe it as part of the plane wave approximation model [33].However pronounced asymmetry form was not explained clearly. Signs soliton picture offset was observed.

Compound $(NH_{4)2}ZnCl_4$ and $(NH_{4)2}ZnJ_4$ also were first investigated by NQR in Krasnoyarsk **IF** [39,49]. In the first of these compounds, in the temperature range from 271K to 266K, anomalous behavior of NQR spectra in which 16 high-temperature phase of singlet lines are mapped to 12 NQR lines below 266K. In the intermediate temperature range was registered incommensurate phase. In $(NH_{4)2}ZnJ_4$ similar type anomaly was observed at 222K in 4K (Figure 1.6). In these compounds, involving other methods, later was detected and other phase transitions indicated in Table 4.1.

RF methods have been reported and studied incommensurate phases in the $(NH_{4)2}BeF_4$ and $\{TMA\}_2ZnCl_4$ (see the references in [33]).

Thus, a simple observation made by NQR can detect incommensurate phases.

Simultaneously with the work described above, for several years compounds with β-K_2SO_4 and studied all sorts of other methods, and to date there is sufficient information on the properties of the phases and characteristics of phase transitions for each compound. The major method allows to measure directly the value of q_s are diffraction methods.

The main advantages of pulsed rf is the possibility of direct measurement of the spin-spin T_{q2} and spin-lattice relaxation time T_{q1} system. This information, as noted above, is of great value for the study of the dynamics of the system in a critical phase transition region.

Blintz and coworkers [33] were measured by NMR $T_{Q1}(T)$ and $T_{Q1}(\eta)$for the core ^{87}Rb in the compounds Rb_2ZnBr_4 and $Rb_2ZnClBr$. Results were compared with theory. In the P-Jc transition usually observed critical shortening $T_{q1,}$ which, as stated by the authors, was not contrary softly-mode description. In Jc phase in a wide temperature range T_{q1} ivmenyaetsya little with temperature and is abnormally short. Originally it was explained the predominant influence of phason excitations in the entire region of the incommensurate phase. However, studies in the high part of the measurement phase and Jo T_{q1} in metered-doped solid solution $(Rb_{1-x}K_{x)2}ZnCl_4$ (x = 0, 0.02, 0.06) [52] reported significant influence of impurities on the behavior of T_{q1} in Jc phase transition at T_C At x = 0, the value T_{q1} was reduced and observed at T_C T_{q1} races.

In conclusion, the experimental part of the review, we note some kinetic phenomena observed in the incommensurate phases. In studies of systems with dipole density waves

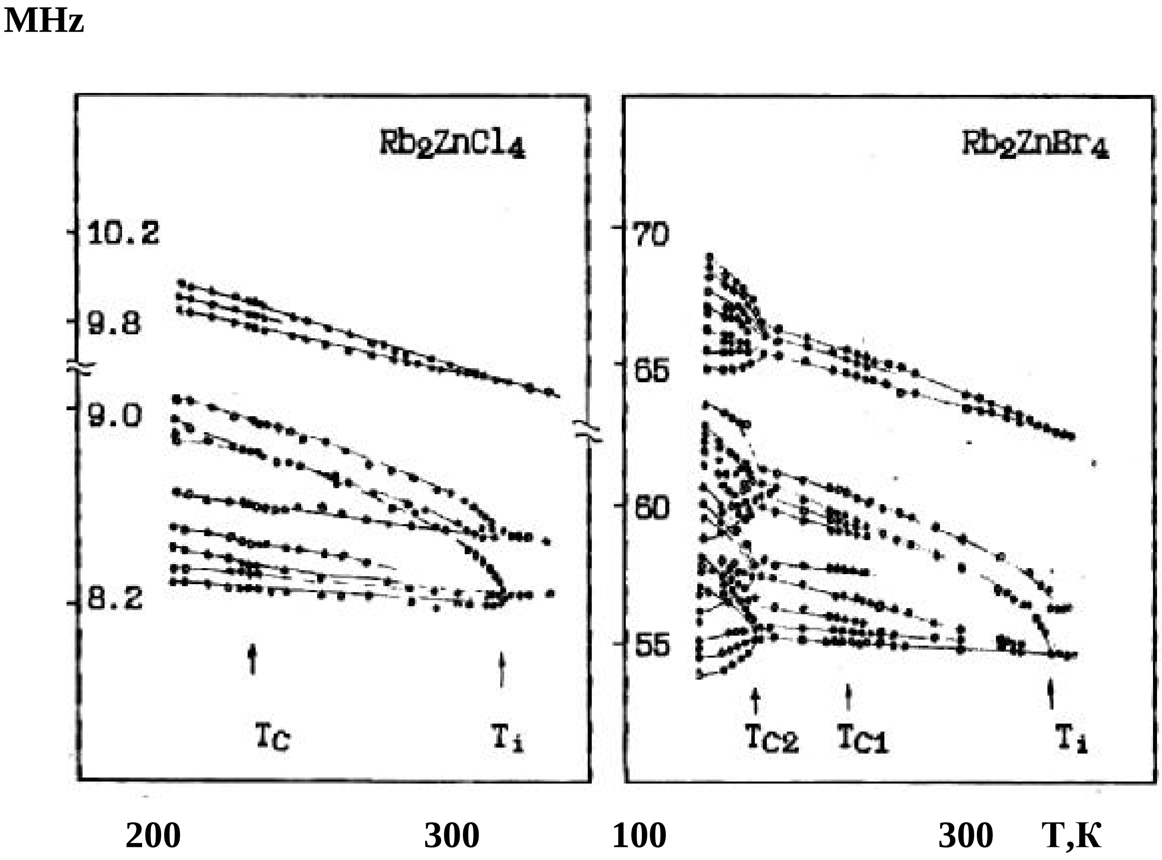

Figure 1.5. Temperature dependence of the frequency of the NQR lines of Rb_2ZnCl_4 and Rb_2ZnBr_4

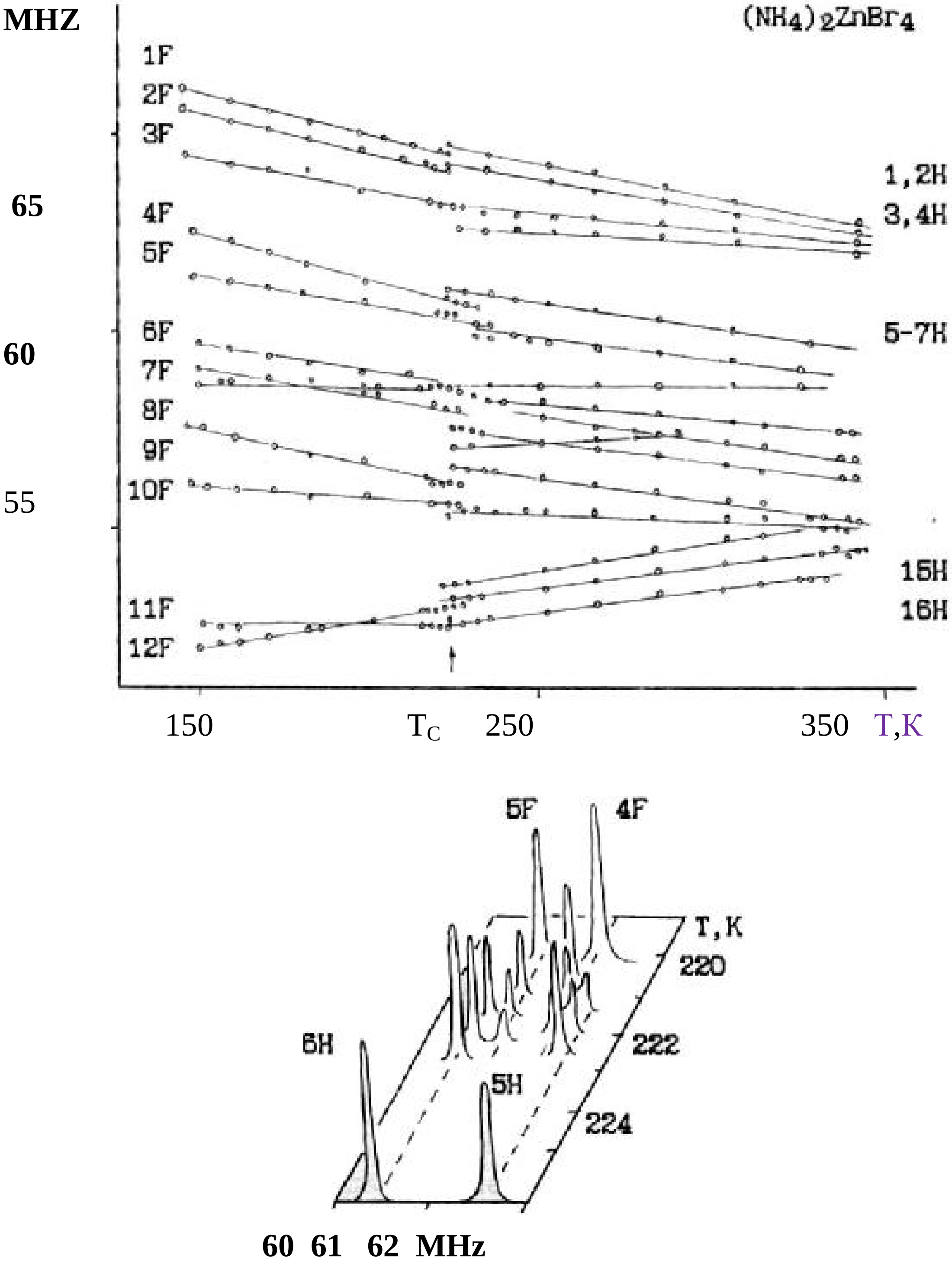

Figure 1.6. Temperature dependence of the frequency and the change in T_C line intensity 5F and 6F NQR spectrum in the $(NH_4)_2ZnBr_4$.

(which include dielectrics and modulated with a structure of β-K_2SO_4) in the incommensurate phase were found by macroscopic nonequilibrium processes that are a little earlier, were seen in systems with charge density waves [63]. One of these phenomena, called global hysteresis is the presence of a kind of hysteretic behavior was observed in the entire region of the incommensurate phase [60,62]. A typical illustration of this behavior is mutually reciprocal transition between states I« II characterized by the magnitude of the inverse susceptibility $1/(c-c_o)$ (corresponding to the cooling mode (I) or heating (II) when the direction of the sample temperature in the opposite Jc phase near T_C [62]). When the temperature stop $T_{stop} > T_C$ trend approximation value $1/(c-c_o)$ to some equilibrium state III. However, if after stopping, the direction of change of temperature is stored, the temperature during the reverse stroke, when the temperature $T_{'S}$ observed small leap 0.01% of the measured macroscopic susceptibility. The temperature $T_{'S,}$ up to a temperature hysteresis stop coincides with the temperature T_S [61]. This phenomenon has been referred to the effect of thermal memory. Additionally in studying samples doped $Rb_2ZnBr_{4,}$ it was found that the form of the hysteresis curves of dielectric measurements depends on the prehistory of the sample [60]. Initially, these nonequilibrium phenomena explained by the interaction of the modulation wave soliton configurations with mobile defects. In this model competition soliton-soliton and soliton-defect interaction at fixed external conditions for quite a long time leads to the establishment of a quasi equilibrium system micro configuration. Conditions change and subsequent recovery, after a time shorter than the diffusion of defects, their distribution is correlated with the quasi-equilibrium conditions for the data configuration of solitons. However, theoretical estimates to quantify the magnitude of this effect in real crystals [62], as well as direct electron microscopic observation of the actual configuration of the walls transform domain disproportionate Rb_2ZnCl_4 and 2H-Ta_2Se [53] pointed out that the main mechanism of the transformation of the soliton strktury are the processes of formation (destruction) of anti-germ incommensurate phase (stripple nuciies) [62,63]. The unit consists of a single nucleus (P = 2) or more (P > 2) regions with incommensurate structure, surrounded on all sides by the other incommensurate structure. Structures differ in the magnitude of the phase

$$j_{li} = j_{O} \ \frac{2\pi}{p} n_{li}\ ; \quad (n_{li} = -(p-1),\ -1,0,+1..\ p-1))$$

and separated soliton walls. The walls of the embryo in their intersection to form a special (topological) defect. With the growth or dissolution of embryos there are significant elastic force impeding change its volume (in the case of the strong interaction of the topological defect with a matrix structure of the crystal). Due to this, the system has significant internal friction, preventing movement of the defect and an inhomogeneous stress. Development of the latter may result in an increase of the same type at the expense of other domains, as well as affect the amount of phase change in the domain walls

$$j - \frac{2\pi}{p} j_{O} \ ^{1} \ 0$$

§ 1.4. Investigation of incommensurate phases in dielectric crystals at high pressure.

After the initial accumulation of experimental information. Study of incommensurate phases in the temperature scale, its amount was insufficient to prove or disprove any of the theories disproportionate state. Efforts experiments were aimed at expanding research using other external parameters. One of them is thehydrostatic pressure

Fig. 1.7 and 1.8 shows the phase P-T diagram of some compounds. These diagrams have been prepared by various methods. The most important from the point of view of the structure are the diffraction data. One of the first studies of molecular dielectrics with an incommensurate phase at high pressure was performed on a crystal of thiourea $SC(NH_{4)2}$ Fig.1.7 [53]. In this connection method neutron diffraction were tracked change in pressure of the wave vector of the incommensurate modulation. At atmospheric pressure, J_C phase due to softening of one of the static modes in the center of the Brillouin zone. Under pressure dew point is marked deviation from the center of fashion, followed by a tripling of the unit cell volume.

In $NaNO_2$ incommensurate phase is also associated with the softening of one of the modes of nature relaxation at zero frequency. In this connection disappears incommensurate phase at low pressures, is also assumed that the incommensurate phase in Cs_2HgBr_4 disappears when the load [54].

Any studies under pressure this class of compounds by RF unknown to us. Among the compounds having ferroelectric properties and having, as it turned out during our research, incommensurate phase, work on the high pressure NQR was held on proustite Ag_2 AsS_3 Fig.1.76 [56,57]. It has been suggested disappearance incommensurate pressurized state. P-T phase diagrams of some of the compounds A_2BX_4 were initially identified using dielectric measurements. Figure. data obtained are presented in [58], and Fig.1.8b in [59]. The first type of compounds with a structure β-K_2SO_4 studied in detail the crystal was pressurized $\{TMA\}_2ZnCl_4$ (Fig.1.7b) [55]. Neytron diffraction method it was filmed isothermal variation of the wave vector $q_{S,}$ traced the region of existence of the incommensurate phase and found a structure with multiple larger unit cell. Character changes q_S adequate behavior such as "devil's staircase". Thus by the time of our study were quite scarce data on disproportionate phases under pressure, and most of them have been published during the execution of our program.

From the analysis of the physics of incommensurate systems in dielectrics family A_2BX_4 structure β-$K_2SO_{4,}$ it is seen that there is a broad range of issues requiring further experimental clarification. First, the lack of detailed structural data on family type β-$K_2SO_{4,}$ where at the beginning of our work was carried out initial studies of all seven of its representatives (of 25 projected).

The resulting macroscopic diffraction and radio spectroscopy data indicate significant differences in the structural transformation of compounds as the wave vector and sequence of structural transformations. In various compounds below the transition to the incommensurate phase was observed significantly different multiplicity spectra and different degree of ordering of the structure dynamics. Not quite clear was the question of uniformity of phase transitions P « J_C and J_C « F. Also highlights some of the difficulties in explaining the shape of the line in the incommensurate phase on the basis of

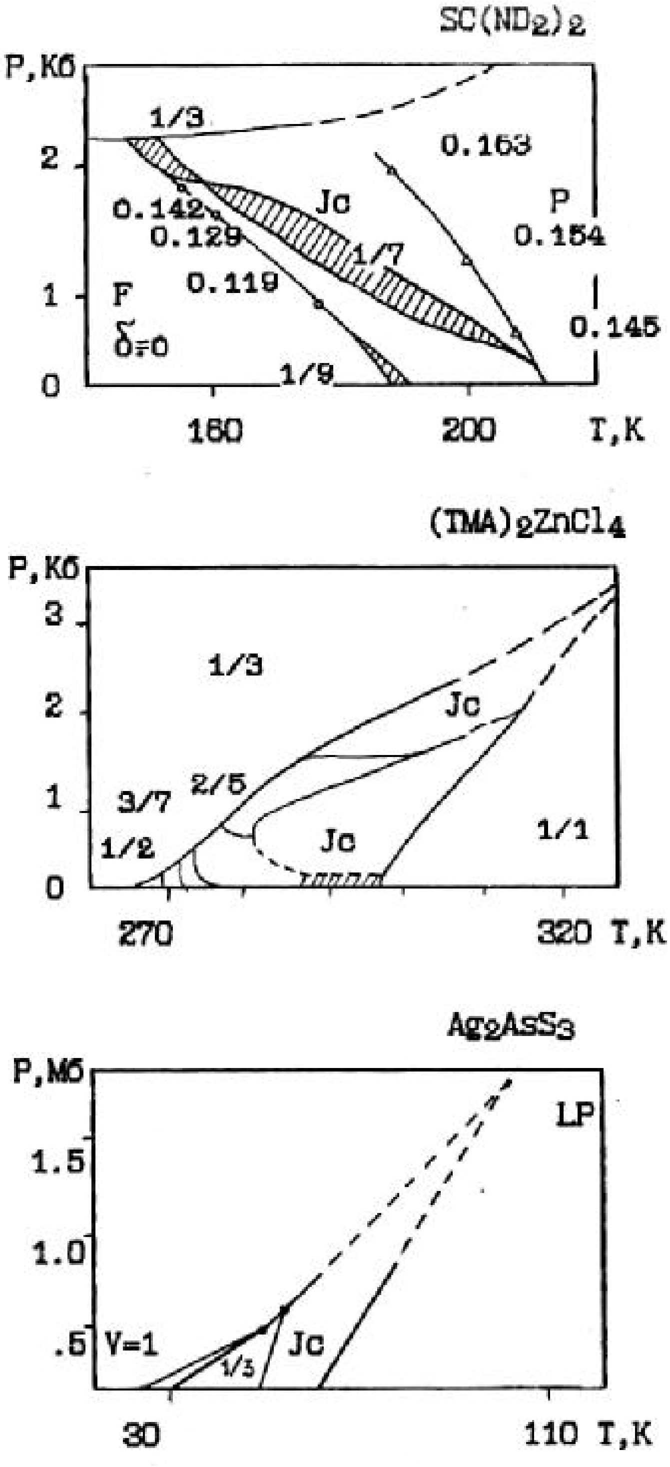

Figure 1.7. Phase diagrams of dielectrics: a) thiourea; b) $(TMA)_2ZnCl_4$; c) proustite.

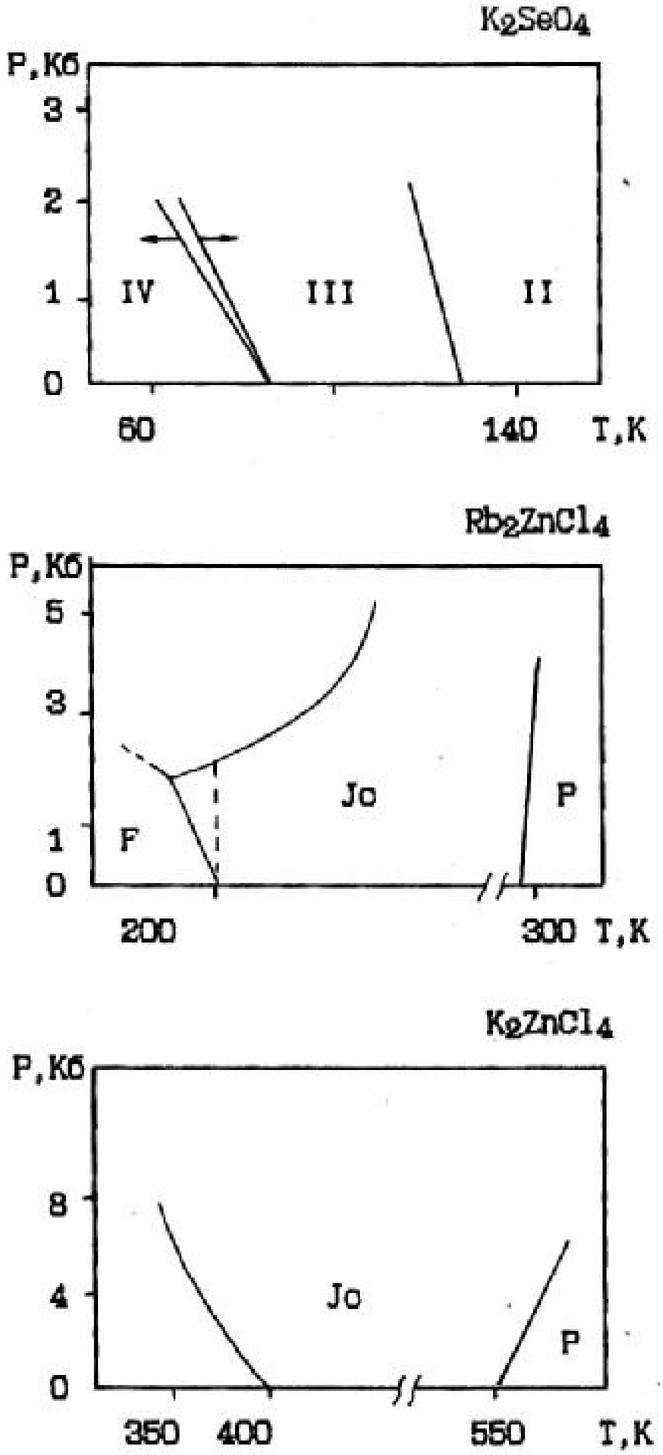

Figure 1.8. P-T phase diagrams of compounds A_2BX_4 obtained by -measurements.

continuous semiclassical theory Dzyaloshinsky-Landau, whereas non-classical type theory Izinga indicate the behavior of complex or simple type "devil's staircase".

Because NQR method, in many cases allows a quantitative interpretation of the structural and dynamic transformations near phase transitions, as well as to feel a slight change in the local structural environment of the quadrupole probe subsystem of the crystal, there is a strong, virtually confirmed the reasons for its use in the study of the subject systems. Even the simplest information to monitor changes in multiplicity intensity and width NQR lines contains important information about changes in the crystal structure and chemical environment, the nature of phase transitions and spin dynamics. More detailed studies, such as the study of the frequency dependences of ν (T), I (T), uv (T) and the change of the relaxation times T_Q T_{Q1} and $T_{Q2,}$ and others, allows to draw conclusions

about the type and nature of the motion of molecular segments or electronic excitations directions of chemical bonds, etc. The advantage of NMR NQR before the winner is sensitivity at high frequencies >10 MHz, where exactly are the NQR frequency halogen nucleus belonging to the majority of the members of the family $A_2BX_{4.}$ Furthermore NQR has the advantage of relative simplicity of the experimental formulation, especially at high hydrostatic pressure. This simplification, however, made up for the back while trying to implement a tribute to the experimental data in the options atomic motions as a microscopic theory of the quadrupole relaxation is based on the specific solid model and crystal chemical bond theory, which, as you know, in these compounds, only beginning to be developed. NQR advantage before EPR - not violated local electronic environment of the matrix.

Tetrahedral or close to the structure of segments BX_4 not densely packed β-K_2SO_4, leads us to expect the possibility of significant local and collective distortion when the external parameters. And it can be assumed that with the NQR method should be obtained valuable, in terms of solid state physics and phase transitions, information. Experimental task in the first stage is a generalized phase diagram β-$K_2SO_{4.}$ On the other hand one can study the structure of the electronic environment of the nucleus - a task more difficult and laborious, and most successfully solved in the presence of all primary data from NQR, NMR and diffraction methods for all compounds of group A_2BX_4 structure β-$K_2SO_{4.}$

We have formulated the following research areas:

1) Controlled diffraction and NQR synthesis of compounds A_2BX_4 major cations and anions (A = $NH_{4,}$ Cs; B = J), near the border the crystal structure stability β-$K_2SO_{4,}$ to detect them with this structure sequence of phase transitions involving incommensurate phase.

2) Application of the method of NQR under high pressure to determine the domains of existence of the structural evolution of J_O phase in Rb_2ZnBr_4 under high hydrostatic pressure. A more detailed study of the NQR (in combination with other methods) $Rb_2ZnBr_{4,}$ to find in this connection behavior such as "devil's staircase" or long-period structures.

3) Explanation of the reasons for the unsatisfactory description of the forms of radio frequency absorption lines in the incommensurate phase of $Rb_2ZnBr_{4.}$

In preliminary studies, after setting growth compounds A_2BX_4 with major ions and detection in a number of these structures β-$K_2SO_{4,}$ scheduled tasks were also associated with an additional question:

4) Assessment of the degree of spin-phonon, spin-spin dynamics in the synthesized compounds.

Chapter 2. Equipment and measurement technique.

§ 2.1. Receiver sensitivity sensor NQR and conditions optimum adaptation to the measuring chamber.

As is known, the sensitivity of the receiving path to radio spectrometer NQR absorption signals defined set of parameters [27]. Thus, according to the survey [64], S / N ratio of the signal to noise ratio at the receiver output can be represented as:

$$S/N=\frac{\alpha NQ\xi r^{2}}{\sqrt{4kB)QN^{2}\nu_{0}T_{r}\sqrt{r+R_{ecv}T_{ecv}}}} \qquad (2.1)$$

where a - nuclear spin contribution, N and r - the number of turns and the radius of the solenoid, Q - Q-factor of the receiver coil, B - receiver bandwidth, T_c - temperature of the resonator, ξ - the filling factor of the resonator, R_{eq} T_{eq} - equivalent resistance and temperature receiver, ν_o - quadrupole resonance frequency.

In this section we will carry out examination of the conditions that must be considered when designing NQR cameras to increase the quality factor of the receiving circuit. As is known, this value is limited by the condition $Q < 1{,}5\nu_o\tau_{im}$ where τ_{im} - lifetime free induction signal. In NQR typically Q <150. However, the location of the sensor in the NQR shell, which is a body of a device external influence on the sample, the Q value is significantly reduced due impendansnoy sensor communication with the shell of the device. This relationship can be expressed as follows [65]:

$$Q=\frac{\nu W}{P} \qquad (2.2)$$

where W - energy stored in the resonator, P-power loss associated in particular with the dissipation of energy in the environment of the resonator. To calculate the losses it is necessary to estimate the energy W. As we know the energy of interaction between two conductors is expressed through the inductive factor **L_{12}**

$$W_p=\frac{1}{8\pi}\int\left(\vec{H}\,\vec{B}\right)dV \sim \frac{L_{12}J_1J_2}{c^2} \qquad (2.3)$$

where J - volume currents. In case the interaction of the solenoid (radius **r** and length **l(l)**) with a cylindrical shell (radius **R**, the length **L** and the thickness **H**) according to [66] has an analytical expression:

$$L_{1/2}=\sum_{k-1}^{N}\int_{0}\int_{-1/2}\frac{r(R+H/2)\cos\varphi\, d\varphi\, dL}{\sqrt{\left(\frac{L-1+1/N}{2}-k\frac{1}{N}\right)^{2}+\left(R+\frac{H}{2}\right)^{2}+r^{2}+2\left(R+\frac{H}{2}\right)r\cos\varphi}} \qquad (2.4)$$

where **N** - number of coil turns, **φ** - polar angle. Integral in the general case is calculated numerically, but **L** → ∞ is expressed in terms of elliptic functions. In the frequency range (**ωR**<c) can be obtained for the magnitude **P** loss following expression [65]:

$$\frac{\partial W}{\partial t} = P \ : \ \frac{\pi^2}{\sqrt{\sigma}}\left(\frac{r^2\mu n\omega J_0}{c^2}\right)^2 + \ldots \qquad (R>r) \qquad (2.5)$$

where (**μ** and ***б*** - magnetic permeability and conductivity of the shell, and take into account the higher-order bias currents, giving an increasing contribution at **ωR** = c.

Knowing the energy of a cylindrical solenoid [65]

$$W = \frac{2\pi r^2 nJl}{c^2}\left(1 - \frac{8r}{3\pi l} + \ldots\right) \qquad (2.6)$$

we can evaluate how the cavity **Q** depends on some dimensional parameters:

$$Q \ : \ \frac{2l\sqrt{\sigma}}{\pi r^2\mu\omega^2}\left(1 - \frac{8r}{3\pi l} + \ldots\right) \quad (\text{With } R> r) \qquad (2.7)$$

For high frequencies (in this case more than 10^8Hz) observed other addiction [66, 67].

The estimates show, in particular, that the **Q** value decreases with the increase of the radius **r** of the solenoid proportional to its square. Midrange in losses will contribute as part of the capacitive impedance of the system.

Returning to the value of the ratio of school, we can see that from the point of view of the geometry of the coil placed in the shell, school increases with the radius and the length of **S/N** ≈ $\mathbf{r}\sqrt{\mathbf{l}}$. However, the length of the **L** shell in the real world is always limited and decreasing **L – 1(l)** will increase energy leakage near the ends of the solenoid [67]. Therefore, we can assume that when choosing some optimal geometric relationships between the dimensions of the shell and coil, SN ratio can be increased by increasing the radius of the coil. Expression (2.7) is rather illustrative indication to select geometry and material characteristics of external consoles NQR. In our case, this is due to the fact that a large part of the diapason of frequencies used, is in a quasi-stationary region field (**ωR** ≈ c) (the mids). Therefore, prior to making the designs consoles external influence, we chose the optimal geometry by measuring the quality factor resonators NQR directly on layouts and finished products.

It was established experimentally that SN ratio increases with increasing radius of the receiver of the NQR sensor up to a value which is approximately half the size of the internal outer shell. The magnitude of the energy loss depends on the magnetic and conductive properties of materials. As shown in [68] and it follows from (2.5), a conductive shell for high frequency loss value decreases with increasing the conductivity of the shell. In the case of dielectric shells made loss due to the bias currents, and increase with frequency. The magnitude of dielectric loss is essentially independent of the geometry of the shell.

These principles have been taken into account in the design world and improve termopristavok NQR for research and used in the development and manufacture of high-pressure chamber with increased sensitivity to signals NQR (see § 2.2 and 2.4).

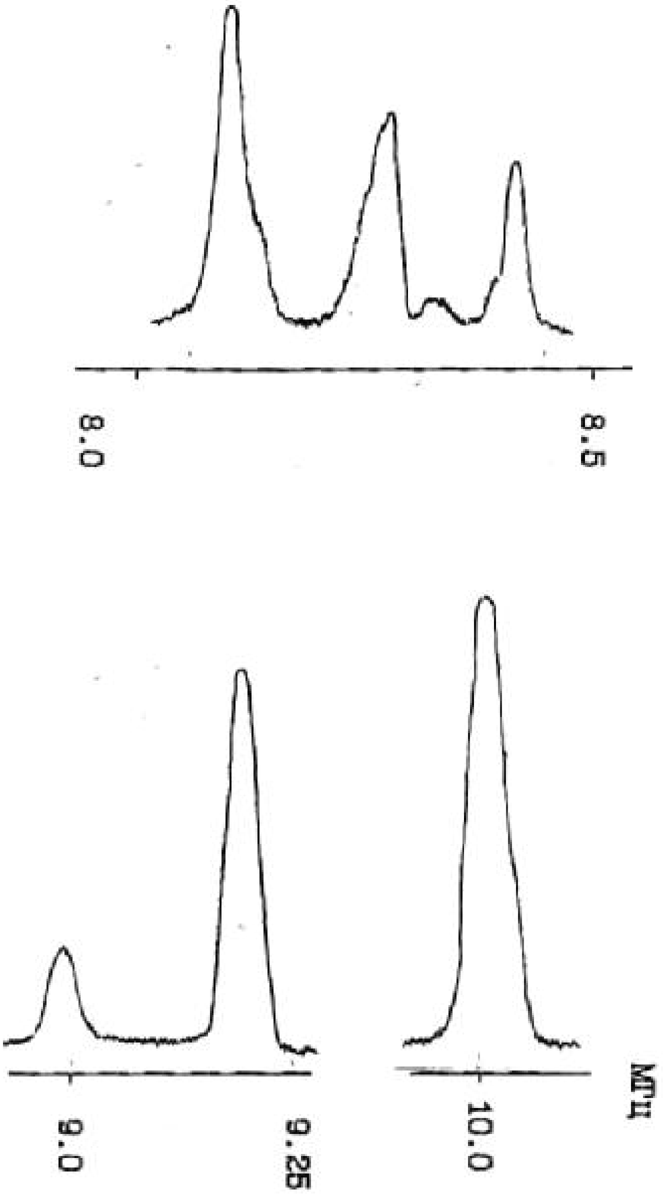

Figure 2.1. NQR spectrum ^{35}C1 in K_2ZnCl_4 at room temperature

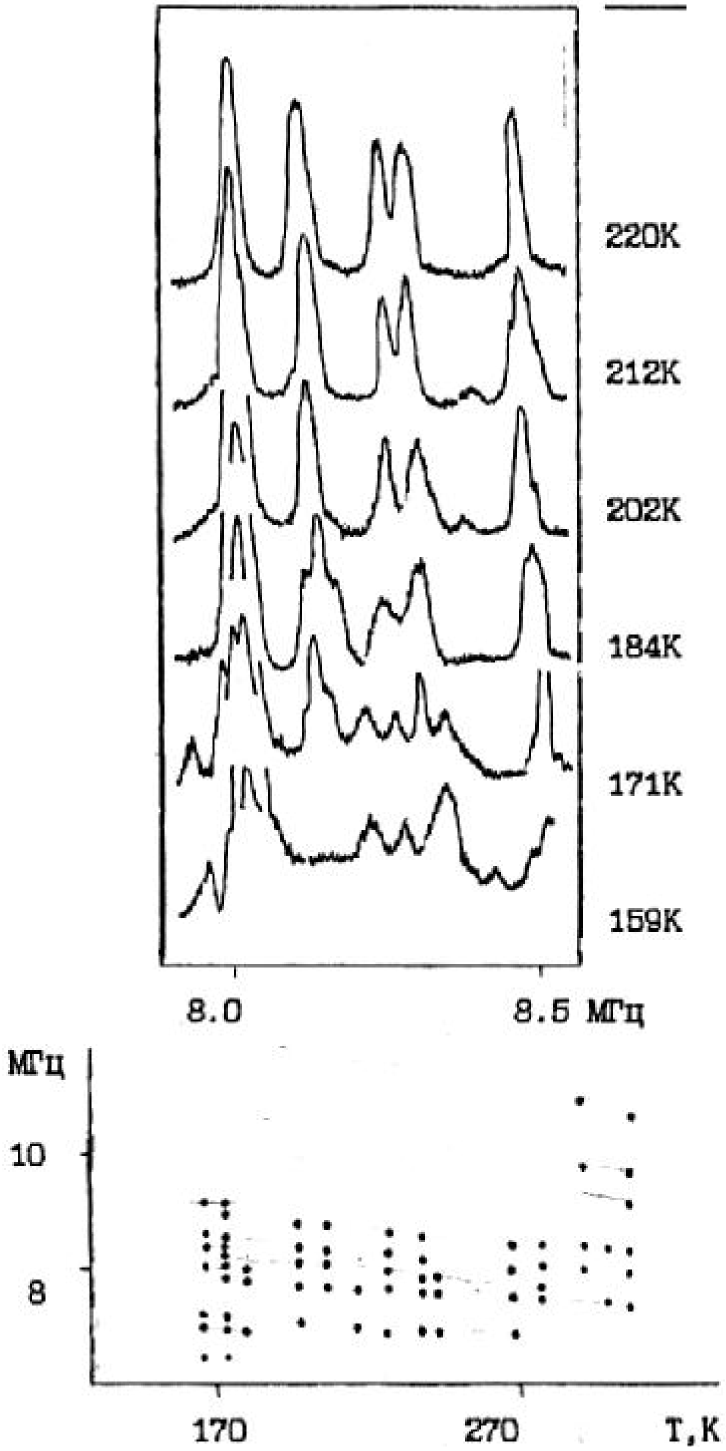

Figure 2.2. The temperature dependence of NQR spectrum and in K_2ZnCl_4 in the range of 8-8.5 MHz.

Originally optimal matching method (OM) was tested at check NQR signals from nucleus $^{37}C1$ and $^{35}C1$ compound K_2ZnCl_4 with a structure of β-K_2SO_4. This compound was initially investigated by the NQR spectrometer superregenerativnogo type in a chemistry lab minerals Klaytona sity, Australia, Scaife [44]. At ambient temperature was revealed six signals from nucleus $^{35}C1$, in the frequency domain with 8-10MHz ratio S/N = 6--12 units. At liquid nitrogen temperature signals are absent. Later, at the Institute of Materials Attica, NQR in K_2ZnCl_4 found three
phase transition at $T_i = 553K$, $T_{C1} = 403K$ and $T_{C2} = 145K$ [37]. When this was recorded only part of the full spectrum of ^{35}Cl NQR near 560K and below 290K. Signal to noise ratio was in the range 0—12 units. The first attempt to study this connection, we noted only weak NQR signals at liquid nitrogen. Application of the method allowed us to fix the OS full NQR spectrum (Figure 2.1) at room temperature (RT). S/N ratio was 10--25 units. In the frequency range 8,5-8,0 MHz NQR observed spectral lines are not marked in [37]. Fig. 2.2 shows the temperature variation of the NQR spectrum of K_2ZnCl_4 and the temperature dependence of the frequency $\nu(T)$. For high-frequency part of the spectrum at T = 290K, unlike us Milian observed broadened singlet absorption line NQR. At T = 173K observed anomaly associated with the redistribution of intensities and frequencies of the spectrum. Simultaneously with our measurements, different researchers using mutually complementary methods observed phase transition in this temperature range [69,70]. However, some significant variations in the temperature of this transition and reusability of data. As explained later, it was the result of significant non-equilibrium processes characteristic of this class of compounds I.

§ 2.2 The temperature set-top spectrometer for studying phase transitions.

Standard termopristavka ISS (ИСШ) spectrometer series, the fan with the principle of mixing the gaseous medium to equalize the temperature gradient on the sample did not meet the requirements of our traditional measurements. Its disadvantage is a) a high temperature gradient to 3 K/sm; b) a great time for temperature stabilization.

The design of the heat chamber, where the heat setting is performed by blowing coolant opposite directions two-way screw channels, Rout in the copper shell, also had drawbacks, the main one of which is a large factor of the inductive-capacitive sensor relationship with NQR.

To achieve the objectives of our research the author has developed and tested new thermal cameras. Figure 2.3 shows liquid heat chamber for research NQR. The basic idea inherent in the design of the thermal cameras, is the replacement of the gas on the liquid medium, providing better heat transfer properties. The main difference lies in the design hermetically sealed housing (3) place the sample location and input axis (4a) of the fan and removing conductive material from the NQR sensor (2). For this inner housing chamber (1) was made of PTFE with a sealing compound in removable input coils NQR. Liquid completely fills the entire volume of the chamber. Small evaporation silnoletuchih replenishes fluids communicating through PTFE hose (6) to maintain the system level. Temperature sensor (5) housed in a shielded casing away from the sample. At the bottom there was a heat chamber shielded stove (7), which was used in the auxiliary heating. The whole system was placed in a standard Dewar flask, made in the form of two communicating vessels.Changing the temperature and maintaining the nitrogen purge was

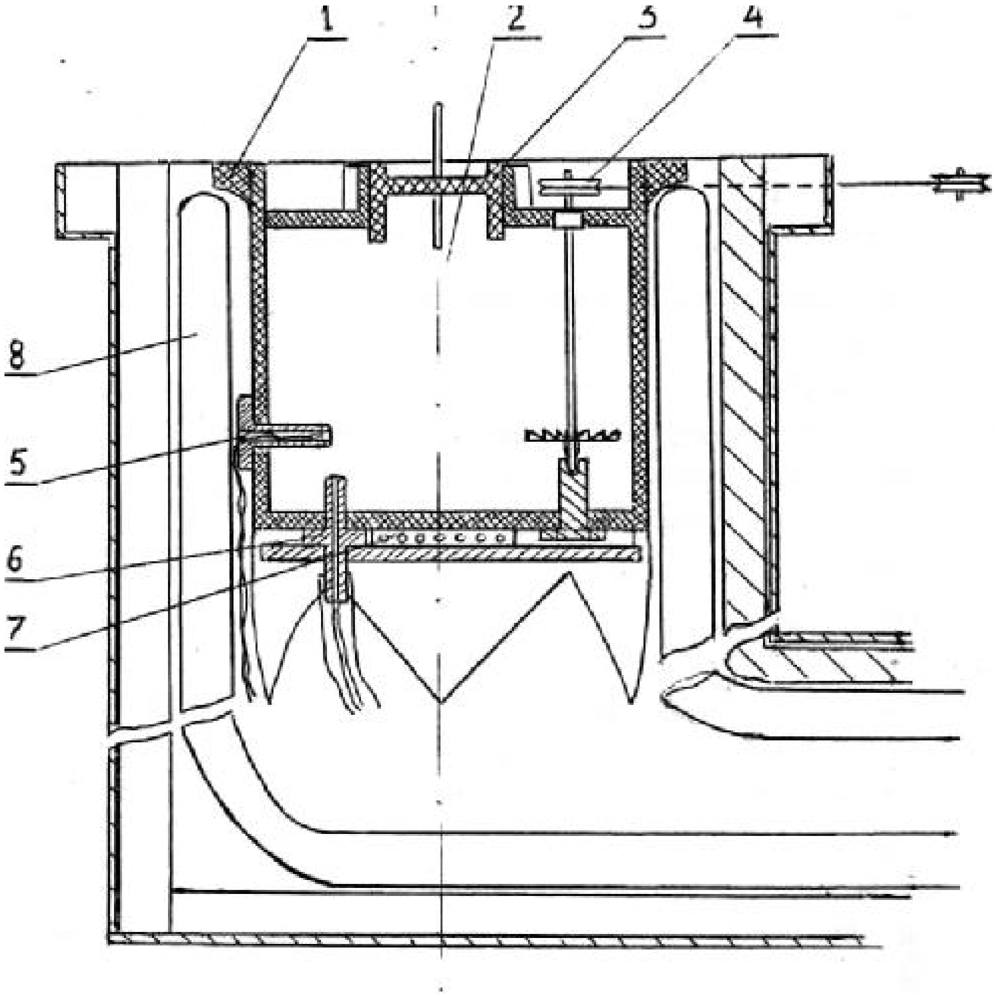

Figure 2.3. Liquid-gradient heat chamber for NQR Science.
1. The body; 2. NQR sensor; 3. Seal sensor; 4. The agitator; 5.termopara; 6. Platinum thermometer; 7. Heater; 8. Dewar.

carried out through a tube connected to the second portion dewar. As the refrigerants used n-pentane (liquid state region 138 <T <3208K) hexane, transformer, silicone oils, glycerol (T = 600K), and other inert liquid sample. The temperature gradient in the zone of the sample out (to 0.01 K/cm).

The disadvantage is the need to change the thermal cameras or olive liquid (which could be carried out during the measurements) in different temperature ranges. At temperatures below 140K (the crystallization point of pentane), its characteristics are deteriorated. To overcome these drawbacks, chamber design required improvements. The result has been designed, tested and used in the study of phase transitions in Cs_2ZnJ_4 and $(NH_4)_2ZnJ_4$ heat chamber shown in Figure 2.4. Its features is the use of an external circulation mode gas purge. In the first case the fluid circulates in the plane of the heat chamber (1) in the upper part of the conjugate through the sealing compound (d) directly to a bayonet flange gasket spectrometer (3). In the case of a gas purge gas (mixture) is blown through the lattice (4) promoting samoperemeshivaniyu hydrodynamic flows. Temperature range when running in automatic mode,determined by the characteristics of the circulation thermostat (for U-16 is 210K - 400K). Outside this range, additional stabilization of the temperature applied. The temperature gradient in the region of the sample out. Time alignment when the temperature gradient was from 2 to 10 minutes. In the gradient mode, the gas temperature at the sample was 0.1-0.2 /sm.

Minimum distance sensor NQR spectrometer to releasably nest and exclusion metallic structural elements described in thermo-console NQR allowed to achieve maximum inductive capacitive matching inductor NQR with alarm transmission paths ISSH spectrometer. Using the receiver coils with an increased (compared with standard) diameter (20 mm) allowed to increase the signal-to-noise ratio (S/N) 5-8 times.

§ 2.3 Synthesis of samples.

Most of the compounds A_2BX_4 used in our experiments, was grown in the laboratory of the Institute of Physics of crystals. L.V.Kirenskogo AS RU. From aqueous solutions of crystals grown V.A.Grankinoy. Bridzhmen method of melt compounds synthesized to I.T.Kokov. Connection Cs_2ZnJ_4, $(NH_4)_2ZnJ_4$ and others for NQR studies were synthesized by the author.

During crystallization from solution, the deviation from the stoichiometric ratio of the starting chemical components AX and BX_2 was chosen empirically, taking into account their degree of hydration. The composition of the samples was identified based on the reference [71] and periodic data [72, 73, etc.].

Connection of A_2BX_4 (K_2ZnCl_4, Rb_2ZnBr_4, Cs_2ZnJ_4, Cs_2CdJ_4,$(NH_4)_2ZnJ_4$) usually crystallized in the form of single-crystal plate splices up to 40mm and a thickness of 5mm . Were synthesized as large single crystals. compounds of other compositions (A_2BX_5, ABX_3, etc.) have had other forms of habit. Some samples of A_2BX_4 to remove impurities, subjected to repeated recrystallization (Rb_2ZnBr_4. Cs_2ZnJ_4). Polycrystalline, blocky or monobloc crystals (Cs_2CdJ_4, $(NH_4)_2ZnJ_4$ were prepared from the melt.

Due to the difficulties in carrying out the exact chemical analysis (which was carried out with precision 2%. only for Rb_2ZnBr_4), the degree of purity of samples was evaluated by the criteria proposed by Hamano [52,72]. According to the cited studies, the magnitude of the concentration of impurities in the compounds Rb_2ZnCl_4 and Rb_2ZnBr_4, significantly

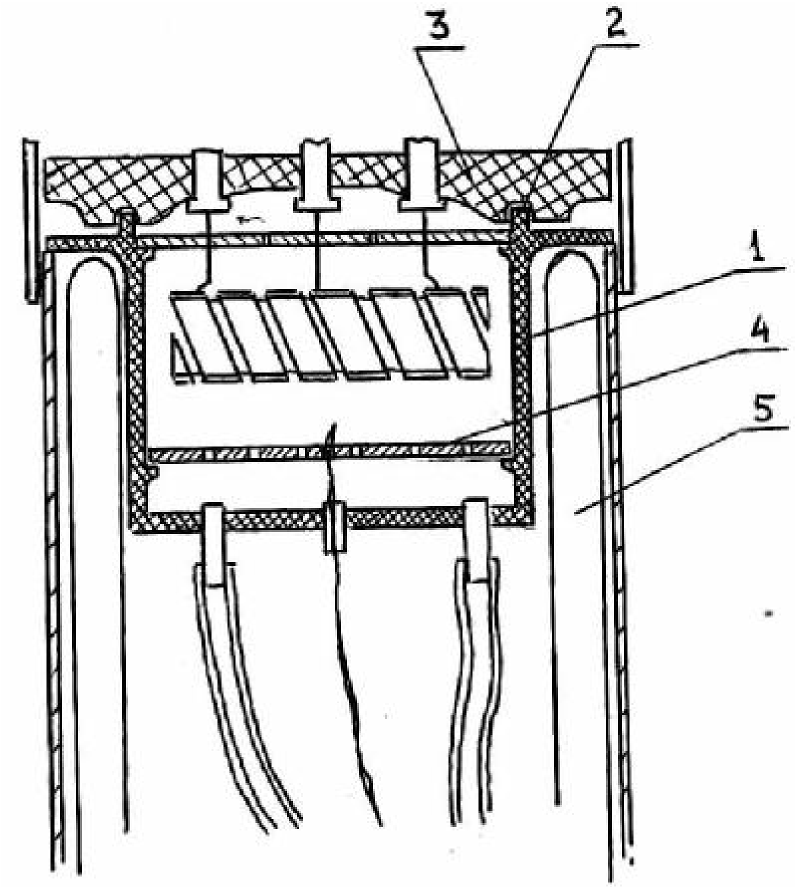

Figure 2.4. Gas-liquid heat chamber NQR :. 1. The body; 2. Sealing compound; 3. Flange spectrometer; 4. Grille; 5. Thermal insulation casing; 6. Thermocouple.

affects the amount of thermal hysteresis of the phase transition at T_C ferroelectric phase, as well as on-time behavior quadrupole spin-lattice relaxation time T_{1Q}. For undoped samples hysteresis decreases significantly and there is racing For example, for the compound , where in hysteresis phenomena are significantly dependent on the concentration of impurities, the amount of thermal hysteresis $\Delta T = T_C^c - T_C^h$ samples from various stages of crystallization in this case was 8 -- 3 K.

An additional criterion was the degree of purity of the NQR spectral linewidth in the ordered phase. For the most thoroughly homogeneous width of the synthesized compounds were sintletnyh lines 100-90 kHz.

§ 2.4 Apparatus for NQR studies under high hydrostatic pressure.

Since 1972 year, the Institute of Physics L.V.Kirenskogo USSR Academy Krasnoyarsk Serebrennikov V.L. and Moskalev A.K., [74,75] developed a high-pressure apparatus applied to radiospectroscopic methods. Such equipment, including the need to study phase P-T diagrams of dielectric crystals. Particularly relevant is the use of this instrument for the study of disordered structures neglected, what are incommensurate phases. Detailed description of the devices and technology of high pressure is presented in the monograph [74]. In this section we present the basic principles of experimental and some technical details on which created a new and improved traditional experimental setup.

Typical complex laboratory equipment used in research of structural phase transitions in crystals NQR, including at high hydrostatic pressure is shown in Figure 2.5. It consists of the following components: 1) spectrometer NQR 2) changes in the system, control and maintain the temperature and pressure (SIKPD).

The main units SIKPD are high-pressure chamber (1), the multiplier (8), a pumping station (9), Electronic Stability and pressure measurement (10). High pressure (HPC) is in direct mechanical contact with flange-receiving slot of the spectrometer transmission unit in a heat-insulating and shock-proof housing. At its bottom, a bomb attached to a multiplier, in which the working chamber through the oil passages (12) from the pump station (9) Hydraulic oil is supplied. End transmits pressure to the piston first multiplier, and further through the piston is created pressure buildup in the medium surrounding the sample (as the medium used hydrostatic pentane mixture with the transformer oil.) The temperature and pressure of the liquid around the sample were measured respectively copper-constantan thermocouple and manganin gauges. Measurement and control of temperature and pressure using standard measuring circuit using potentiometers P309 and P363/Z and bridge resistors P39.

Thermal stabilization system consists of a cold finger (11), which passed the vapor stream of nitrogen, and the electronic device (4) with a system of heaters thermostabilizing elements of the system. At positive temperatures using liquid coolant, thermostabilizing circulator.

The study applied a few high pressure chambers In the high-temperature measurements were carried out in a cell made of a titanium alloy BT-6C [74,75]. At low temperatures and used camera HPC1 HPC2 made of beryllium bronze (BrB2).

Chamber HPC1 designed to operate over a wide range of pressures (up to 1,.5 GPa (= 1,5 Kbar)). Its design is presented in Figure 2.6. The camera body (1) has an outer

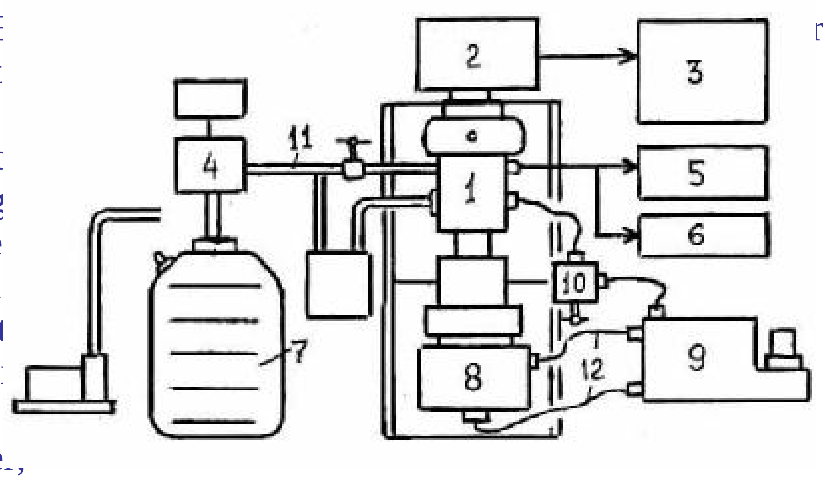

Figure 2.5. F ransitions NQR at
high hydrostat

1. Pressure c
2. Receiving
3. NQR spe
4. Electroni
5. Temperat
6. Pressure
7. Dewar;
8. Multiplie
9. Pumping station;
10. Device stabilization system pressure;
11. Thermal inputs;
12. Oil - input.

diameter of 80 mm. Inner through-channel (2) with a chamber diameter of 16 mm. At the top of the channel is the radio frequency coil NQR (3). Electrical inputs of coils are soldered to the bottom of the high-voltage electric inputs (4). Contact with the spectrometer unit provided top of the electric inputs. Recent resin-sealed channels ED-20 filler. One of the channels used for output

conductor pressure sensor and thermocouple. Coaxially receiving coil is a silver foil shield (5). Obturator with a set sealing bronze-copper-lead-rings (7) fixed bearing nut (8). The lower part of the HPC is installed on the multiplier. All parts of the camera heat treated to a hardness of 3540 units in the scale of HRC.

Usage tapered seal wiring impulse withstand voltage up to 2.5 kV at a pressure up to 10 kbar. Electric high capacity electric inputs was about 10 **p**F. Q factor specially manufactured receiver coils mounted in the chamber, was Q = 12¸ 18 units at 50 MHz Range interface receiving and transmitting paths of the spectrometer is within the 5¸ 6 MHz.

In the operation of the high temperature compartment HPC1 been ascertained that the quality factor of the NQR sensors in these cells is not sufficient for detailed studies in the field of spectra disproportionate phases. In addition, the presence of significant inductive coupling sensors with camera body, significantly restricted range of frequency matching paths spectrometer, in connection with which tracked a narrow frequency range of spectra and worse accuracy. Another disadvantage is imperfect system input sensors for measuring P-T parameters. Siting in the vicinity of high-voltage electric wires caused additional deterioration of merit and immunity NQR sensor and on the other hand, increased the high-frequency and capacitive crosstalk on themselves P-T sensors. Small amount of volume of the pressure medium, a high value of the residual pressure (about 0.4 kbar) after decreasing from larger values create more difficulty in the experimental work in the field below 0.6 kbar. To address these shortcomings, and in accordance with the task was developed and produced a new high-pressure chamber HPC2.

The design is presented in Figure 2.7 HPC2. The camera body (1) (external diameter 80mm) has an inner diameter of 40mm working where and placed RF NQR sensor (2).

The channel (3) for movement of the piston (4) has an enlarged diameter 20mm. By implementing the new design of the obturator (5) has been reduced to three times the length of high voltage electrodes (6). Diameter electric inputs for channels has been increased to 2,5 mm. Connection and sealing shutter with the camera body is provided with special mounting clips (7) with the counter buttress thread. Used in this type of seal chamber is specially designed by us for large diameter channels and is based on the hydraulic chamber through the mating of the parts bronze ring of triangular section (8).

To enter P-T sensors using an additional seal (9) located on the side of the camera. It is attached to the snap ring (10). The same ring is used to attach the nuts (11) sealing the capillary nozzle (12) through which the hydraulic fluid pumping work and message of the working volume of the chamber through the valve with atmospheric pressure.

Shielding PT sensors from inductive capacitive coupling coil NQR is achieved by installing a thin-walled silvered screen The screen is also used to reduce the inductive capacitive coupling coil with the camera body. Heat exchange with the coolant used two copper jacket (14) with single-sided spiral groove.

Under this design were manufactured receiving sensors up to 22mm diameter. Sensors electric inputs and coated with a layer of silver of about 1 micron. Q factor coils mounted

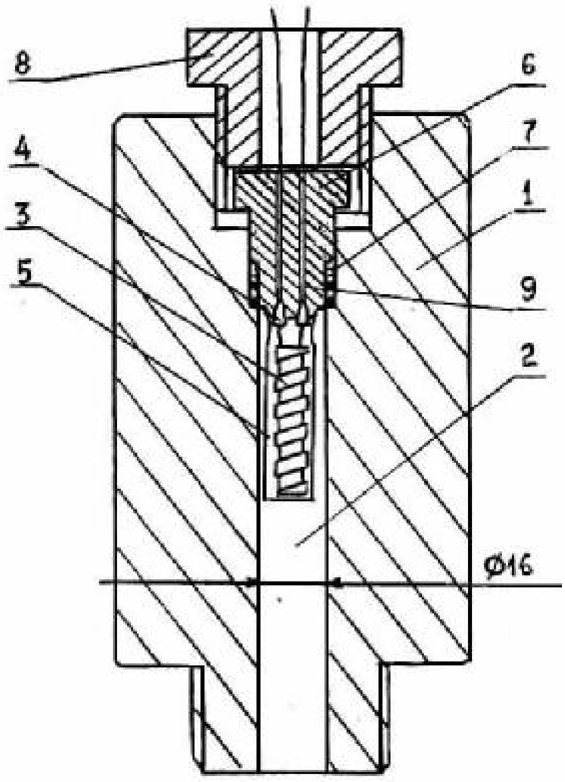

Figure 2.6. The design of high-pressure chamber (CHP1) for NQR study.

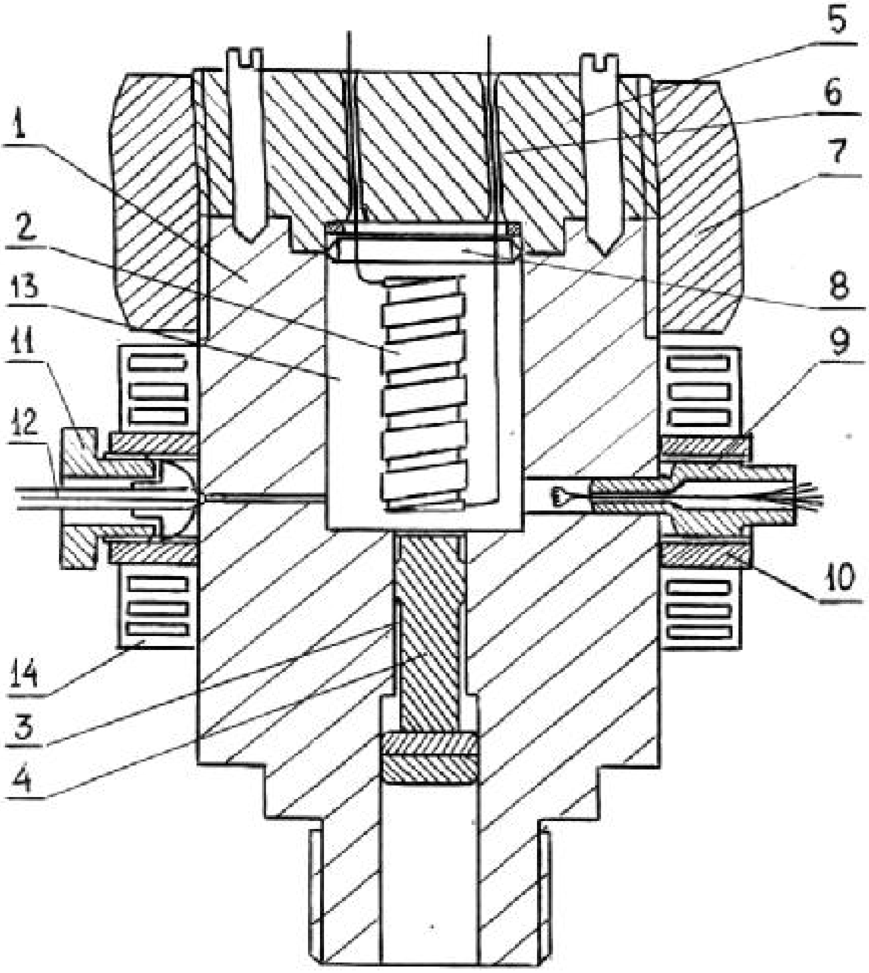

Figure 2.7.The design of high-pressure chamber (HPC2) with large inner diameter.

t 8¸ 10mm diameter - Q 80¸ 100 at diameters 20mm - Q » 60. The signal-to-noise ratio increased
o in HPC1.
nproved frequency-amplitude matching NQR sensors with alarm transmission paths spectrum.
ased to 12 MHz, which, in particular, has allowed further simultaneously capture NQR spectru
tion of the nucleus in the structure of Rb_2ZnBr_4.
equency measurement of the signal amplitude and the ratio S/N became comparable with its own st
cameras spectrometer (Table 2.1).

omparison of errors changes in temperature, pressure, frequency, and the signal/noise ratio under di
conditions.

alue s	T degree	bar	Frequency	Intensity	S/N for different frequencies	te
hamber	± 0.05	-	0.5±0.02%	»5%	100 ¸ 10	
		±100	1±3%	»50%	40 ¸ 0	
	± 0.5	±10	0.5±1%	25% ¸ 15%	80 ¸ 0	
	± 1	±200	2±3%	»80%	20 ¸ 0	

High-ressure hamber (
*

CHAPTER 3 The sequence of phase transitions in compounds A_2BX_4 (X = J).

In this chapter we provide experimental data (the study of phase transitions in the compounds of Cs_2CdJ_4 (CCJ); Cs_2ZnJ_4 (CZJ) and $(NH_4)_2ZnJ_4$; involving mutually complementary methods, the main of which is the NQR try organize and discuss these data.

NQR study sequence phase transitions in Cs_2CdJ_4.

Initially, the synthesis and study NQR ^{127}J compound Cs_2CdJ_4 were taken in 1983.laboratory IP SB AS USSR diplomnitsey Skripichnikova V.V. [76] under the leadership of A.K. Moskalyov In the available samples revealed the presence of two phase states, which were attributed to crystalline hydrates Cs_2CdJ_2-H_2O and the mixed state of Cs_2CdJ_4 + Cs_2CdJ_4-nH_2O. Get resilience nonhydrating connection failed, therefore the studies were limited supervision absorption signals NQR ^{127}J at 77 K and the temperature dependence of the dielectric constant e(T) and conductance G(T). By anomalies in the temperature dependence was assumed the existence of phase transitions at T^+_1 = 187K, T^+_2 = 207 K, T^+_3 = 231K with a temperature hysteresis ΔT »14K.

In 1986 year studies were continued in [139]. Crystals Cs_2CdJ_4 were grown from an aqueous solution by the Bridgman method. In studies of NQR ^{127}J for the transition (1/2« **3/2)** at a temperature of 77 K, we observed three NQR signal from the samples grown from solution. After annealing the samples at temperatures above 400K, was observed in all samples (at 77 K) 16 lines in the spectrum of the quadrupole resonance.

Studies have shown that under various conditions are realized two different crystal modifications of a substance Cs_2CdJ_4 - α and β. Modification of α - Cs_2CdJ_4 is stable in conditions of high humidity and changes in modification -Cs_2CdJ_4 under forced drying of samples, for example, after warming the crystal above 420K. When the thermally induced in the α-β transition was not observed decrease in the weight of the sample (within 2%) [77], and the NMR dataindicated the absence of crystalline bound water in the -modification (within 2%). On this basis it was concluded that the α-phase is a structural modification of the polymorphous compound Cd_2CsJ_4. β-modification is metastable and the storage of samples under conditions of high atmospheric humidity (h ³ 55%), during the hours £1-20 goes into α-form.

NQR studies were performed in the temperature range 77--450K using the optimal matching [78-81].

To a temperature of 130K were measured in liquid thermal chamber with temperature stabilization 0.1K. From the α-form was not observed any anomalies in the NQR temperature range studied. Temperature dependence of the frequency of β-Cs_2CdJ_4. presented in Figure 3.1. The data clearly indicate the existence of three phase transitions at T_{C1} = 335K; T_{C2} = 260 K and T_{C3} = 184K. In the high-temperature phase observed three spectral lines that usually characterizes the connection β-K_2SO_4-type structure and phase symmetry D^{16}2h (Pnma). However, above T_{C1} signals are detected only by the decay of free precession. At T_{C1} NQR signals disappear and reappear only in the vicinity of T_{C2}, where their spectral form is typical of the incommensurate structure. On this basis it was concluded that in the temperature range 335-260K has incommensurate phase. In the G1 phase observed four NQR signal approximately equal intensity. Phase transition from the phase Jc in the G1 phase accompanied by a slight temperature hysteresis 2K (see inset in Figure 3.1). When approaching T_{C3} intensity NQR lines from the G1 phase and decreases sharply below 184K appears 16 spectral lines, the intensity of which increases with decreasing temperature. At 77K all 16 lines have equal intensity. Thermal hysteresis in the transition G1 « G2 is absent and there is coexistence of phases G1 and G2 in the temperature range 2K.

From a modification in the temperature range from 390K to TCA-observed three NQR lines ^{127}J, marked on Figure 3.1 in broken lines. The ratio of the intensities of these lines 1:2:1. Stroke frequency (T) is linear with ¶n$_I$/¶T = 1,5*10^{-2} MHz /K, ¶n$_{II}$ /¶T = 1,18-10^{-2} MHz /K, ¶n$_{III}$ /¶T = 5,4*10^{-3} MHz /K. Relaxation measurements β-Cs_2CdJ_4 showed that phase P spin relaxation times are at the limit of time resolution and equipment up for T_{Q1} <50µs and T_{Q2}<10µs this phase NQR signals are recorded only by induction. NQR signals in the absence of phase Jc can be explained by a decrease in time T_{Q1} and T_{Q2} abroad temporal range of the spectrometer. In the G1 phase of the value of the spin-spin relaxation time $T_{Q2}{}^{3}$ 10µs.

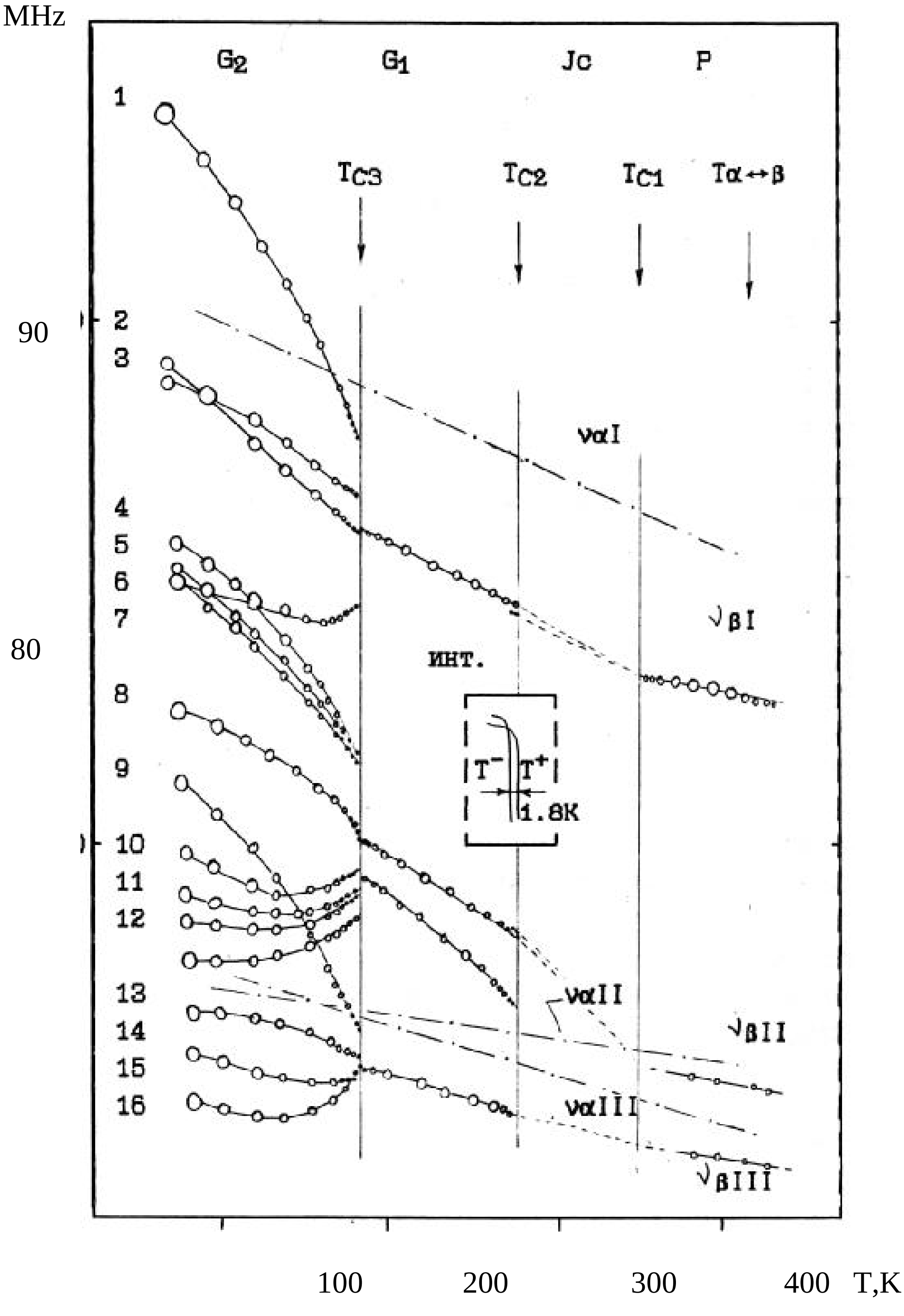

Figure 3.1.The temperature dependence of the NQR frequencies ^{127}J in Cs_2CdJ_4

This, along with a uniform contribution irregularities present contribution to NQR signals. However, the spin-lattice relaxation time is still below the threshold of measurement $T_{Q1}<50\mu s$. Figure the temperature dependence of the time T_{Q1} and T_{Q2} near $T_{C3.}$ With increasing temperature of the G2 phase is observed critical shortening of these times. In the absence of thermal hysteresis G2« G3 and observation of phase coexistence in a narrow neighborhood of $T\text{-}T_{C3} \approx> 2K$, it was assumed that the phase transition T_{C3} is close to the tricritical point. Phase transitions of β-modification were also investigated methods us colorimetry, electro-optics [78.139].

According to X-ray diffraction data given NQR sequence was established as follows symmetry transformation [79]:

Pnma (Z=4) « Jc « $P2_1/n$ (Z=4) « $P\bar{1}$(Z=8)

In the phase system was found Jc incommensurate satellite reflections with $\mathbf{q}_d$ varying from 0,25***** to 0,24***** with decreasing temperature [78].

α -modification of the Cs_2CdJ_4 was identitsirovana Center structure $P2_1/m$ (Z=2). Thus NQR relaxation measurements indicate its dynamic stability (T_{Q1}=>1ms, T_{Q2}>200s) compared to -form.

§ 3.2 Study the sequence of phase transitions in Cs_2ZnJ_4 NQR ^{127}J.

Initial data on the study compound Cs_2ZnJ_4 NQR presented in [45]. Continuous method at room temperature observed three rezonananyh absorption signal from the nucleus of ^{127}J and only one absorption line at temperature of 77K.

In 1988, the compound Cs_2ZnJ_4 originally synthesized and studied by NQR author, and then were held and more comprehensive studies [78-82,138].

Cs_2ZnJ_4 crystals grown from ZnJ_4 aqueous solution at 313K. According to our diffraction studies, at this temperature, the compound has an orthorhombic structure with space group symmetry Pnma-Dah^{16}. NQR spectra were recorded by the optimal matching in gas-liquid heat chamber in the temperature range 77 400 K. At room temperature (RT) at the transition 1/2« 3/2 nucleus ^{127}J observed three absorption lines at the frequencies8.87; 75.50; and 72.75 MHz with an intensity ratio other than the ratio of 1:1:2 (the latter position should reflect symmetry nucleus ^{127}J at positions I, II, III and (III ') structure Pnma). Fixed ratio of intensities and frequencies, but different from that registered by super regenerative NQR [45]. At 77, we observed eight singlet spin-echo signals and three NQR signal decay of free precession (MTP). One of the precession signal whose intensity was greatest, was close to a single frequency signal is observed at TCA [45].

In a wide range from 120 to 400 K the temperature dependence of high-frequency components of the spectrum is linear with $d\nu_I/dT = 5,87*10\text{-}^{2}$; $d\nu_{II}/d\nu = 1,51*10^{-2}$ $d\nu_{III}/dT = 1,19*10^{-2}$ MHz/K. Below 120 K the temperature dependence of the NQR frequency spectrum and its multiplicity change (Figure 3.3, 3.4). At a temperature T_i = 118K the first phase transition is observed, which is fixed on the anomalous behavior of the spectra shape Figure 3.4 and 3.5, and the spin-spin T_{Q2} and the spin-lattice relaxation time T_{Q1} nucleus iodine Figure 3.7.

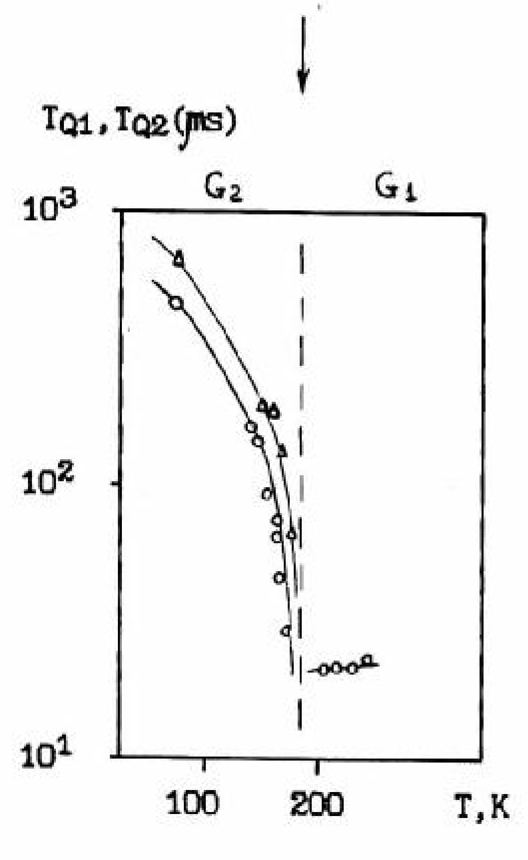

D- T_{Q1} ; O - T_{Q2}

Fig. 3.2. Temperature dependence of the time T_{Q1} and T_{Q2} of the quadrupole relaxation of ^{127}J in Cs_2ZnJ_4

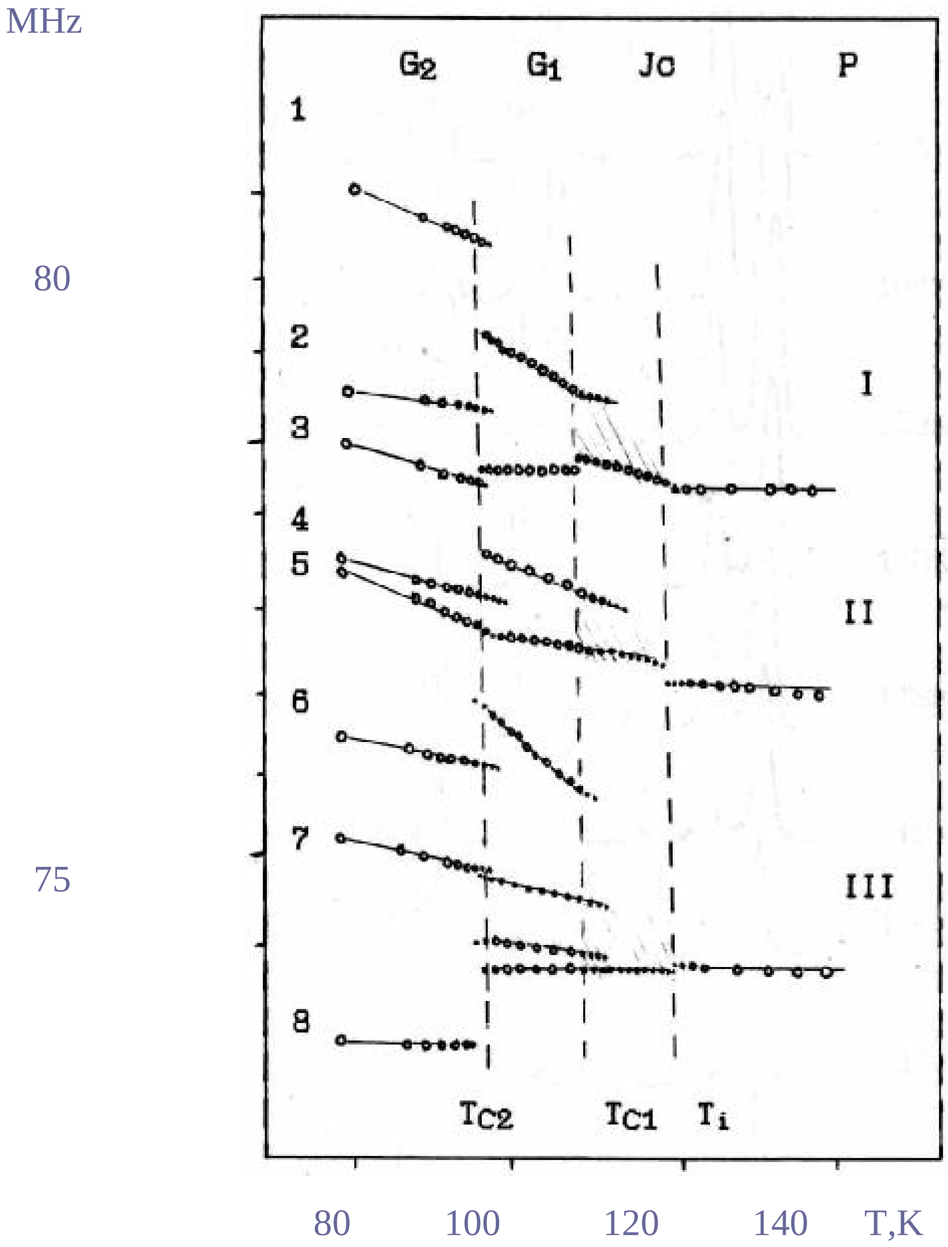

Fig. 3.3. The temperature dependence of the NQR frequencies in the ^{127}J in Cs_2ZnJ_4

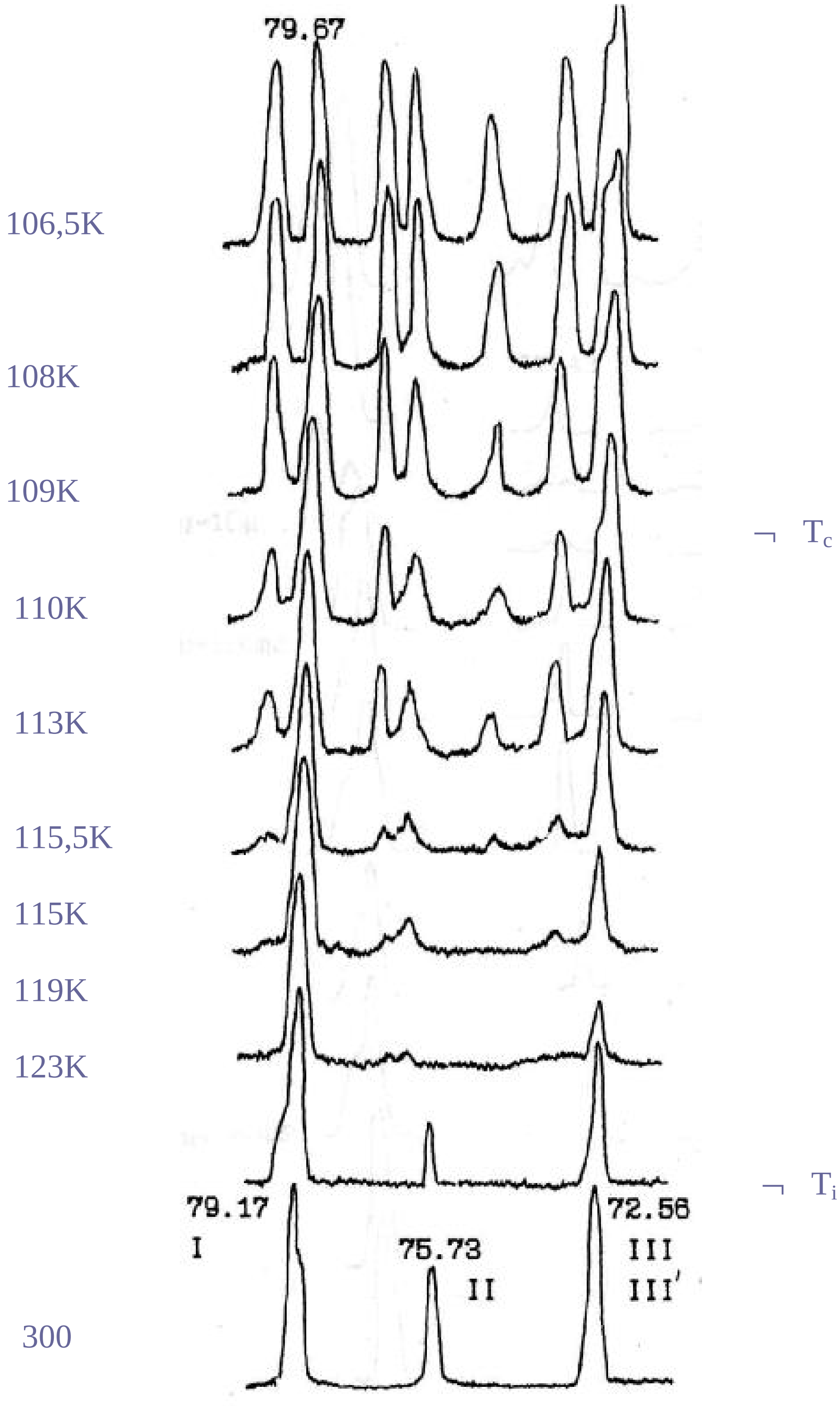

Figure 3.4. Type ^{127}J NQR spectrum of Cs_2ZnJ_4 near T_i

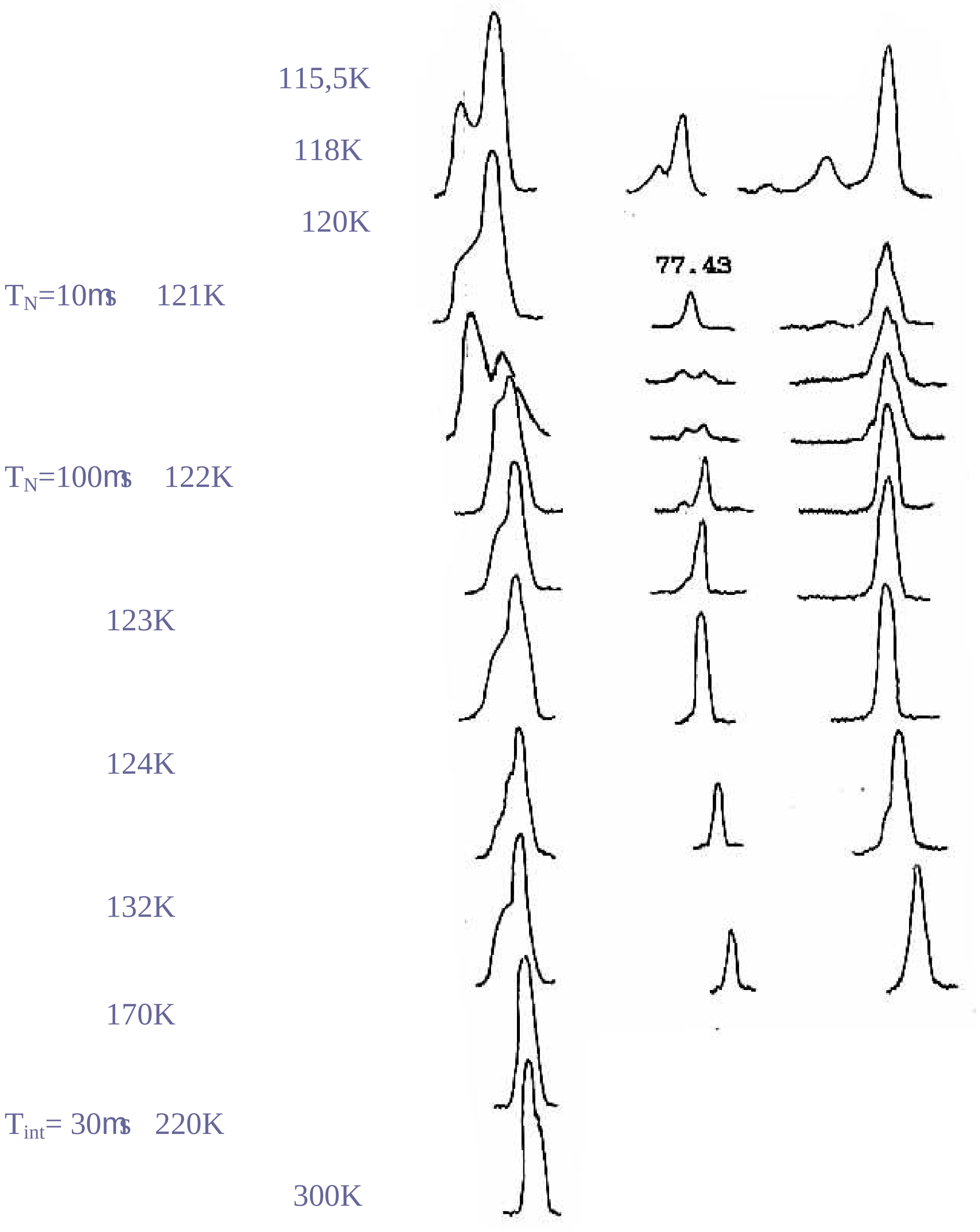

Figure 3.4. Type ^{127}J NQR spectrum of Cs_2ZnJ_4 near T_i

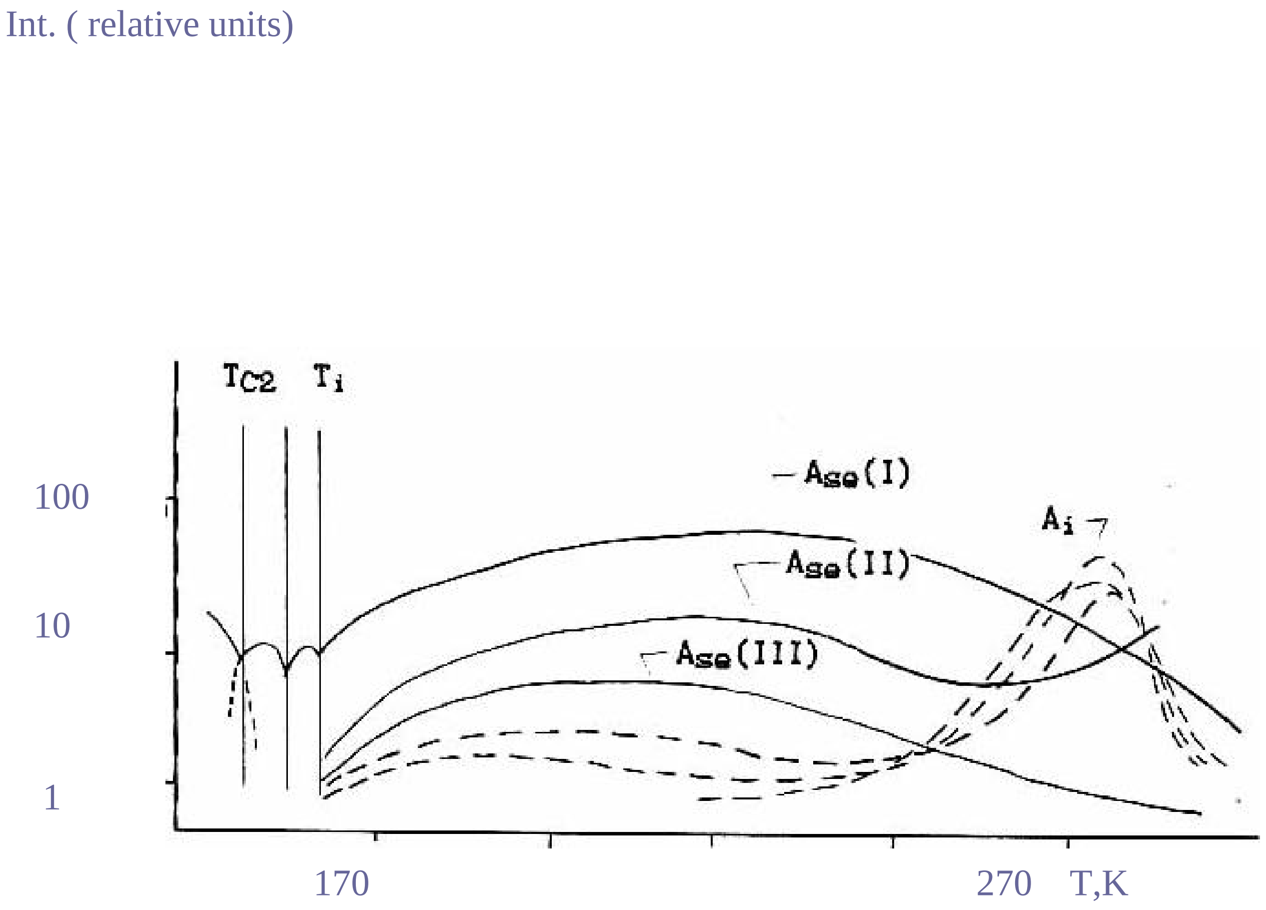

Figure 3.6. Changing the signal amplitude of the spin-echo (A$_{se}$ and induction (A$_i$ on the temperature at some parameters of the pulse setting.

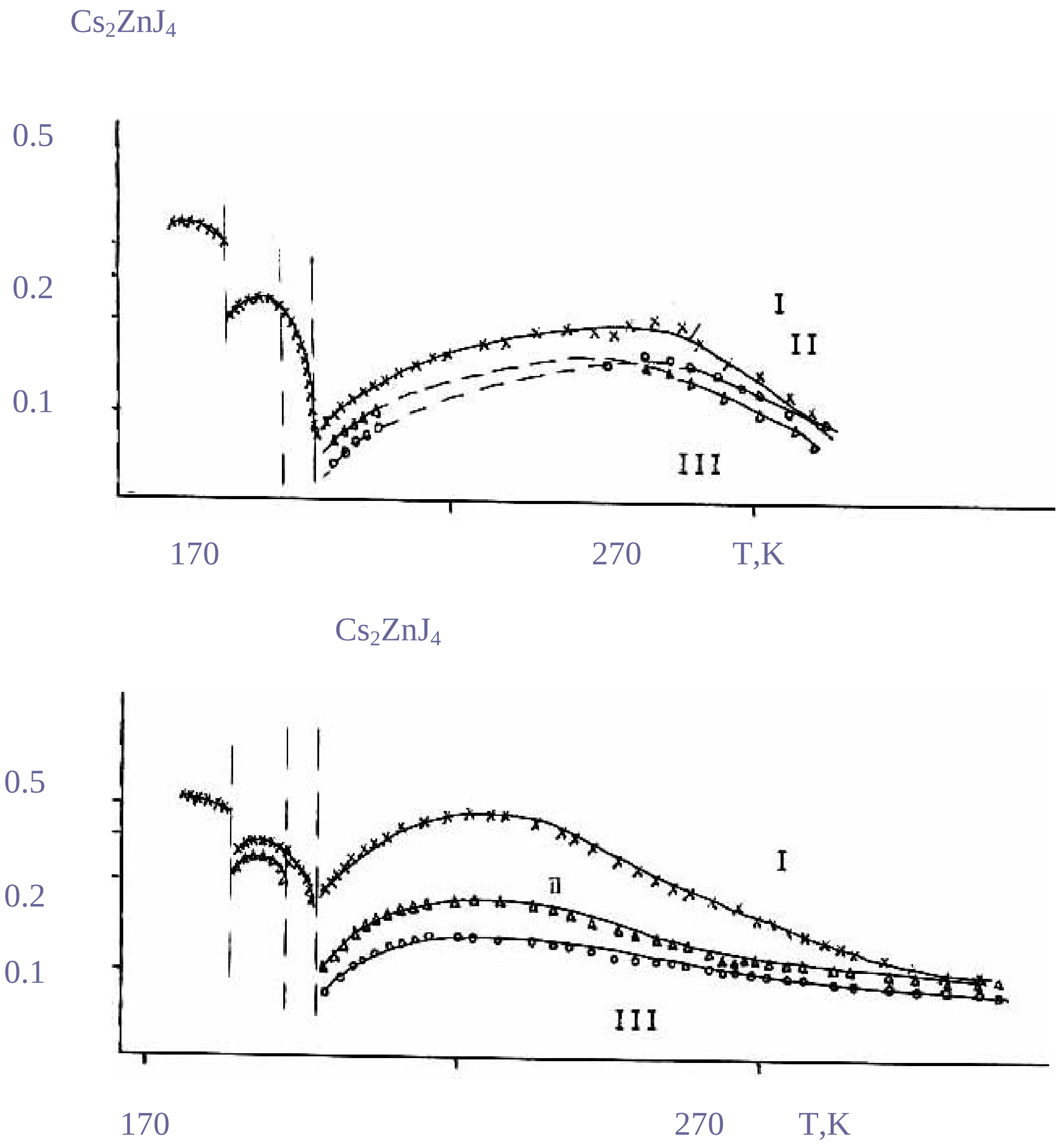

Fig.3.7. Temperature dependence of the time T_{Q1} and T_{Q2} cpinovoy relaxation in Cs_2ZnJ_4

As we approach the T_i peak intensity of the lines decreases (Figure 3.6) **I** have high-frequency component of the spectrum, long before $T_{i,}$ there is a marked asymmetry of shape. For the other two lines of the spectrum asymmetry is observed at lower temperatures. When passing the phase transition diminishes the intensity of lines in the field of asymmetric wing, a new spectral component. The change in the spectrum can be interpreted and register as the existence of three closely spaced components whose frequencies are continuously follow through $T_{i.}$ Below 118K spectrum shape is typical for the incommensurate phase (Figure 3.5). It should be noted that the optimal matching method for the first time were able to observe the full range of NQR in incommensurate phase tsezevogo compound ($Cs_2BX_{4)}$ with iskhodnoi structure Pnma. The advantage of the optimal matching can be demonstrated by comparison with similar measurements [87,88], where T_i near signals are not observed. The hysteresis transition at $T_{i,}$ the peak intensity changes along lines I, I and III, no.

Although continuum frequency distribution, limited terminal peaks typical of the NQR spectrum of the incommensurate phase in the temperature dependence of the line shape, there are significant deviation from existing models [34]. Directly below T_i less intensity "singularity" of the spectrum is very blurred and far from the form predicted by the model. However, with decreasing temperature, shrinks to a spectrum intensity corresponding to a peak that becomes pronounced in the middle well disproportionate phase. Line III below T_i is split into two strongly overlapped continual distribution, one of which is weaker in intensity. High-frequency part of this distribution appears above the noise level only in the middle temperature range nesoraamernoy phase.

As the temperature decreases, the sharp change in intensities (Figure 3.6), and notes the jump frequencies, at least the line at frequency 80MHz, tilting frequency dependencies, well fixed phase transition Jc« G1 at T_{C1} =108K. This behavior is also not consistent *with the* model [34], where the frequency of boundary singularities continuously converted into singlet line low-temperature phase. In the G1 phase, we observed eight ravnointensivnyh NQR lines. Hysteresis transition at T_{C1} about 3K. In addition to the continuing progress of the frequency spectrum of the line III in the G1 phase at temperatures of 96-105K at a frequency of 73.6 MHz observed Intense induction signal that accompanies the bass line NQR in this phase, fixed by the spin-echo signal. According to our data here, as in Rb_2ZnBr_4 observed cross-relaxation resonant excitation of a certain level of connectivity Cs_2ZnJ_4 within the contour line of the low-frequency phase G1.

At 96K observed a pronounced phase transition G1 « G2. with the number of lines in the spectrum does not change, change their frequency. Observed phase coexistence. Hysteresis transition is absent. Coexistence region depends on the quality of the samples and for the more perfect crystals is »2K.

Temperature dependence of time and T_{Q1} and T_{Q1}, measured by the resonant response of the absorption of iodine nuclei in positions I and III of the crystal structure of tetra cesium iodine zincate indicates existence of a critical slowing down at T ® $T_{i.}$ In this case directly with $T_{i,}$ due to approximating the values of the relaxation time to the limit of time resolution of the spectrometer (»30-20ms for T_{Q2} and »100ms for T_{Q1}measurements were performed with low accuracy.

Near $T_{C2,}$ also observed critical slowing down prior to the jump relaxation times at first-order transition.

At temperatures above T_i NQR signals consist of heterogeneous as well as from homogeneous component. At the same amplitude value the contribution of these signals igmenyaetsya with temperature (Fig. 3.6). Below 273K is most clearly expressed spin echo reply nucleus and above this temperature observed area where in the equipment range temporal resolution prevails uniform contribution fixed by the decay of the free precession. There is a slight frequency shift (≈ 50 kHz) between the longitudinal and transverse components of the nuclear absorption. These data indicate a significant spin-relaxation properties of the system. In the available time scale, we performed measurements only time T_{Q1L} and T_{Q2L} (Figure 3.7). As can be seen from the figure, clearly a decrease in T_{Q1L} and T_{Q2L} positions of the nucleus in the structure **I** Cs_2ZnJ_4, whereas nucleus positions II and III (III') the spin-spin relaxation in a wide temperature range varies only slightly.

Note that in the Cs_2ZnJ_4 according NQR no polymorphism and expression of non-equilibrium phenomena. However, at a frequency of 83.3 MHz, by induction, we observed an unidentified NQR signal. Temperature dependence of the frequency of this signal is linear in the temperature range from 300 to TKA, with a small value ¶n/¶T »0,85 kHz/K Signal amplitude during cooling-heating cycle varies as shown in Figure 3.8. In the cooled signal value increases rapidly approaching the T_i. When the sample is heated in a wide temperature range, a more smooth-change.

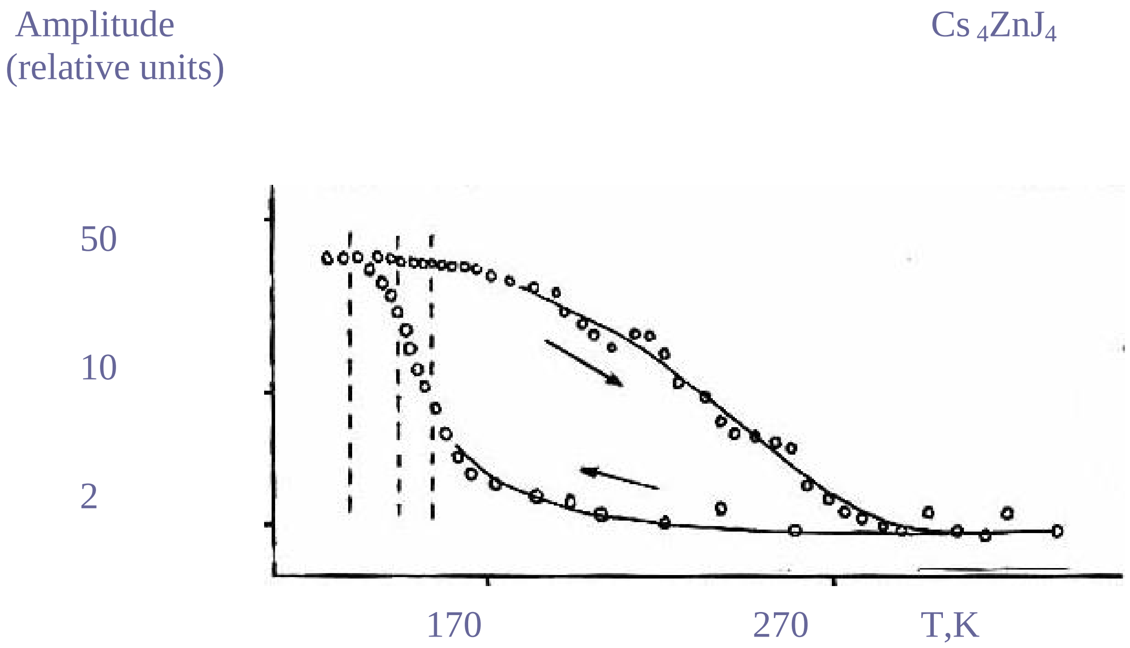

Figure 3.8. Temeraturny stroke amplitude of the signal decay of the free precession frequency 83.3 MHz.

Cs_2ZnJ_4

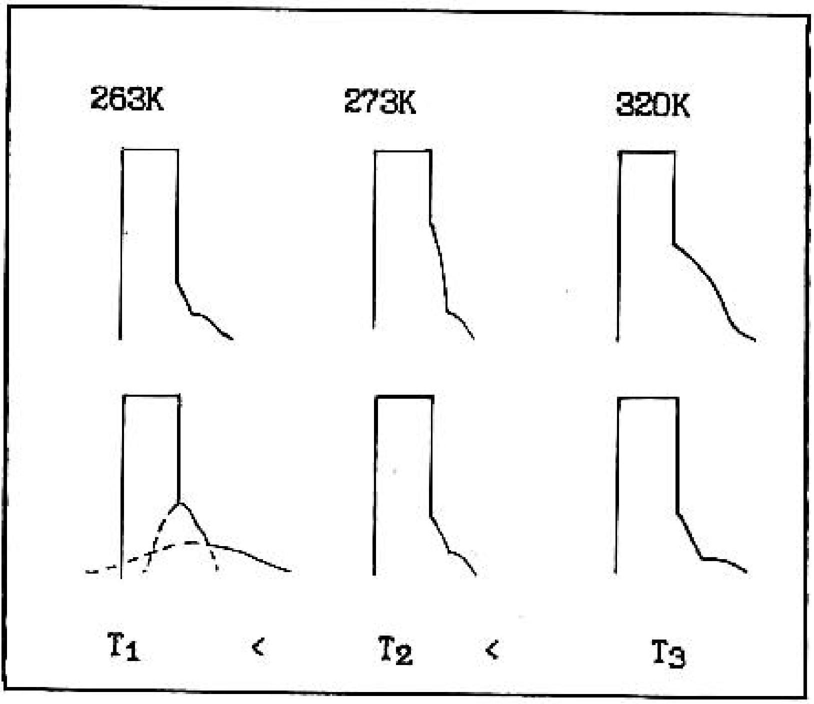

Fig. 3.9. Two-exponential decay envelope shape of the free precession.

As is well known and customary for all the compounds of structure β-K_2SO_4, the phase transition in the paraelectric willows Jc phase transition is of the second kind, but for Cs_2ZnJ_4 observed phase coexistence region near the transition point T_i, which usually characterizes the transition as original. On the other hand, the original transition should be observed temperature hysteresis width of the order of the phase coexistence region. However, from our data suggest that hysteresis effects are fixed only by the homogeneous unidentified NQR signal (Figure 3.8). According to this we can assume that in the Cs_2ZnJ_4 (see below and also Rb_2ZnBr_4), there is a microscopic substructure affecting the nature of the phase transition, and hysteresis of the main structure is masked by a large temperature region of frequency overlap of homogeneous and inhomogeneous contributions to the signal NQR. Microscopic nature of observed substructure is confirmed by the presence of trivets cross-relaxation absorption of one of its levels with the level of the basic structure of the NQR frequency 73.7 MHz. Thus there is reason to assume that the phase transition to the incommensurate phase is smeared in a 100K above T_i Around the same area observed asymmetry of the line shape NQR redistribution contributions homogeneous and heterogeneous components NQR signal plateau in the temperature dependence of the spin - lattice relaxation, strong anisotropic scattering by point radiographs. At a temperature change in the slope 280K measured temperature variation electro-piezo-optical coefficients dDn_1 and dDn_2 [78], the softening of the optical mode [89]. Thus, in this temperature range is marked with non-standard behavior of macroscopically and microscopically smooth blurred anomaly at 240-270K. Anomaly is associated with a slight restructuring and is accompanied by changes in the spin dynamics of the system.

To describe the observed behavior of the NQR spectral parameters we performed additional NQR study. It turned out that the form of induction decay signals at frequencies of I, II and III is at least two-exponential (Fig.3.9), wherein it is not connected to the interlevel spin transitions of 5/2. This indicates the existence of two systems in the dynamics of the scale of the spin-lattice relaxation time - short T_{Q1s} and long T_{Q1sL}.

With increasing temperature, the shape of the envelope of the induction signal is clearly observed redistribution of these deposits. The existence of two time scales fixed and spin-echo sequence. Line shape at different setting conditions (Figure 3.5) revealed that the frequency dependence of the complex spectral line $_I$ can be represented as shown in Fig.3.10.

Analysis of the spectral data in the NQR Cs_2ZnJ_4 may be conducted under the assumption that between the high and incommensurate phases of the intermediate region. By lowering the temperature of 330K, where there are narrow homogeneous line (which can be explained by the high mobility of iodine ions [97]), the temperature is lowered NQR line shape is broadened by developing fast motions of the atoms are concentrated in clusters and are in the resulting double-well (configuration) potential. After T_{CI} and T_C transition atom selects a specific position so that rotation occurs cooperative ZnJ_4 tetrahedra in opposite directions with the equilibrium configuration of positions filled building.

Less clearly described behavior, as will be shown below, is also observed in $(NH_4)_2ZnJ_4$ and Rb_2ZnBr_4 (signs: an extensive area of dynamic disorder, the presence of an incommensurate phase, a two-time scale dynamics, the existence of substructure).

Very similar behavior was observed in another type A_2BX_6 crystals [20].

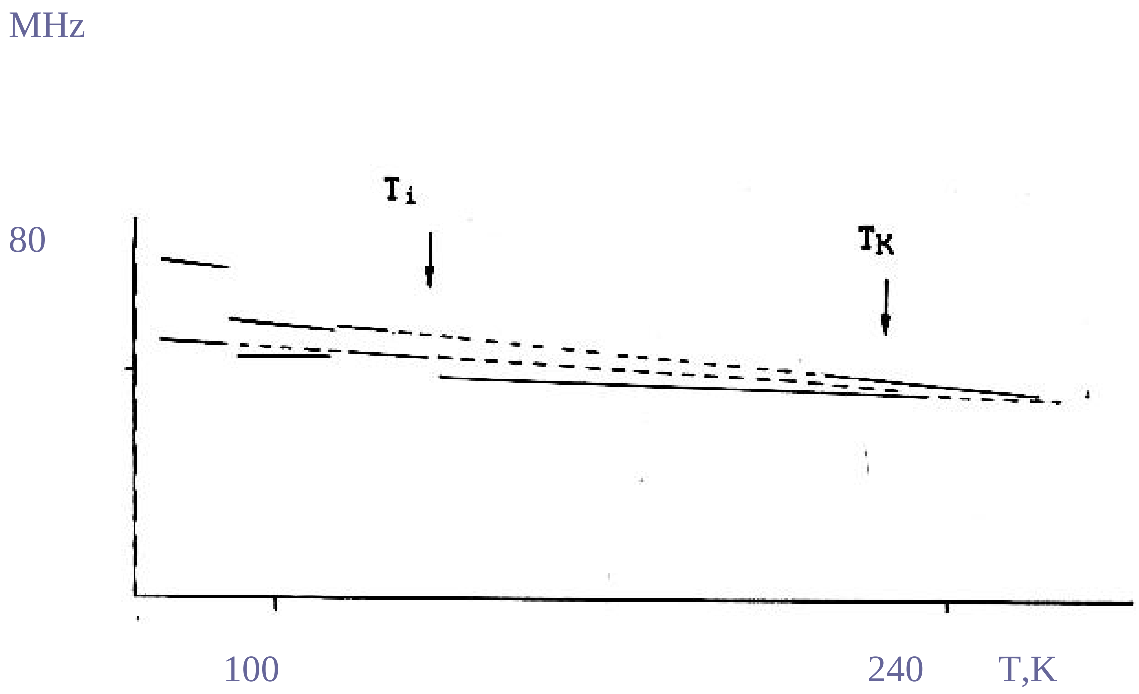

Fig.3.10. Scheme of the temperature dependence of the frequency components of the nonsinglet line (I) Cs_2ZnJ_4

In addition to the NQR data, we have made and the x-ray diffraction studies dielectric Cs_2ZnJ_4 at temperatures ranging from 300 to 93K [85]. Dielectric changes along the c axis showed a peak in T_i and fractures T_{C1} and T_{C1}. These data correspond well to similar measurements Gezi [90], made around the same time. X-ray diffraction, it was found that at room temperature the crystal has a rhombic pseudohexagonal cell D_2^{16h} with parameters: a = 10.835; b = 8.318; c = 14.440**A**; c/b = 1/3, Z=4, which allows this compound is sure to carry the structural type -K_22SO_4. When the sample is cooled from 237 to 107K view radiographs does not change. At 107K radiograph well displayed in the orthorhombic cell with a = 10,744; b = 8.231; c = 14.341 . At 108K a splitting of some X-ray line.

Character splitting indicated monoclinic distortion of the cell. By analysis of the extinction reflexes involving elektroopticheokih and NQR data has been proposed that has a G_i phase structure with a spatial group or $P2_1(Z=4)$ with a polar or nonpolar axis **b** $P2_1/n(Z=8)$. Below 95K on X-ray data, has a triclinic cell distortion. General analysis of structural data (including NQR) gives G_2 phase space group P1(Z=4).

However, radiographs in Jc phase initially failed to fix superstructure reflections. Only in high-precision X-ray studies performed at the University of Orsay (France) F.Denovue was recorded appearance satellite reflections below T_i, with the value of the wave vector [91]

$$\mathbf{q_d = (\ 1 + d\ )\ \ a^*/2,\ d \approx 0{,}15 \qquad at\ T = 112.}$$

Thus in conjunction CS_2ZnJ_4 discovered and investigated the phase sequence:

$$\mathbf{Pnma(Z=4)\ \text{«}\ \ Jc,\ q_d = (1+d)a^*/2\ \text{«}\ \ P2_1/n(Z=8)\ \text{«}\ \ P\bar{1}(Z=4)}$$

The transition to the incommensurate phase is accompanied by an extensive pre-transition region and the specific evolution of the line shape transition NQR signals.

§ 3.3 NQR Studies of phase transitions in $(NH_4)_2ZnJ_4$.

Synthesis and crystal growth tetrayodtsinkata ammonium author performed using chemically pure $\mathbf{NH_4}$ and ZnJ_2, which were taken in stoichiometric ratio, a method of evaporating an aqueous solution and melt ive.

In the first case, crystallization is carried out at a temperature of 293 K under conditions **of** low atmospheric moisture for 10-15 days.

Depending on the variation of the starting components of various crystallizations were prepared with different crystal habit. When r excess NH_4J grew predominantly hexagonal prismatic crystals with a diameter of 5 mm. With excess ZnJ_2 obtainedlamellar intergrowths willows crystallites up to 25 mm in length. To remove any residual crystals were washed with a solution of a chemically neutral fluid. A homogeneous melt of colored iodine compound, which after grinding and annealing was a light gray powder. An x-ray test crystals with hexagonal form the habit of no interest.

Methods of NQR investigations was the same as described above. Temperature measurements were carried out in 380-77K.

Studies have shown [92] that observed at room temperature from6 to 8 NQR lines at 77 and 16 lines of varying intensity. Analie number and intensities of the spectral lines samhles different methods of growth and crystallization allowed to correlate them on two structurally different states. So to a certain structure ***and*** spectral lines correspond to type νaI - νa5; and-other structure in lines νI, νII, νIII (in-line). Fig.3.11.

Later studies were conducted on samples two N1 and N2. From sample Nl at T-290K fixed intensity of the NQR lines at frequencies νa1 - νa5 and structure, and from the sample N2 simultaneously observed NQR signals of a and β-structures in proportion intensely about 1:1. At 77 K from both samples were also observed and in-line type NQR, and from sample N1 signals approaching the noise level of the spectrometer. Upon annealing the samples (T = 380K) within 4 hours, an increase in the intensities of the NQR signal type b. Spectral line type ***and*** traced throughout the temperature range and do not have any anomalies in the temperature dependence of ν(T) (dashed lines in Fig.3.11) and intensities I(T). Stroke frequency NQR lines in the linear type to ***T)*** 170K with $_{I}/T = 34,5$; $_{II}/T = 14,8$; $_{III}/T = -2,0$ kHz/K. At a temperature Ti - 165K anomaly in the behavior of the spectra. Peak intensities of the lines ν and νIII diminish lines and νI νIII when passing through the Ti vary in frequency (Fig.3.11). The second anomaly is observed at Tci = l26K, where there is a change in the multiplicity of the spectrum. The low-frequency component is split into three lines with an intensity ratio of »1:2:1, and the high frequency components pass into the two NQR lines each. When the transition 1/2 - 3/2 fixed 12 NQR lines ^{127}J.

Temperature changes in the group of high-frequency lines indicate the temperature of the third spectral anomaly : $T_{C2} = 87+2$К.

At temperatures 210-370K NQR signals from b state of the crystal are observed as a spin-eco signal $A_{se,}$ and in the free precession signal decay $A_{i.}$ With increasing temperature, the amplitude of signal A_{se} for all of the component ν. Fig.3.12 spectrum decreases, and the amplitude ratio of $A_{se}(I) : A_{se}(II) : A_{se}(III)$, characterized by the ratio of 1:1:3. Amplitude A increase of the noise level and reaching a maximum at T»310K, fall at higher temperatures. After annealing the sample at T^{3} 310K and subsequent cooling, the quantities A_{se} and A_i decrease in size, but restored after low-temperature cycles. Such changes in NQR spectra reflect the resonant nature of the observed relaxation of nonequilibrium phenomena. However, due to technical limitations, these affects on this compound investigated is not sufficiently clear.

Based on a comparison with the data obtained by this NQR for compounds Rb_2ZnBr_4 (Fig. 3.13, etc.), $Rb_2ZnCl_{4,}$ Cs_2ZnJ_4 and other assumption was made that the investigated compounds belong to the structural type β-K_2SO_4 symmetry transformation of the scheme:

$$\begin{array}{ccccccc} D_{2h}^{l6}(Pnma) & \overset{165K}{\ll} & Jcl & \overset{126K}{\ll} & Jc2 & \overset{87K}{\ll} & C_{2v}^{9}(Pn2_1a) \\ (Z=4) & & & & & & (Z=12) \\ V=l & & & & & & V=3 \end{array}$$

The phase between 126 and 87K interpreted as disproportionate, rather arbitrary, and is likely to increase in the period phase $q_S = 2/5$ or 3/8) and the symmetry Pn21a.

Focus on a comparison of the spectral data obtained by us NQR with similar data for other compounds A_2BHal_4 (Hal = Cl, Br, J) and consider-their compliance with femenologicheskoy model [34], proposed to describe the shape of the resonance lines in the incommensurate systems.

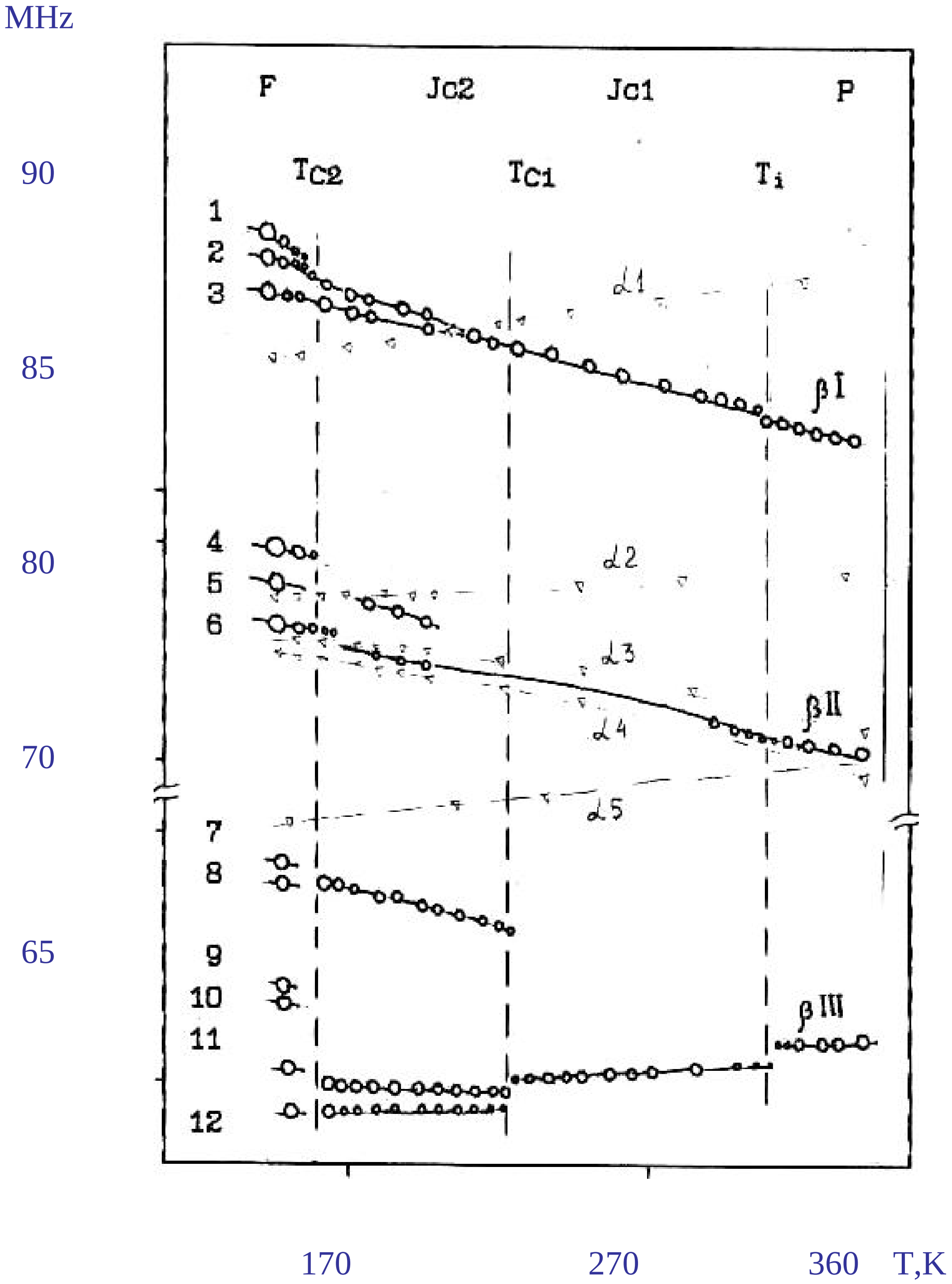

Fig.3.11 Temperature dependence of the frequency spectrum of the NQR ^{127}J in **$(NH_4)_2ZnJ_4$.**

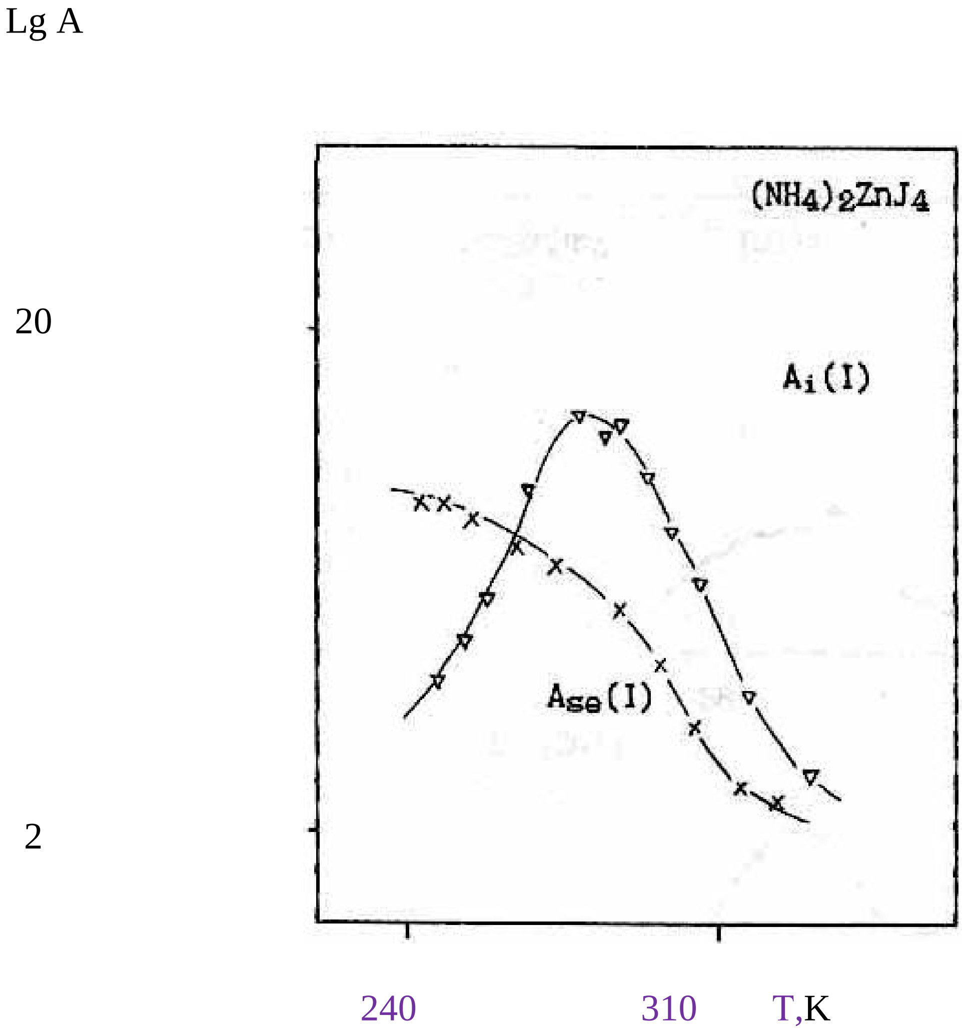

Fig.3.12. Changing the values of the amplitudes A_{se} and A_i in **$(NH_4)_2ZnJ_4$**

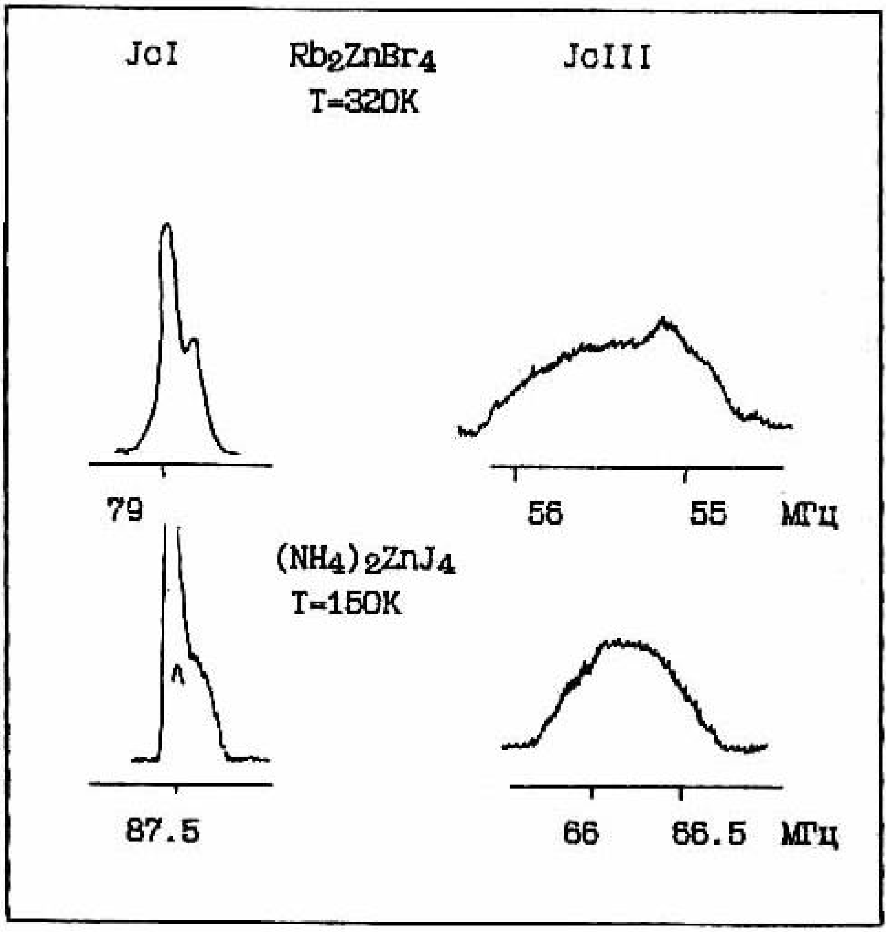

Figure 3.13. The comparison of the NQR spectra of Rb_2ZnBr_4 and $(NH_{4)2}ZnJ_4$

Table 3.1 shows the known NQR data for compounds A_2BHal_4 with an incommensurate phase. These data include: 1) the relative splitting of the extreme components of the spectrum near T_i: $_{I-III}$ = [$_{I}$-$_{III}$]/$_{III}$; the values of the temperaturecoefficients of /n*¶n/¶T

Table 3.1

A_2BHal_4	n_I MHz	n_{III} MHz	Dn_{I-III} %	$\frac{1}{n}\times\frac{dn_I}{dT}$	$\frac{1}{n}\times\frac{dn_{III}}{dT}$	$\frac{n}{n_0}$ %	T_{Q1} (m
ZnJ_4 (AZJ)	87.0	66.0	31	$3.9*10^{-4}$	$-3*10^{-5}$	280	150
$ZnBr_4$(AZB	66.0	61.5	<26	$3.0*10^{-4}$	$-1.9*10^{-4}$	400	160
$ZnCl_4$	9.8	8.0	<27	$2.6*10^{-4}$	$+1.3*10^{-4}$		1000
Cl_4 (CHC)	14.15	11.68	*22	positive	negative		-
Cl_4 (KZC)	9.94	8.08	*20	positive	negative		600
J_4 (RZJ)			>19	positive			
Br_4 (CUB)	93.5	78.6	19	$2.3*10^{-4}$	$+1.6*10^{-4}$		
BT_4 CCCB)	65.9	57.36	15	positive	positive		-
J_4 (CCJ)	83.2	71.5	16	$7.4*10^{-5}$	$+ 4*10^{-5}$		100
Br_4 (RZB)	64.0	55.0	16	$2.5*10^{-4}$	0	320	
Cl_4 (RZC)	9.7	8.3	16	$4.4*10^{-4}$	$+2.4\ 10^{-9}$		
J_4 (CZJ)	79.5	73.9	7	$7.4*10^{-4}$	$+1.5-10^{-4}$	200	400
Cl_4 (CZC)			8	modulation Cs по ЯМР [127]			
Br_4 (GZB)	62.73	67.62	9	no Jc ?			
dCl_4 (RCC)				structure Immm			

3) the average half-width of the resonance signals latched by spin-echo above T_i ; 4) The maximum values of the relaxation times T_{Q1} and T_{Q2} the position I Pnma structure of the compounds studied, where the nucleus of halogens.

Comparison of the relative spacing between the high frequency ν_I and ν_{III} low frequency NQR lines in the high-temperature phase near T_i, shows that the largest amount of splitting $D\nu_{I-III}$ celebrated for ammonium compounds (up 31%) and the smallest for cesium (up *7%).* This fact is explained by difficult from the standpoint of crystal, because radius of the cations NH_4, Gs and close in magnitude and indicates that the cleavage is determined sufficiently dynamic environment nucleus halogen. Some correlation of splitting $D\nu_{I-III}$ observed size of the halogen atom: for compounds A_2BHal_4 same A and B, the splitting decreases with decreasing radius Hal. Due to the fact that the "smaller" Hal atoms polarizability than this may indicate a significant chemical (electronic) contribution to the nature of this splitting. At temperatures close to T_C and 77K major outer frequency splitting observed in average in the compounds with the larger ions. This is in agreement about the importance of data on the dipole-dipole interaction in these compounds. Nor is there any patterns between types of atoms B (Zn, Cd) and the general character of the temperature dependence of frequency: when changing varieties atom B, is transferring to another compound crystallochemically or structural class. This implies that the stability of the tetrahedron defined by the electronic environment.

Significant linewidths temperature phase indicate the presence of structural or chemical disorder in these crystals. Suggest the following details in shape. Hal_I spectral distributions (the position of the nucleus in the structure of halogen I Pnma). If in Cs_2ZnJ_4 line shape in the position of Jc faze Hal_I presented low-intensity and high-intensive low frequency component, the compounds of RZB, CHB, CCB, CCJ observed reverse arrangement in the intensities of these components.

In this case, cesium bromide intensely ratio of these components is about 20, and in the second part CCJ only observed when T_C low intensity as a small wing . As will be described in Chapter 4 of RZB in increased pressure in the Jc phase component intensity ratio discussed approaches unity and becomes comparable with the add-on for AZB and AZC. Since the shape of the line is determined, in particular, the transverse spin relaxation (T_{Q2}), to a marked difference indicates a different character dynamic environment nucleus deviated from position I (II and III) structure Pnma. Most clearly seen when compared Cs_2ZnJ_4 with other cesium analogs.

Temperature dependence of the frequency below T_i unusual and can not be explained by known types (rotary, Vibratory, torsionalny) atomic motions. In the nature of the temperature slope of the NQR frequencies in compounds A_2BX_4 celebrated their graduation large values of sharply positive for high frequency components, to smoothly negative for the lower frequency component of the NQR spectrum. This, along with other data about indicates significantly different character movements and dynamics of structurally nonequivalent nucleus Hal.

When comparing our data with the results of stationary NQR methods [37, 44, 45], there are significant differences. It follows from our relaxation measurements of the T_{Q1} and T_{Q2} due to the fact that when using the latter can be detected only homogeneous (long-lived), contributions to the absorption signal, whereas the use of spin-echo technique allows us to observe inhomogeneously broadened signals. But even in the latter case there are time limitations instrumental that does not allow enough correct record form broad frequency distributions, as in the case of Cs_2CdJ_4, even with an increase in sensitivity of the method, the signals in the Jo-phase is not fully observable.

Briefly summarizing the results of NQR spectral data presented in this chapter, we can note the following: First, the experimental data obtained under static spectral characteristics indicate a fundamental difference in the nature of their temperature evolution compared to phenomenology model [34]. Secondly, there is a significant impact on the nuclear dynamics observed frequency spectral characteristics of NQR.

Time measurement T_{Q2} spin-spin relaxation in and [103,109] indicate the need to consider the temperature change of the width of the singlet spectral line in Jc phase, whereas in the existing model, the width of individual components of the continuum distribution was chosen to be the width of the line paraelectric paraphase . However, NQR data for Cs_2ZnJ_4 (and especially our studies RZB [109]) shows that this assumption is not always competent, since the relaxation times and T_{Q1} T_{Q2} in Jo phaseincrease rapidly with decreasing temperature, and the intensity of the two end peaks for all of the observed frequency distributions near T_i differs by more than an order of magnitude. The observed shape of the spectra are not always the result of hardware distortion, since the relaxation time $T_{Q2,}$ at least at low temperatures Jo phase, the relation $T_{Q2} > t_1$; t_{INR}; t_2.

Comparing our data with the X-ray data on the measurement of the mean square displacements of atoms in tetrahedral ZnCl paraelectric Rb_2ZnCl_4, where it was established that there are two equal-probable provisions tetrahedra into each other by the libration movement (Fig.3.14) and summarizes literature data on the values of the mean square displacements of atoms in the other $A_2BX_{4,}$ to some extent consistent with those of the NQR and Raman [42] that the phase transition P-Jc in the compounds studied close to the type of order-disorder. It should be noted that not form symmetric spectral distributions comparable to those observed by us, detected RF methods and systems of other crystalline, such as in compounds with CDW charge density waves (see e.g. 2H-$TaSe_2$ [95,96]), used ion conductors with superlattice ordering (Ag_2HgJ_4 [97]), organic-dimensional conductors CH_x-trans [98] etc. [100]) and even in solid helium-3 not [99]. In all these cases, the observed asymmetry of the resonance line was associated with the anisotropic diffusion of spin or charge against the backdrop of two large-scale spatial or temporal scale. Similar forms registered by EPR in the study of the vibronic interaction A and orbital states in complexes with octahedral symmetry [102]. Overall data analysis allows to chart a path radiospectroscopy explanation NQR experiments in this class of compounds in the direction of electron-nuclear movements in two ambitious timeline.

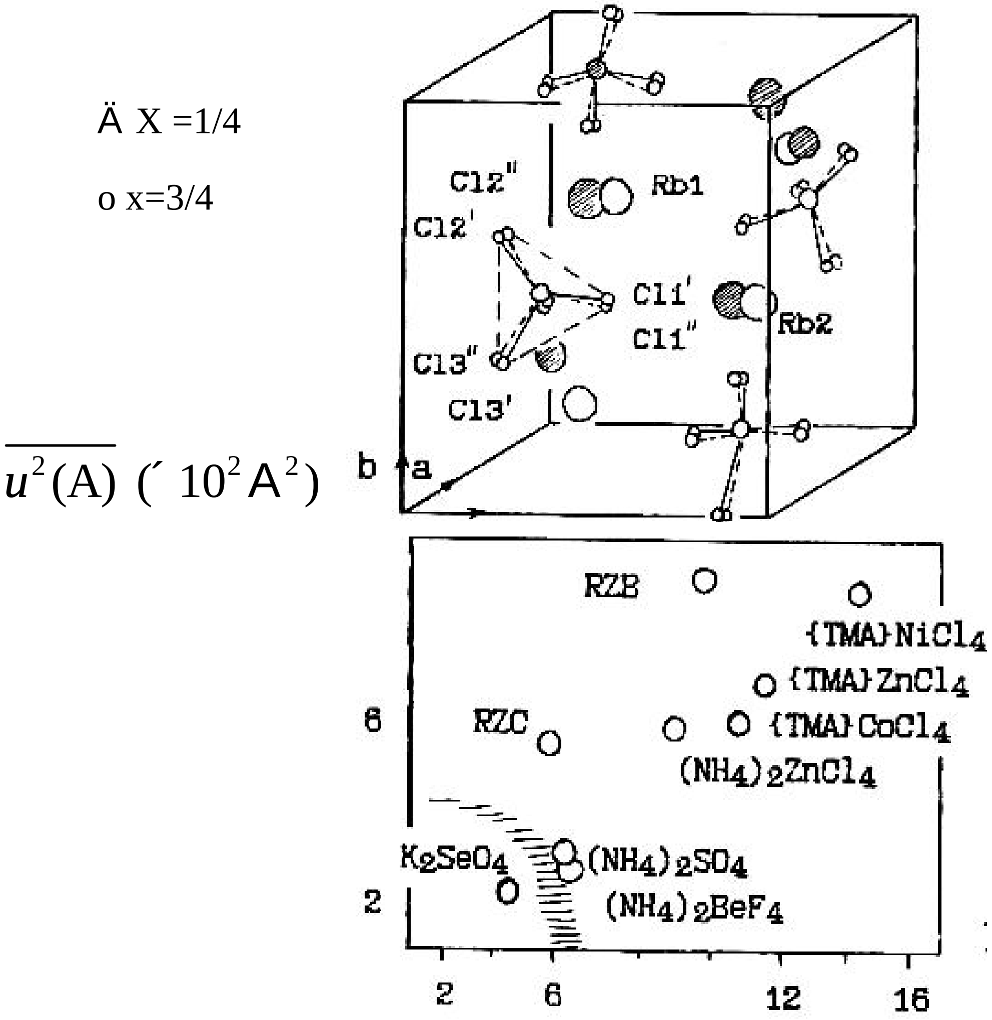

Fig.3.14. *a.)* Libration movement ZnCl$_4$4 tetrahedra in the high-temperature phase Rb$_2$ZnCl$_4$ according to [41].

b) standard deviations of the atoms grade **A** and **X** for certain compounds A$_2$BX$_4$ at room temperature.

§ 3.4 Polymorphs in the family A$_2$BX$_4$ with -K$_2$SO$_4$.

It follows from our data, the compounds Rb$_2$ZnBr$_4$ (see § 4.1), Cs$_2$ZnJ$_4$, K$_2$ZnBr$_4$ [125] and, presumably, (NH$_{4)2}$ZnJ$_4$ and Rb$_4$ZnJ$_4$ and others may crystallize or relax to more stable crystal structure, described by the space group $_1$ (type structure Sr$_2$GeS$_4$). Consequently, the structure type β-K$_2$SO$_4$ in these compounds are metastable. As you know, many of the compounds A_2BX_4 also crystallize into structures in space group Pnma or $P2_1/m$, and few of them reliably or supposedly presented simultaneously these two structural modifications [86]. In Table 3.2, the compositions are A_2BX_4 in which: 1) the only observed structure Pnma; 2) was observed structure Pnma and $P2_1/m$; 3) was observed only structure $P2_1/m$.

My can assume that marked us polymorphic transition α-A_2BX_4 « β-A_2BX_4) is characteristic for the various compounds and can be implemented for other compounds shown in Table A_2BX_4. However, significantly different relaxation times of the structure to the structure and observed us for Rb_2ZnBr_4 (weeks), and for K_2ZnBr_4, Cs_2ZnJ_4 (several minutes), indicate that polymorphic transition may be unrealized in normal conditions. However, we know of no data on detailed studies of the conditions of the transition between these modifications, although these effects were observed and studied in other crystalline objects, and in particular in disordered polymers and molecular crystals with cis-trans isomeric structure chains [43].

According to our research and NMR data on the measurement of the heat capacity [77] in all the compounds A_2BX_4 grown from aqueous solutions or have been in contact with the atmosphere is always a small amount (less than 2%) loosely bound water. On this basis, we can assume that the transition β-α is carried by surface orientational ordering of β-α structure in the dipoles of water molecules. Comparison of the spin relaxation times for the α and β structures indicates that dynamically disordered metastable β structureconverted into a more structurally ordered dynamically stable structure. The possible existence of crystal structures with varying degrees of dynamic stability is predicted by mathematical methods of stability theory for systems with interaction ANNN [104, 130]. As follows from these studies in some symmetrical classes of such systems are possible bifurcation from stable solutions with conditional period of the structure N-1 to dynamically meta-stable states with N = 1,2,3,4 followed by higher order bifurcations to large periods and increasing the degree of instability. How shown in [104] cases N=3 and N=4 and N=2 at some parameters of interatomic interactions are special, because realized only through the bifurcation some dynamically unstable solutions with N=1 (which we can compare the structure Rnma). In the vicinity of a line bifurcation with different solutions in different periods are mixed and separated by raising away from this line.

This approach can, to some extent justify the presence of a dynamically more stable modifications under consideration for compounds which space group $P2_1/m$ has no common subgroup communication with the space group Pnma.

Table 3.2.

1 Pnma	**2 Pnma, $P2_1/m$**	**3 $P2_1/m$**
Rb_2ZnCl_4	**K_2ZnBr_4 [125]**	**Cs_2CoJ_4**
Cs_2ZnJ_4	**Rb_2ZnBr_4 [125]**	**Cs_2MgJ_4**
K_2ZnCl_4	**Cs_2CdJ_4 [125]**	**$KsCoJ_4$**
$(NH_4)_2ZnCl_4$	**Cs_2CdBr_4[125,129]**	**$(NH_4)_2CoJ_4$**

$(NH_4)_2ZnBr_4$ Cs_2MgBr_4	Rb_2ZnJ_4 [125,132] Cs_2CdCl_4 K_2CoBr_4 [134] Te_2CoBr_4	Rb_2CoJ_4 $T1_2CoJ_4$ [l32] K_2MnJ_4
	Rb_2MnJ_4	
	CS_2HgJ_4 [133] Tl_2ZnJ_4	

Type β-K_2ZO_4

Pnma	↔	$P2_1/m$
тип β-K_2SO_4		тип Sr_2GeS_4
β-A_2BX_4		α-A_2BX_4

Chapter 4. Sequence of phase transitions in Rb_2ZnBr_4 at atmospheric and high hydrostatic pressure.

In this chapter we present the results of studies of phase transitions in Rb_2ZnBr_4 NQR ^{79}Br, ^{81}Br at atmospheric and under high hydrostatic pressure. External exposure is the factor that allows you to get a fundamentally new information about the sequence of phase transitions, in addition to clarify the issues in the form of the NQR lines incommensurate phases.

The absorption spectra of NQR ^{79,81}Br in the incommensurate phase at atmospheric pressure.

When NQR study of compounds with incommensurate phases in which there are significant non-equilibrium processes, it is necessary, in particular, have procedures quantitative measurement of the resonance absorption signal for given values of other parameters (T, t, ν, etc.). Such a technique can be designed based on coherent spectrometers. Spectrometer type ISSH the absolute accuracy of the amplitude of the transient resonance signal is small. Therefore, in the research process was used to monitor the intensity of the reference method, which consists in comparing the magnitude of NQR signal recorded at different sample metaequilibrium state, with the value of the equilibrium signal, structural stability of the sample. When working with Rb_2ZnBr_4 was matched standard, which amounts to less than 10% volume filling of the receiving coil, and the slopes of the temperature and frequency dependences of the pressure of the two NQR lines absorption were sufficient for calibration.

With this methodological technique were significantly clarified the conditions for obtaining reproducible measurements, and also found some side effects. Thus, it was observed that the absolute peak intensity of the NQR signals from the original Br annealed sample Rb_2ZnBr_4 increases the amount of accumulation of cooling cycles. However, subsequently, when samples originally uncontrolled contact with moist atmosphere, the intensity of the spectra of incommensurate structure decreases again, and in addition, there is the appearance of three absorption lines, which we have designated $\nu_{H,}$ ν_C, ν_B . The appearance of these NQR signals, as was explained, due to the excessive influence of atmospheric moisture on the state of the sample. At the same crystal structure of the sample is gradually transformed into another polymorph. Some samples when grown from aqueous solution completely or partially crystallized in this modification, and there is a complete or partial modification of this transition in prolonged contact with moist atmosphere samples.

To elucidate the nature of this phenomenon, measurements were made on the content of crystalline bound water in these compounds, NMR. The results of measurements are structurally bound water (with an accuracy of 2%) was not detected. With the use of X-ray diffraction studies, and considering the NQR signal intensity ratio 1:2:1 (relaxation times are within the time resolution of the spectrometer), it was found that the structural modification (α) has the space group symmetry $P2_1/m$ ($Z = 2$). Upon annealing the samples above 300K structure Pnma symmetry is restored. Thus β-modification is thermally induced metastable modification of Rb_2ZnBr_4 The frequency dependence of the NQR lines $\nu_{H,}$ $\nu_{C,}$ ν_B modification α-Rb_2ZnBr_4 is presented in Figure 4.1, together with the general progress of other NQR frequency signals from both Br isotopes for -modification.

In addition to the absorption signals in some cases a special form of the NQR spectrum in the high frequency region of the spectral distribution of the isotope ^{79}Br β-modification (ν »78MGz) and additional weak lines at the frequencies 79 and 80MHz. These lines, we denote the index of ν_x ν_y ν_z Figure 4.1 and 4.2. As explained, these signals were a homogeneous signals recession free process. Their presence was not related to the existence or absence of the share structure of α-Rb_2ZnBr_4 in the samples. Particularly clear signals $\nu_{x,}$ ν_y and ν_z manifested after the application to non-hydrostatic deformation patterns. After removal of the load was fixed shape of the spectrum shown in Figure 4.2. As the temperature decreases the frequency of induction of these signals almost coefficients of l/*¶/¶T; 3) the average half-width of the resonance signals latched by spin-echo above T_i 4) The maximum values of the relaxation times T_{Q1} and T_{Q2} the position **I** Pnma structure of the compounds studied, where the nucleus of halogens.

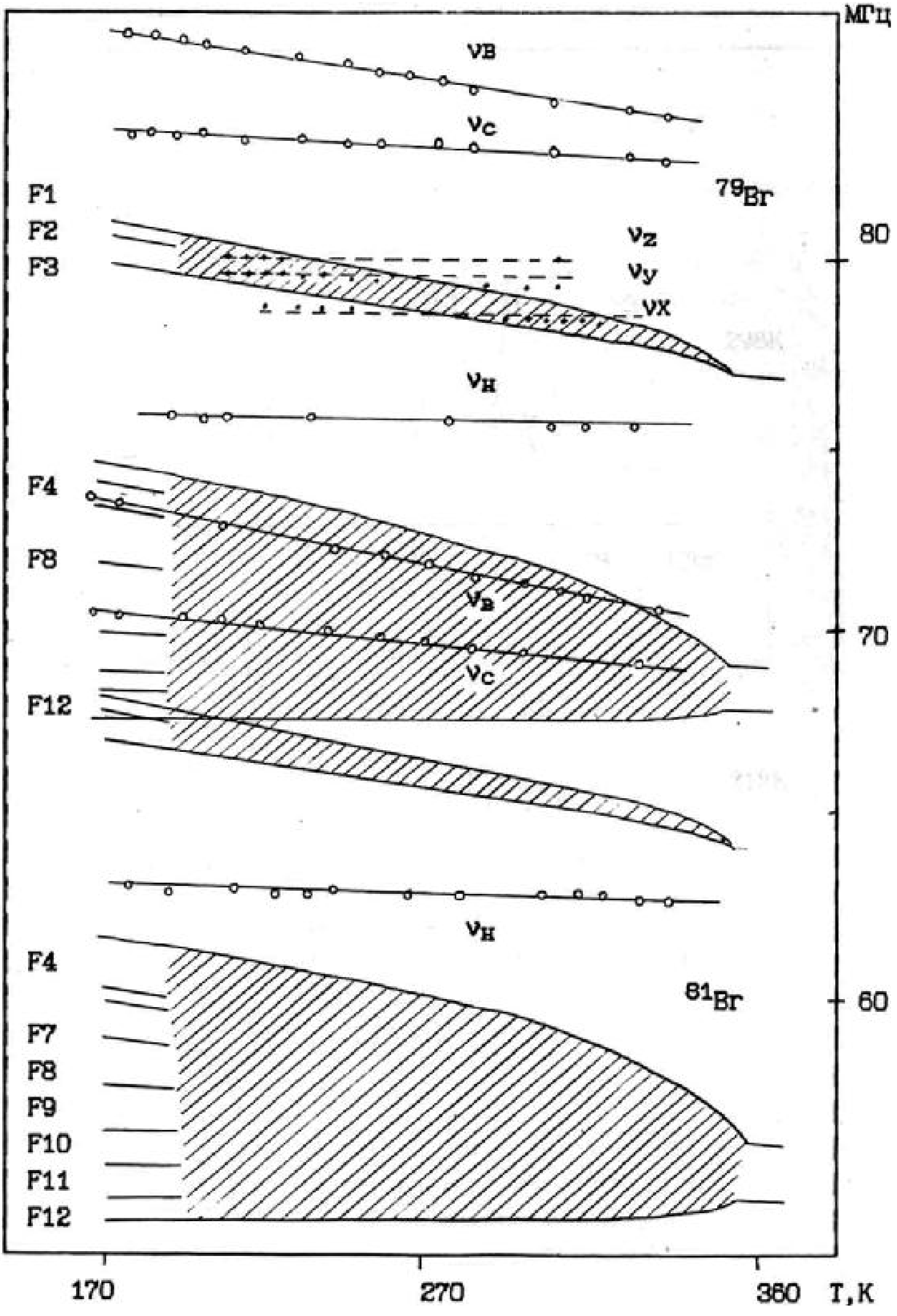

Figure 4.2.View of the ^{79}Br NQR spectrum from samples of Rb_2ZnBr_4 in a stressed state.

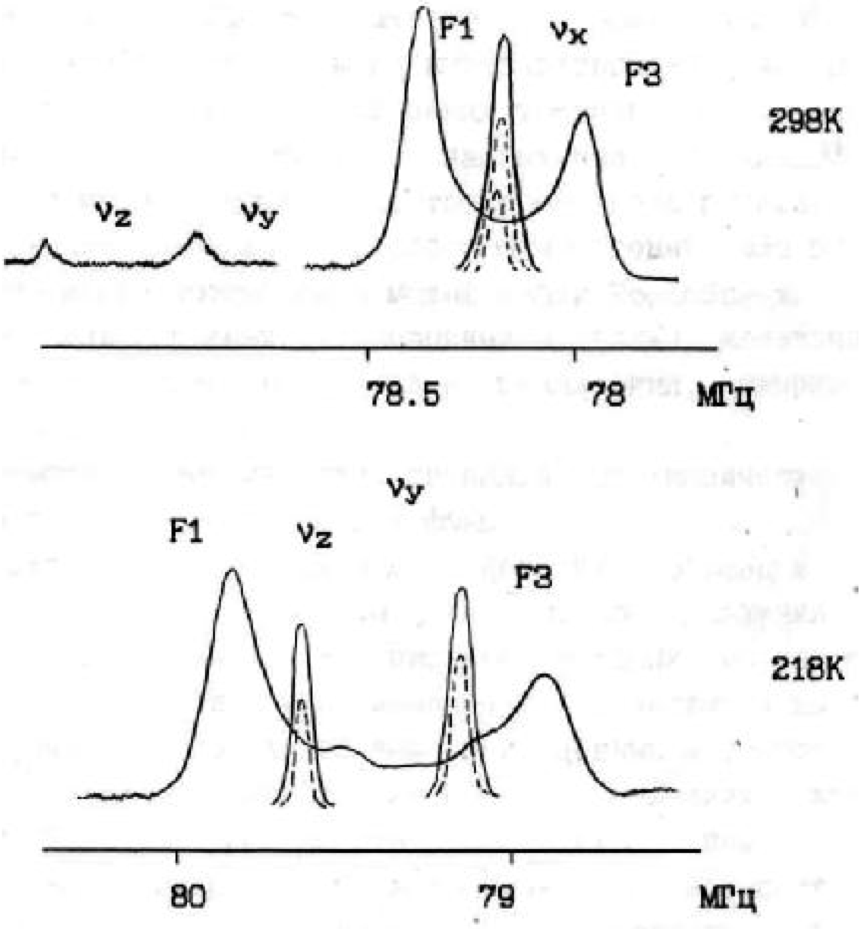

Figure 4.2.View of the ^{79}Br NQR spectrum from samples of Rb_2ZnBr_4 in a stressed state.

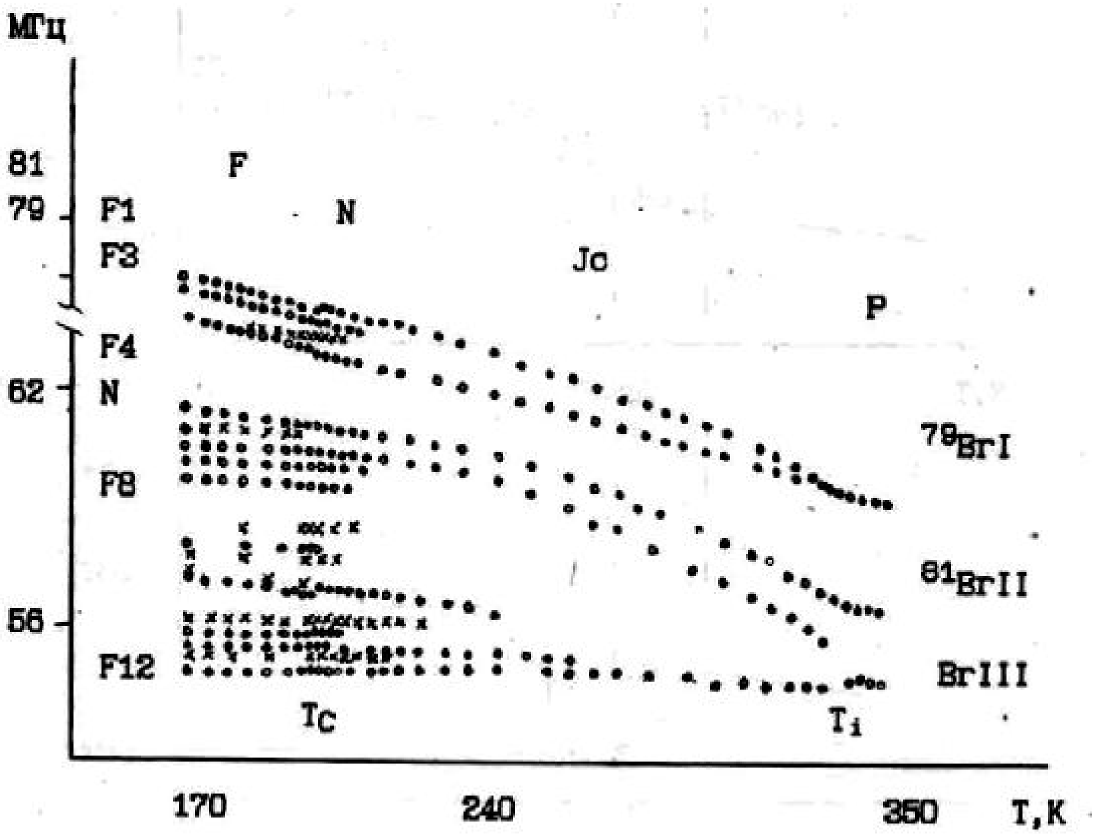

4.3. Full temperature dependence of the NQR frequencies Br in Rb_2ZnBr_4 at atmospheric pressure.

Explanation of this effect is beyond the scope of this paper. We note only that it can be interpreted as the result of cross-relaxation absorption of certain levels, resulting from nonuniform external voltage with quadrupole levels incommensurate structure tetrabromo zincate rubidium [102].

Thus resulting mining measurements were found:

1) Existence of polymorph Rb_2ZnBr_4-α .

2) Impact deformation induced, and also accumulated in the process of crystallization or cooling cycles, the state of voltage samples Jc-phase.

3) The dependence of signal intensity on the amount of cooling cycles in the incommensurate phase.

These results were considered in the preparation of samples A_2BX_4 to research in atmospheric and high pressure method of optimal matching, to which we shall now describe.

Most of the results of research carried out in the following conditions precluding the manifestation above mentioned effects.

Better signal-noise ratio in terms of liquid-gradient thermal stabilization allowed us to meet precision NQR measurements metastable β modification RZB with an incommensurate phase, to clarify and supplement the results published previously [38]. On Fig.4.3 shows the temperature dependence of the NQR frequencies obtained by the author in the temperature range 390-150K. As can be seen in the high-temperature region near T_i managed to track more accurately the frequency dependence of the spectral components Br NQR Fig.4.4. Since the frequency of edge peaks of the spectral distribution of the position of the nucleus Br in the Jc- phase lie above the experimental points of the NQR frequency of the nucleus in paraphrase: J_C phase in the course of the frequency observed in the form of "beak", which is typical for phase transitions with the fluctuation splitting [107]. In the NQR frequencies of nucleus BrI and BrII was monitored more reliable frequency dependence of the splitting. In the region 56MGz below $T_{i,}$ we observed a wide frequency distribution, without any trace of the continuum. It was further found that the NQR signals in the paraelectric phase contain both homogeneous and heterogeneous components. In this case the spin-spin relaxation time T_{Q2S} and T_{Q2L} of these contributions are at the limit of time resolution of the spectrometer ($\approx 20\mu s$).

When measuring the width T^*_{Q2} is most intense line νl, marked difference of its low temperature dependence into a temperature at which the inflection is observed in the frequency dependence of Fig.4.4.

In Jc phase is observed in the behavior of Mild feature spectra, consisting in a slight change in the shape of spectral distributions near 240K. At the same time-frequency spectral shape blurred in 56 MGz (Fig. 3.13) smoothly into a spectral form with three amplitude maximum allowed.

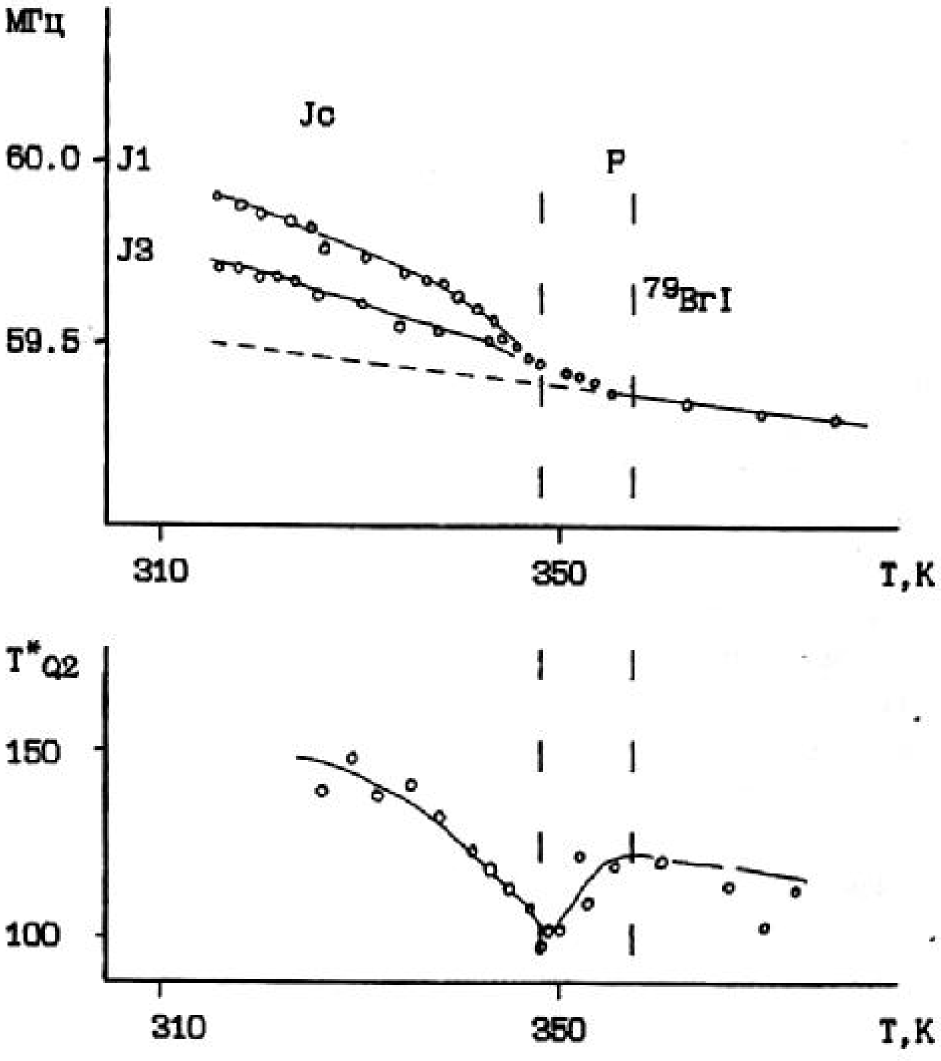

Fig. 4.4. Splitting NQR frequencies the high frequency line and change line width near $T_{i.}$

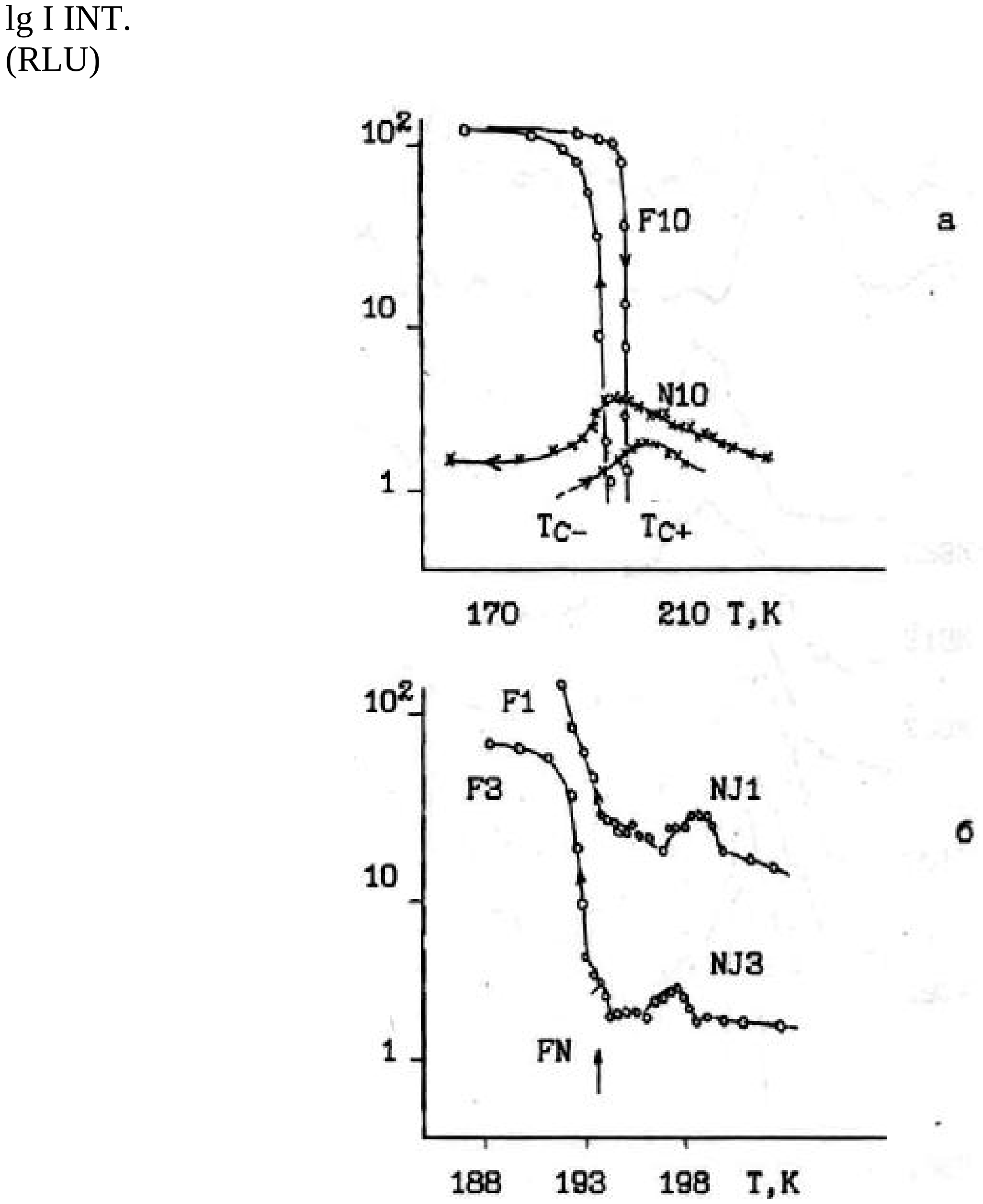

Fig.4.5. Temperature variation of the peak intensities of the lines F, N, and "mixed" type near T_C in Rb_2ZnBr_4.

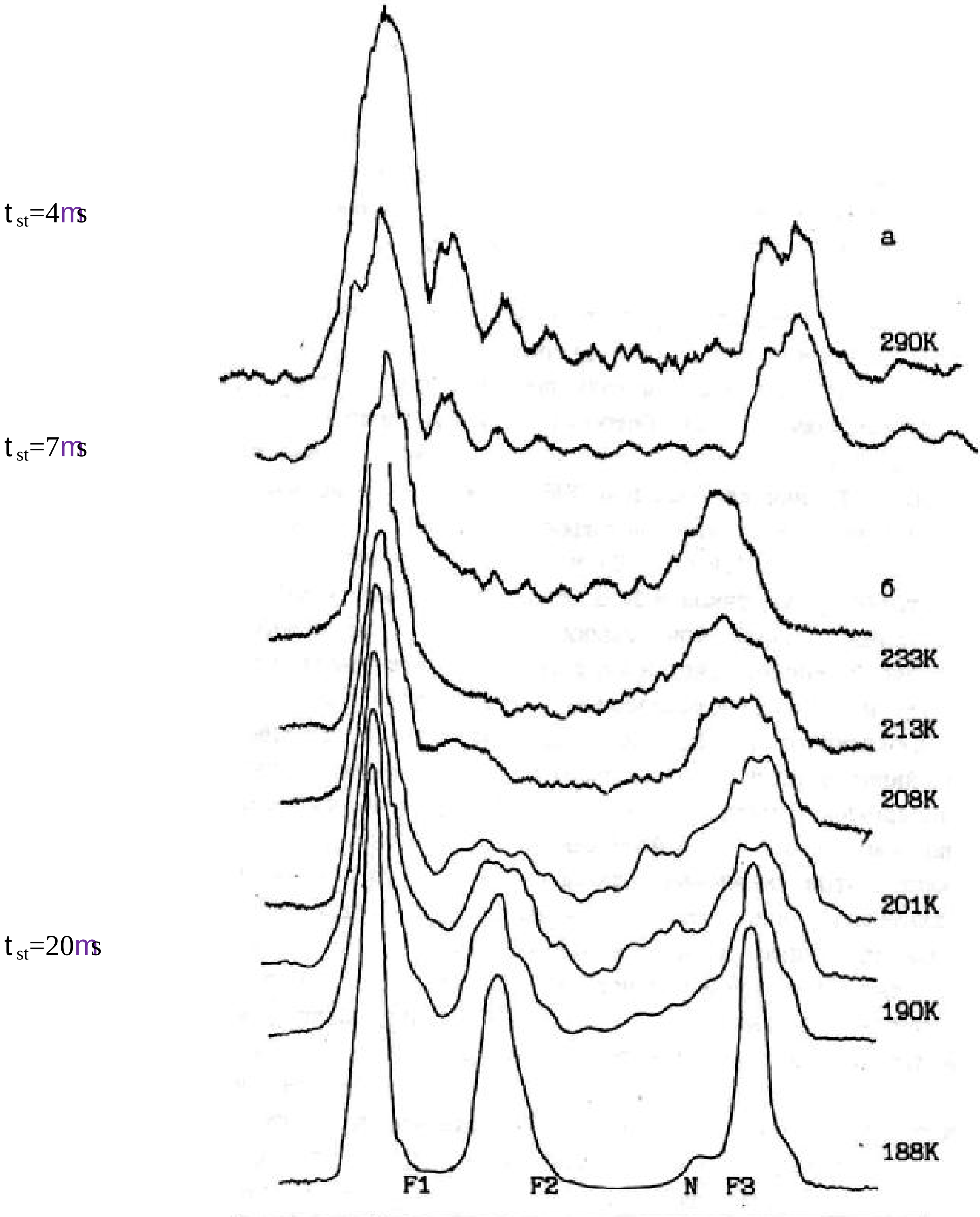

Fig.4.6. ^{79}Br NQR spectrum of the position BrJ structure with special recording conditions: a) isolation; b) non-isolated gate pulse

Below 220K near T_C transition in the spectrum detected NQR lines not previously observed. Their frequencies are sufficiently close to the frequencies previously recorded signals. These lines have a smaller intensity and are marked (x) in Fig.4.3 and 4.5a [108,115]. On Fig.4.5 shows the change in the intensity of the line at the frequency ν=56.8MGz (line F10) and lying next to the new line. With decreasing temperature, initially appears and grows in intensity the new component. Its intensity reaches its maximum value to $T_{C,}$ stabilized in the 3K and decreases with the passage of $T_{C.}$ Appearance and increase in intensity line F10 occurs only near T_C at T £ T_C +3K. The maximum intensity is achieved below T_C-5K and then remains constant.

Near the high-T_C shape distribution at frequencies 80-78 MHz (Fig.4.6) has at least four components, the central part of the distribution sags to the noise level just above $T_{C.}$ The recording of this spectrum (Fig.4.6.) To improve school performed with great frequency sweep and under t_{strobe} £ T_2* and t_2 » T_{Q2} , so the circuit broad line with a short value $T_{Q2,}$ oscillations are observed are associated with the apparatus function or gate integrator [126], or with the effects of the polarization of nuclear dynamics [106]. Omitting the finer details of the line profile, we note in this fourth component of the spectral distribution. With precision studies optimal matching method in this mode were obtained accurate temperature frequency dependence of the spectral components of F1-F3 and N NQR spectrum ^{79}Br Fig.4.7.

Behavior of the intensities of the remaining lines is quite similar to that shown in Fig.4.5, but most of them overlapped with other components of the spectrum, while the temperature-variation of peak intensities of lines located at frequencies overlapping areas, is nonmonotonic Fig.4.56. There is a shift of the NQR frequencies while passing Best T_C measurement accuracy enabled to detect the temperature hysteresis of frequencies, for example, lines F1 and F3 (Fig.4.7).

This change in NQR spectra can be represented as a transformation of an incommensurate phase lines (lines of type J) through the N-type spectral lines to twelve lines F ferroelectric phase. Lines formed in the immediate vicinity of the ferroelectric phase T_C, and do not follow continuously through the transition, as it was previously thought [34]. This is most clearly observed in the group of lines F8-F11 and close lying lines N type. In the frequency overlap lines F and N at T_C recorded small frequency peak races overlap (Fig.4.7). Nonmonotonic behavior of the intensities and frequencies of the lines above T_C indicates that they are unresolved frequency overlap lines F and N-type (spectral lines overlapped FN type), and at higher temperatures are covered by other types of lines N and J (NJ line type). Last gradually converted to the spectrum of the middle region of the incommensurate phase (Fig.4.8).

These experimental data and data on the measurement time T_{Q1} quadrupole spin relaxation of Br [103, 109] indicate the need to revise the model proposed in [34] to describe the shape of the nuclear resonance line in incommensurate phases. Fixed structure of the spectrum allows for the interpretation of the line shape in the framework of the existence of long-period structures. In this case, using the expansion of the atomic displacements on the eigenvectors of the soft mode (1.1) we have:

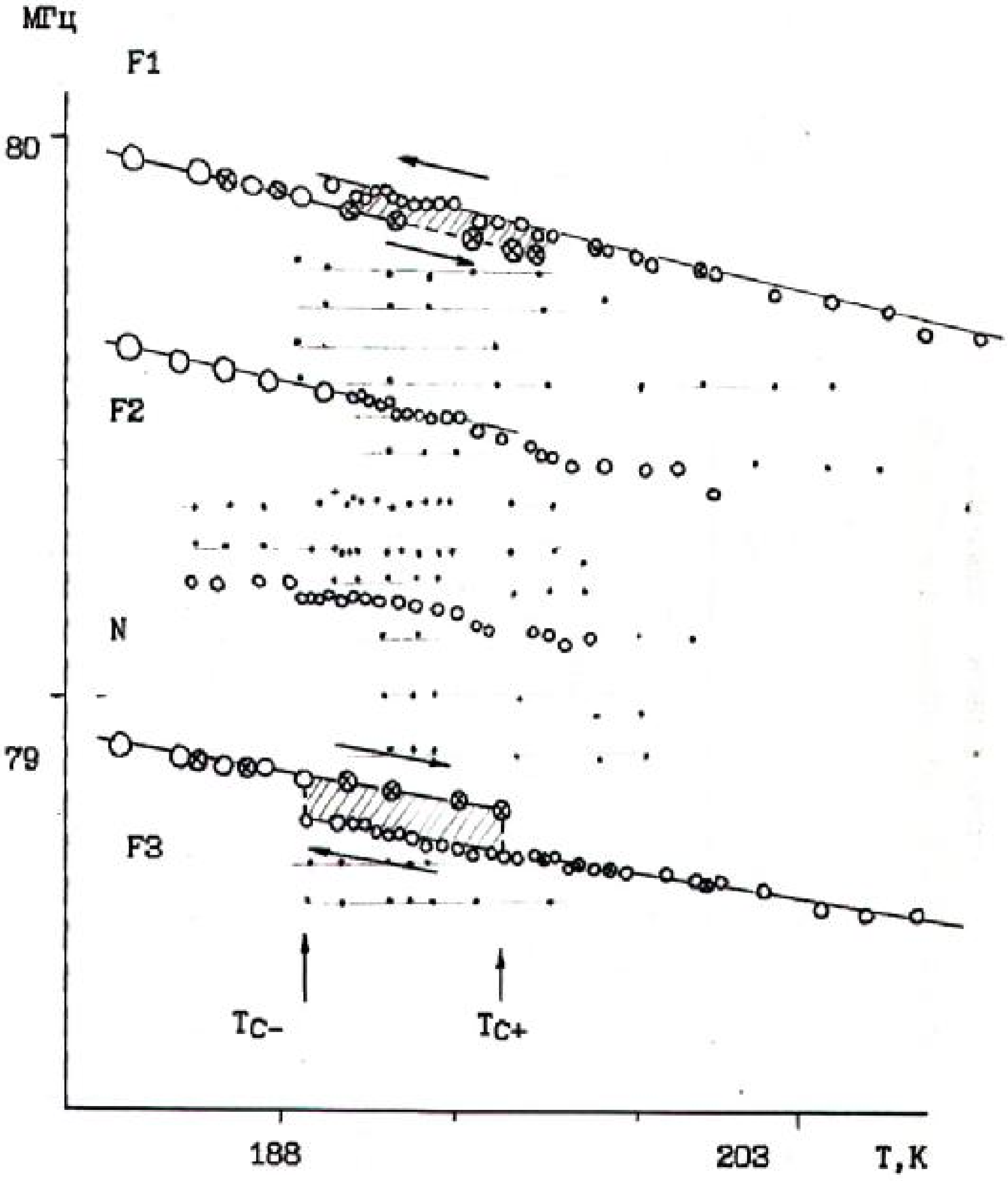

Fig.4.7. … and the

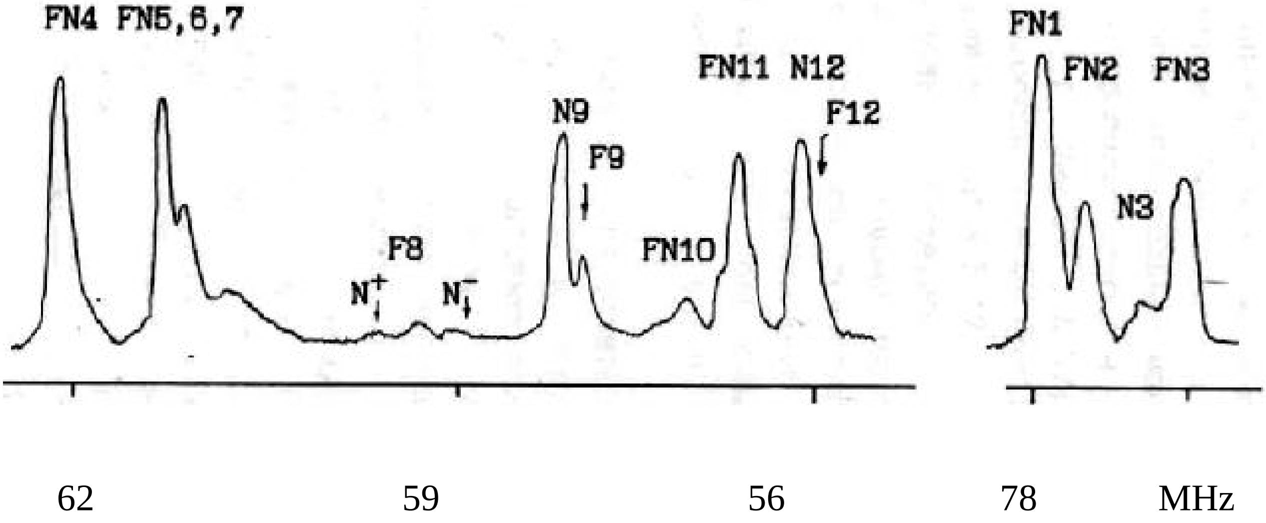

Fig.4.8. View NQR spectrum near T » T_C+2K at atmospheric pressure.

$$u(\mathrm{lkp}) = \sum_{\lambda=1}^{L} A_{\lambda} \cdot \vec{e}_{\lambda k} \exp\{-2\pi i(\frac{N}{M} q_S x_{lk} - \varphi_1)\}... \qquad (4.1.)$$

Spectral density function (1.33) is discrete, and the shape of the line will be the sum of the spectral components of the form g(ν). Taking the calculation of expression (4.1) and in the simplest case, we only consider one rotational mode S_{10} (A_1^1 local approximation, L = l), we calculated the shape of the lines of the long-period structures such as 3/11; 5/17; 9/29; 11/35, with varying angle φ_o in shirokovolnovom approximation. In Figure 4.9 shows an example calculation for modulating 5/17 with different values of φ_0. Increasing the width of the original singlet component g(ν) line shape is close to the continuous frequency distribution (dashed line).At room temperature, the estimated line may be adjusted by experimental verification of the continuum on the assumption that modulation of the 5/17 simultaneously coexists with different values of the phase angle φ and introducing corrections relaxation contour line.

In the low temperature region, where the soliton tapered wall and the main structure similar to the crystal structure of the ferroelectric phase to the value of $q_d = 1/3$, we shall use the expression for the non-linear phase angle φ. The calculations in this case showed that a satisfactory agreement with the experimental line shape can obtain if modulations along with close to 1/3 (5/17, 3/10) briefly introduce a periodic modulation of 1/4, which is indispensable in the local approximation to describe the fourth component spectrum. This assumption means that an increase in the contribution from other modes of symmetry, such as S_3, or from a different view, for example, A_q [93], S_2 fashion, formally analogous to the introduction of non-local description. On Fig.4.10 shows the calculated line shape is obtained by assuming the coexistence of the modulations with wave vectors 3/10 and 1/4, respectively, taken with weights 4:1:1:2. The coincidence of the calculated and experimental forms, as can be seen from the figure, is quite satisfactory.

Thus NQR data at atmospheric pressure indicate that near T_C structure of the incommensurate phase of Rb_2ZnBr_4 can be represented by the coexistence of multiple modulation sequence "satanic stairs. This is not inconsistent (X-ray diffraction data. [110] However NQR data indicate that besides the modulation of 1/3 must be present for at least another one even short-modulation.

For the experimental confirmation of the existence of such a structure, it was decided to expand the area of research through additional parameter - the external hydrostatic pressure. When this was to be expected that in the "devil's staircase" this will change the proportion of one phase at the expense of others, and to facilitate their supervision.

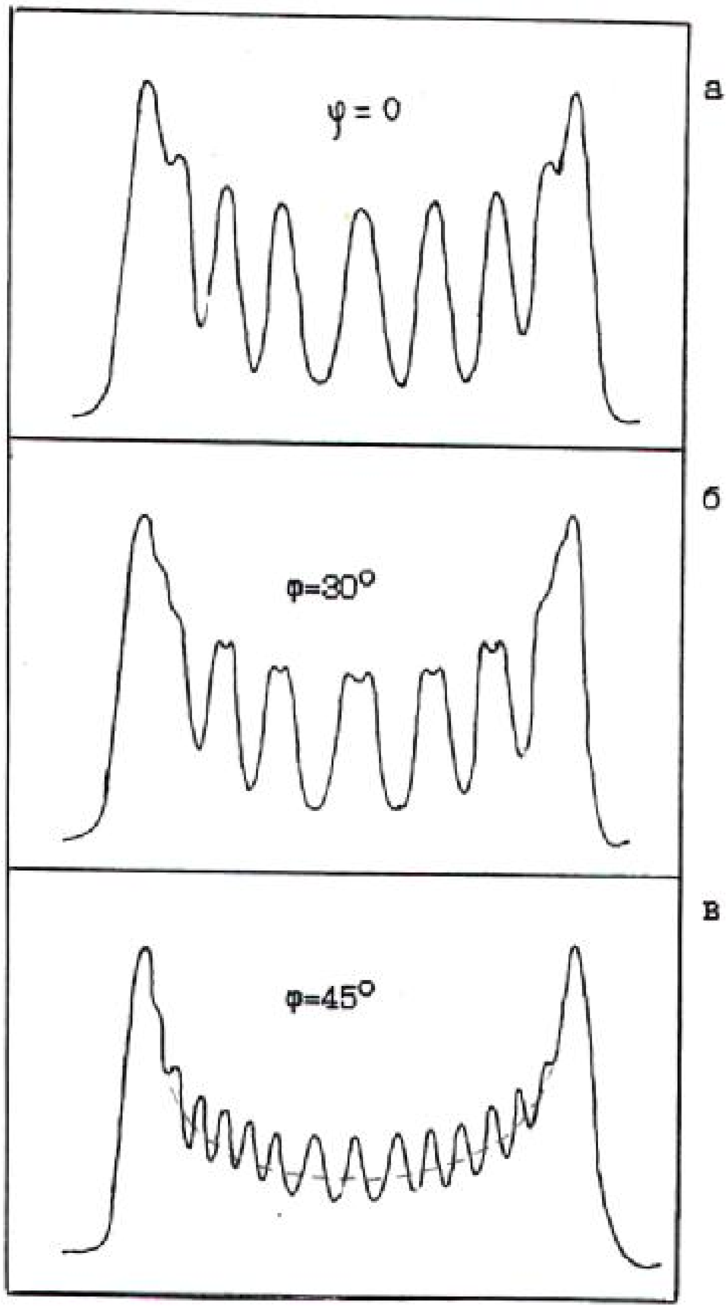

Figure 4.9. Calculated line shape in the long-periodic approximation M/N = 5/17; A_q = 0.

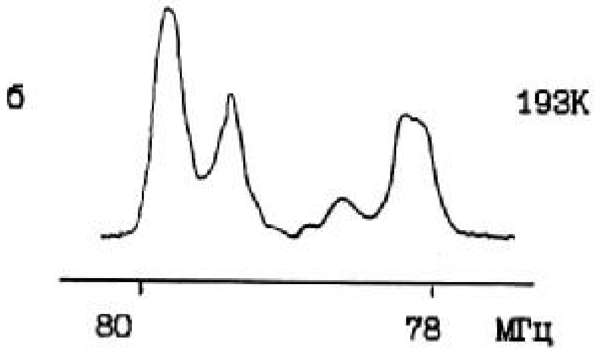

Fig.4.10 a) Calculated line shape in the long-period approximation Coexistence modulations third; 3/10, 1/4; 5/17; respectively, with weights of 4:2:1:1 ($A_q = 0$); b) Experimental

P-T phase diagram of Rb_2ZnBr_4.

In the beginning of this section briefly touch on issues of experimental measurements techniques not mentioned in Sec. 2. During the first stage, which was carried out in 1986-87, decided camping methodical task is to determine the possibility of equipment to record the "disproportionate" spectra at high pressures and determine increases or decreases the temperature range of the existence of Jc structure to such impacts [136,137]. This problem was originally solved by a high-temperature phase transition area using a titanium chamber NQR method and differential thermal analysis (DTA construct a cell for measurement is described in [74]). At temperatures below room used low-temperature cell HPC1. And only later, after the production of the second stage HPC2 managed to meet the challenge of a detailed study of structural changes in the J_c phase. In the study technique was used isobaric and isothermal changes of P-T parameters. The spectra were recorded with a temperature step of 5-10K and step pressure of 0.1-0.5 MPa. Frequency scanning range was from 55 to 78MGz. To control the sensitivity of the receiving path and to assess the impact of non-equilibrium processes in crystalline amplitude spectrum used NQR "frame". P-T field of study in HPC2 was 170-290K at pressures up to 0.4 GPa. Above these pressures and temperatures data obtained HPC1. Total about 20 iso-sections. tracked, recorded more than 300 spectra. The samples of high quality obtained with the growth of single crystals for NMR experiments. Due to the fact that data obtained in HPC2 far been published only in a succinct form, we elaborate on their description in this paper.

On Fig.4.11 open circles marks the position of the differential thermal break in the temperature curve passing P-Jc transition at different pressures. For comparison, in this figure, dotted line plotted P-Jc transition obtained later by Japanese researchers according dielectric measurements [59]. Note that the phase transition temperature T_i and DTA recorded at atmospheric pressure differ by more than 5K.

NQR measurements in the area of T_i conducted on high-line absorption signal from nucleus BrI.

(Presented below is a purely technical information intended for trainees and specialists experimenters. Panoramic reader can omit these routine details and go to end of this section.)

When isobaric changes in the phase transition observed "failure" in the intensity of this line, and at higher pressures, the line was not observable in a greater range of temperatures. These intentions have shown little promise HPC1 use design with a small diameter of the working channel for research NQR spectra near T_i. However, it was found that the temperature T_i with increasing pressure shifts to the high temperature region and the phase transition is smeared P-I (Fig.4.11).

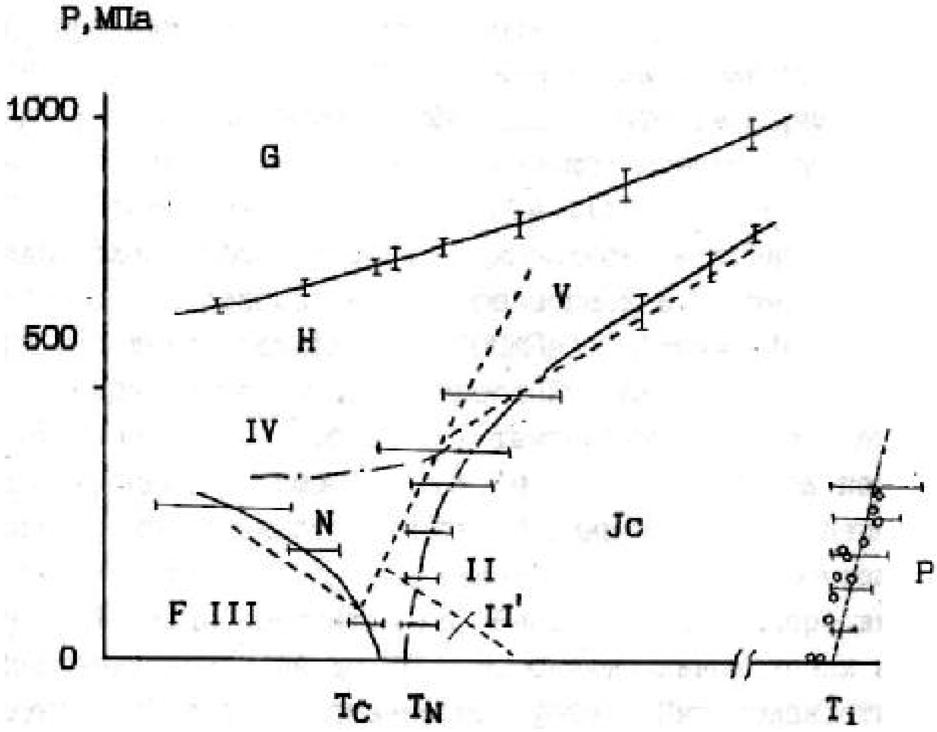

Figure 4.11. DTA data (open circles) near T_i, dielectric [59] (dotted lines, Roman notation) and NQR (continuous lines) measurements in the P-T region of the incommensurate phase of Rb_2ZnBr_4

lg I (RLU)

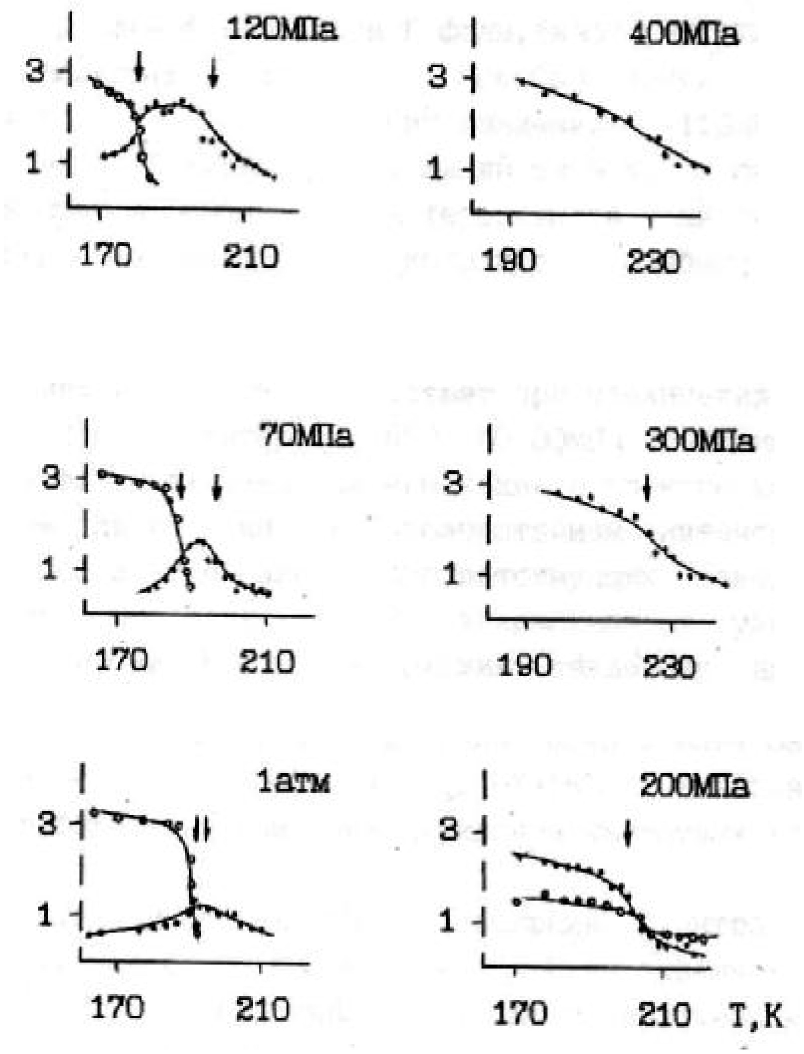

Fig.4.12 The relative intensity of the spectral lines NQR F10 and N10 at different pressures.

Much more informative studies were NQR in the transition from the incommensurate to the ferroelectric phase. At low pressures 100MPa near Jc, there was a marked increase in the intensities of the NQR lines of type N. With increasing pressure, the temperature region where these lines appear in the spectrum, expanding that recorded by changes in relative intensities of the "clean" lines of type N, NJ overlapped and FN and F types of spectral lines. The relative intensities of the course is illustrated by the example of Fig.4.12 lines F10 and N10. In the pressure range up to 250MPa. The spectral lines of these types coexist in the incommensurate phase. Intensities of the lines of type N increases gradually and at pressures higher than 250MPa spectrum consists of 14 discrete lines, which were correlated with the existence in this pressure commensurate phase N.

In isobaric measurements at 200MPa with decreasing temperature, a phase transition to the ferroelectric structure, which is characterized by intense 12 discrete absorption NQR (line Fl - F12). With increasing temperature above 210K spectra intensity gradually decreases. Area of P-T parameters (where the overall intensity of the spectra decreases) designated by us Jc symbol on Fig.4.11 can be roughly separated from the rest of the low-temperature region of the incommensurate phase.

During the measurements, it was also found that the isobaric passages corresponding to high pressures from the incommensurate phase transitions (Jc) in the N phase and ferroelectric phase strongly blurred. Changes in the intensities F, N and overlain groups of lines are so gentle that above 150MPa definition phase transitions becomes difficult. Fig.4.11 on the phase diagram based on the results of isobaric studies [116,118,136,137]. Experimental data suggest the possibility of a more complex structural changes in the N phase. These assumptions were confirmed by us in isothermal studies CPH2 [111,112,116], for a detailed exposition of which we proceed.

Increased pressure in the F phase (isotherm 173, 183 and 188K) possible to observe the following transformations NQR spectra: Fig.4.13, 4.14 and 4.16. Pressures up to 90-110MPa observed only 12 lines of F type. Traces type lines N, due to the lower sensitivity in a bomb than a heat chamber, is not recorded. The above values range complemented weak spectral lines of type N (shaded areas on the spectrum Fig.4.13 and 4.14). Their intensity increases with increasing pressure to ~ 150MPa, and further in the range of DP ~ 60¸ 30MPa stabilized. With further increase of pressure changes in the spectrum are characterized by the disappearance of the lines of type F, increase the intensity of the N lines and the appearance of lines corresponding phase H: H-lines. Intensity increases dramatically past a narrow range of pressures above 250¸ 280MPa and at higher pressures there is powerful resonance lines 14, two of which, at frequencies 65.8 MHz and 66.7 have twice the strength.

On Fig.4.15 presented as an illustration of the baric stroke frequency of the NQR spectrum of Rb_2ZnBr_4 at T = 183K. In the phase transition region the slope of the frequency of moves and jumps NQR frequencies.

Features isothermal evolution of the spectrum in the P-T field is an extension of P-interval overlap (coexistence) lines of type F and N with increasing temperature isotherm. So at 189K coexistence region F and N spectral lines is about 30MPa at 188K 40MPa and at 173K - £10MPa. However, the transition to the isobaric change in temperature in the range 160-200MPa, the coexistence lines of type F, N and H extends over a wide temperature range over 40K and 200MPa isobar on phase transitions in H or F phase was not observed up to 150K. These data indicate that the region of coexistence the phases

183K

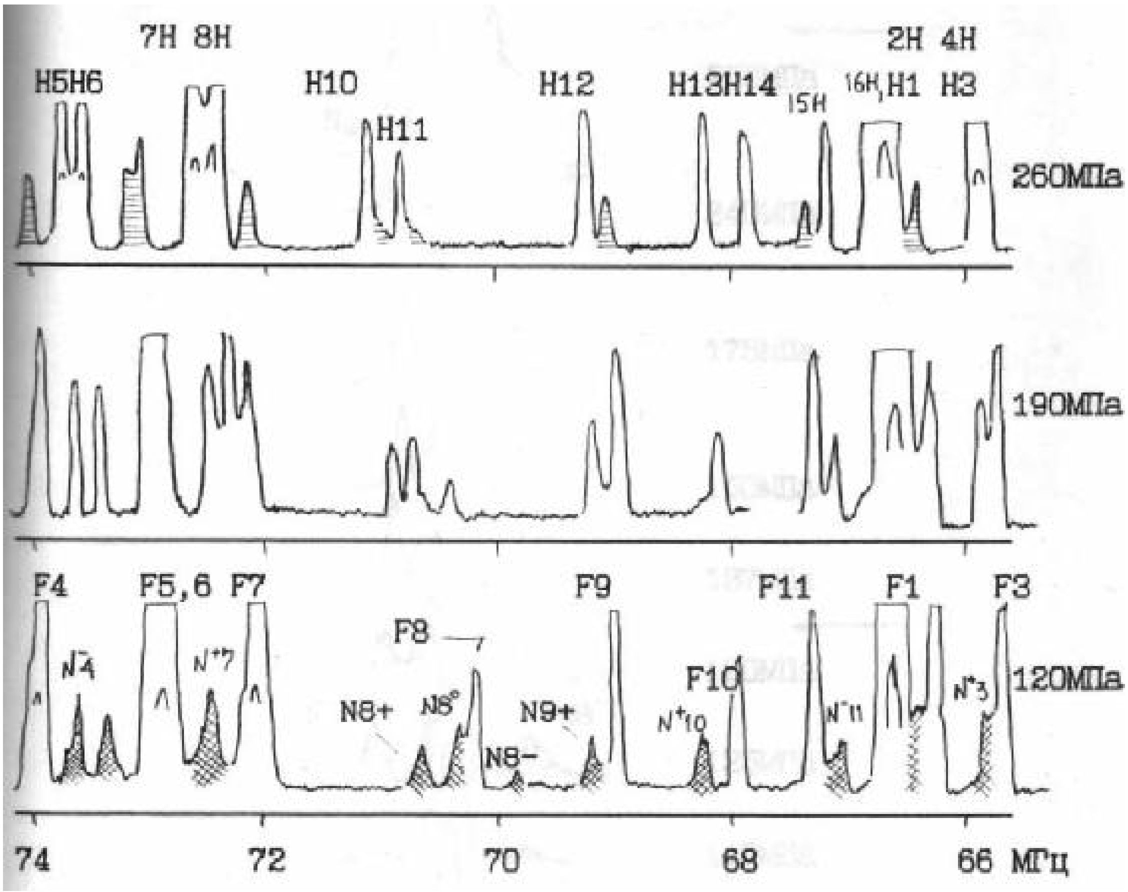

Fig. Full Br NQR spectrum in RZB at T = 183K and different pressures.

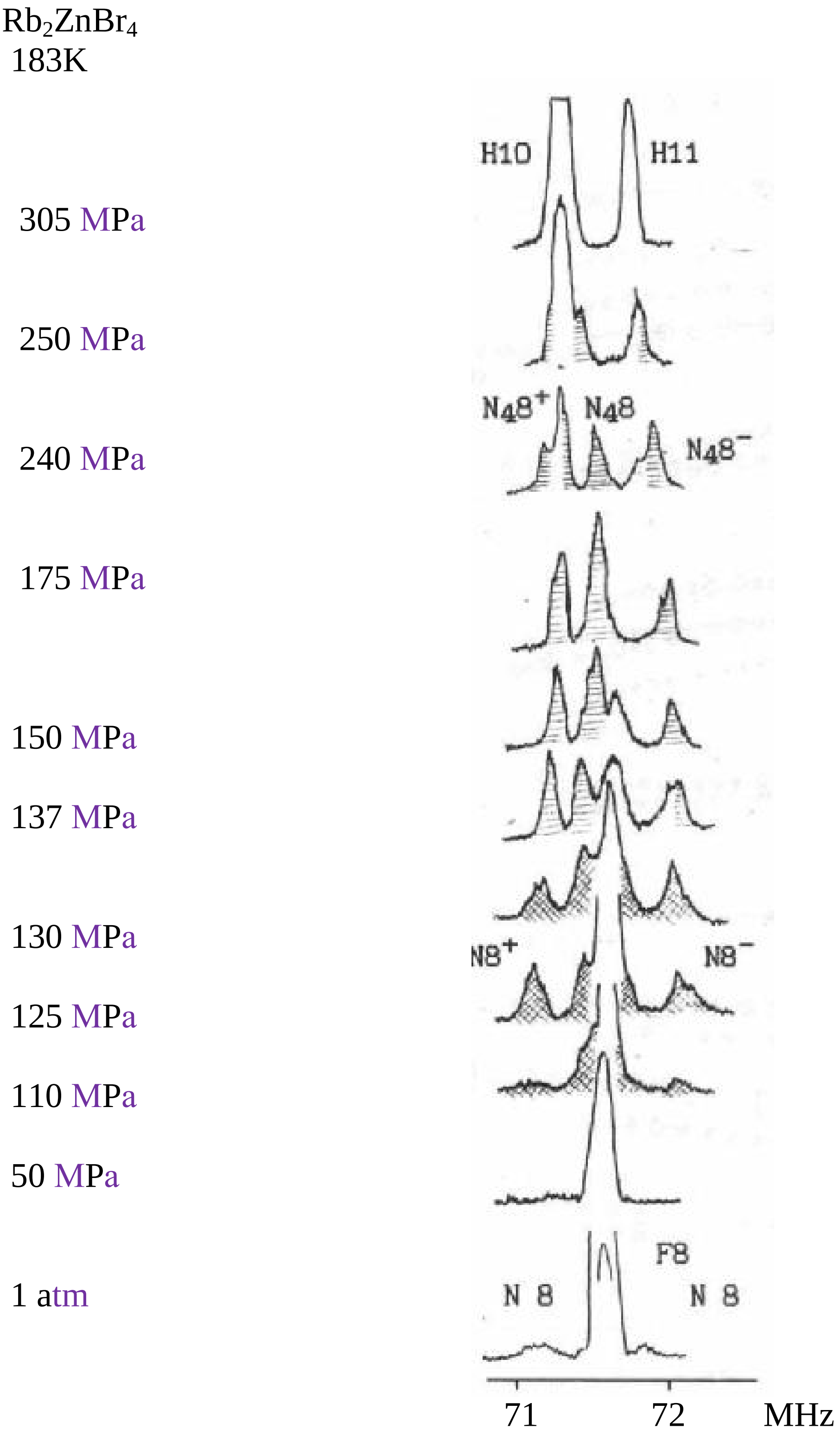

Fig.4.14. Changing of the NQR spectrum with increasing pressure at T = 183K.

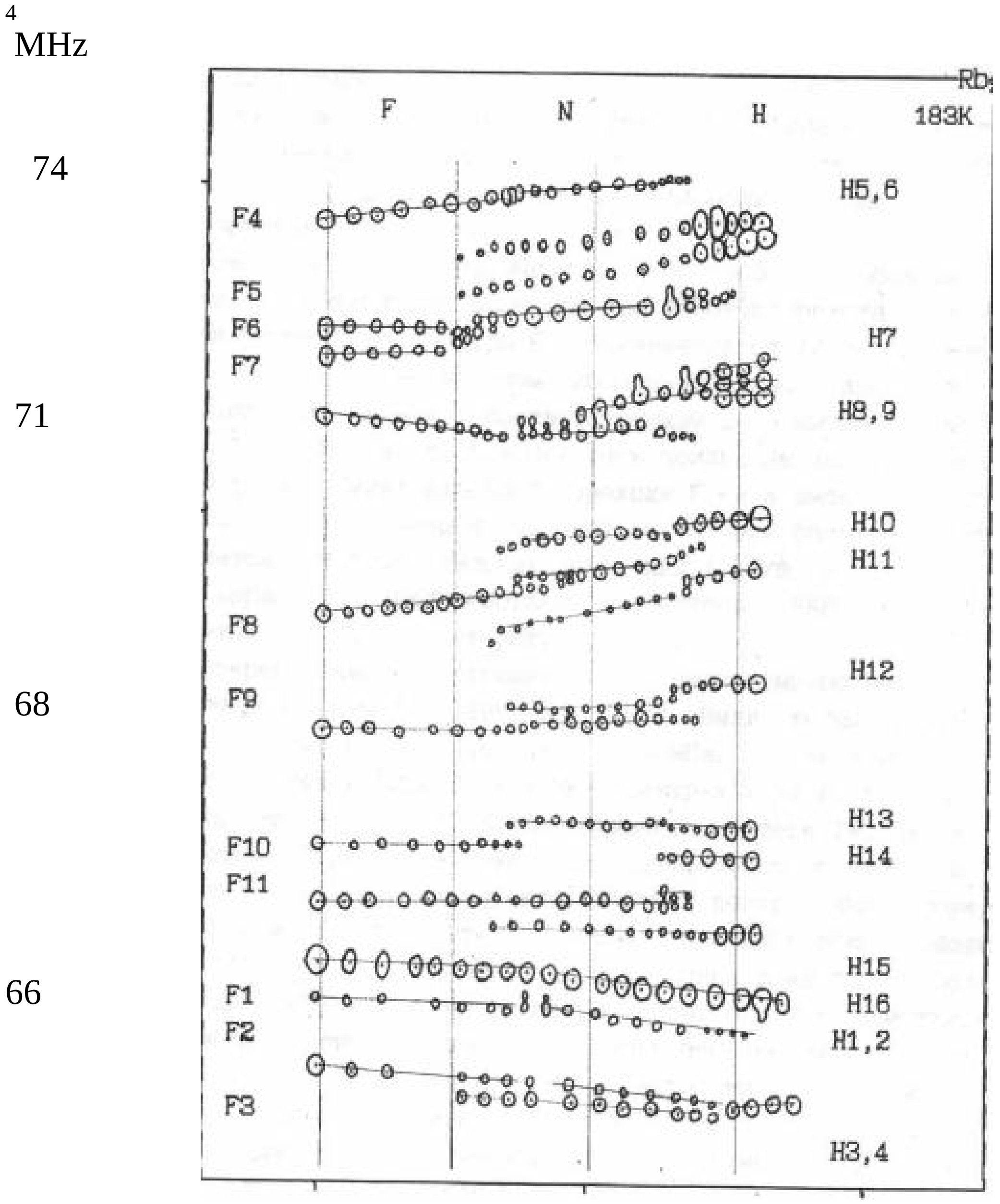

Fig. 4.15. Baric stroke line frequencies of the NQR spectrum at T = 183K.

dependent on the direction of change of the parameters P- T in relation to the P-T-phase lines.

As the pressure decreases from phase H hysteresis of phase transitions. To move H « N DP 20 ¸ 40MPa, the transition F « N DP from 30 to 6OMPa where value increases with increasing temperature.

Thus isothermal method at low temperatures clearly recorded two phase transitions F«N and N«N. Multiplicity NQR spectrum varies from 12 lines of singlet type F, through no less than 20 spectral lines of N type to sixteen NQR lines, corresponding to the high pressure phase N. Both phase transitions in classical featured are first-order transitions. Phase transition line F« N is negative ¶P/¶T Phase transition H« **N** at high temperatures observed at higher pressures (¶P/¶T = 2,86 MPa/K) with a character transformation spectra NQR does not change significantly at temperatures up to 210K.

Isothermal studies in the field of low-temperature incommensurate phase (from 189K to 200K) were performed in detail with step 10¸ pressure 50MPa. Let us consider the general patterns observed in the NQR spectra in this area.

On Fig.4.16 and 4.17 for example isotherms T = 198K and T = 190K presented baric Frequency spectrum lines. Due to the fact that in this area of P-T observed spectral distribution with a complex change in intensity on the pressure dependence (Fig.4.17), except for specifying the frequency of the peak of each distribution, a closed oval contour scheduled spectral distributions that reflect their intensity and area of overlap. On Fig.4.26 and 4.27 are graphs of peak intensities. With increasing pressure, the overall intensity of the spectra increases and decreases the half-width frequency distributions. At a certain pressure, in the absence of frequency overlap, have seen the emergence of new lines (for example N8$^{+,}$ N8$^{-,}$ N11^{+}) Fig.4.17. P-T boundary area of occurrence of these lines at high temperatures is shifted to higher pressures and the phase diagram it is possible to compare a certain P-T line at = 150MPa and 200K (Fig.4.24). When crossing this line is also measured the change in peak intensities most NQR signals. With decreasing, the pressure indicated hysteresis in the position marked abnormalities DP 40MPa.

Thus, all indications in phase N, a phase transition from a phase existing near atmospheric pressure to a phase N4, the previous high-symmetry phase N. A detailed analysis of the spectral data (see § 4.3) shows that the evolution of the NQR spectrum in the P-T region is represented by a more complex way than the coexistence of spectral lines F, N or HN type. At pressures of ~260MPa, clearly observed phase N« H transition.

We now describe the data in isothermal studies CHP2 in the middle region of the incommensurate phase (above 200K). The characteristic form of NQR spectra in this area is presented in Fig.4.18. Fig.4.19 on the example shows a typical isotherm 219K baric frequency dependence of NQR lines, and change Fig.4.20 peak intensity spectral component at the frequency J14 - 67.3 MHz, which is characteristic for the other lines of the spectrum.

At atmospheric pressure, the shape of the spectrum is represented by a small number of resolved components (Fig.4.18a). This form is maintained until the pressure 200MPa, where there is the first anomaly. So blurred spectral distribution at frequencies 69¸ 66,5 MHz (line group conventionally designated J13-J16) above 200MPa varies considerably (Fig.4.18b). Shape of the spectral distribution J5-J6 and J7-J8 also converted by increasing the circuit under their new spectral components. Group lines J1-J4, at atmospheric pressure characterized by a continual distribution between edge peaks above 200MPa

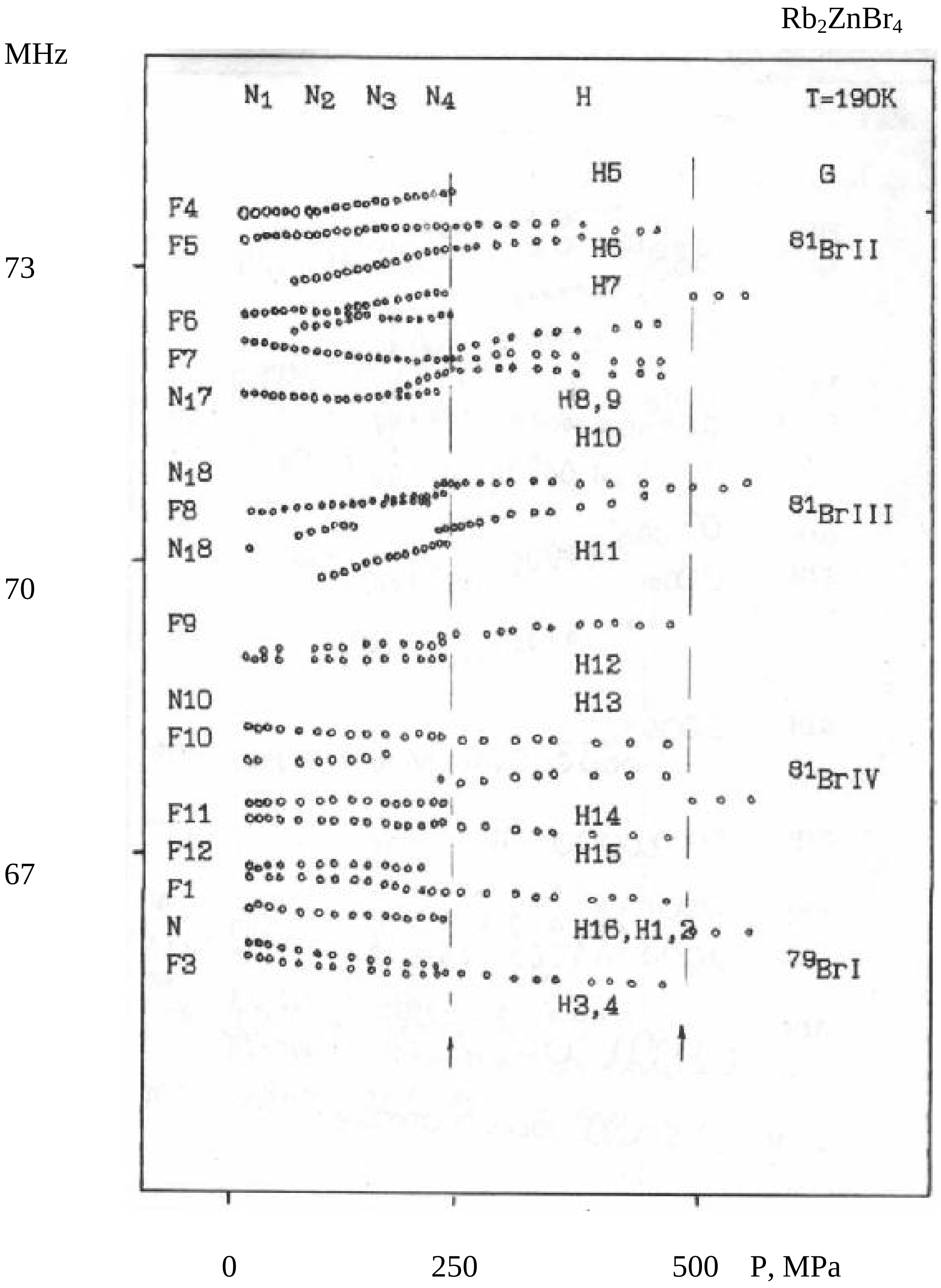

Fig. 4.16. Baric move NQR frequencies at T = 190K.

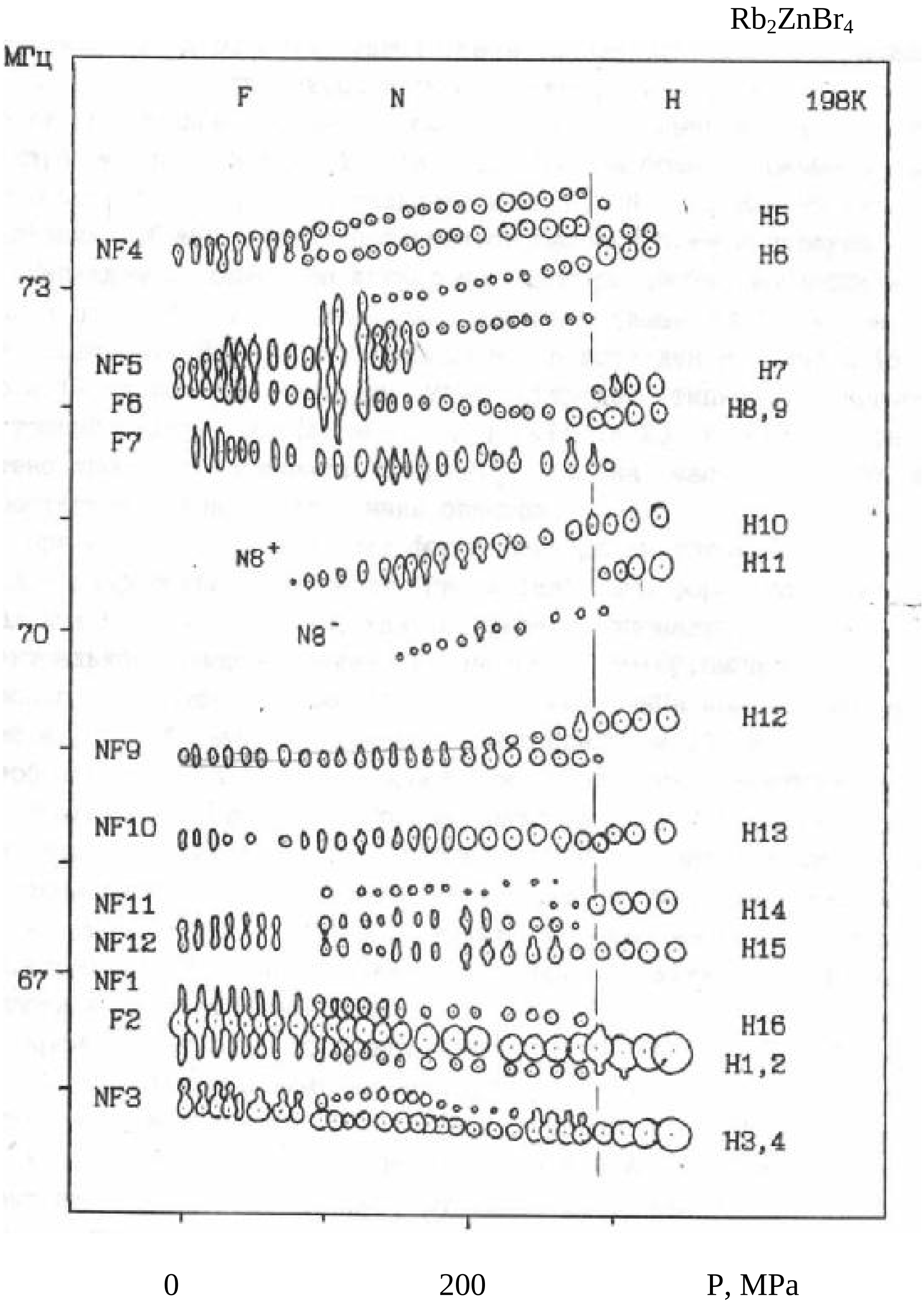

Fig. 4.17. Baric move NQR frequencies at T = 198K.

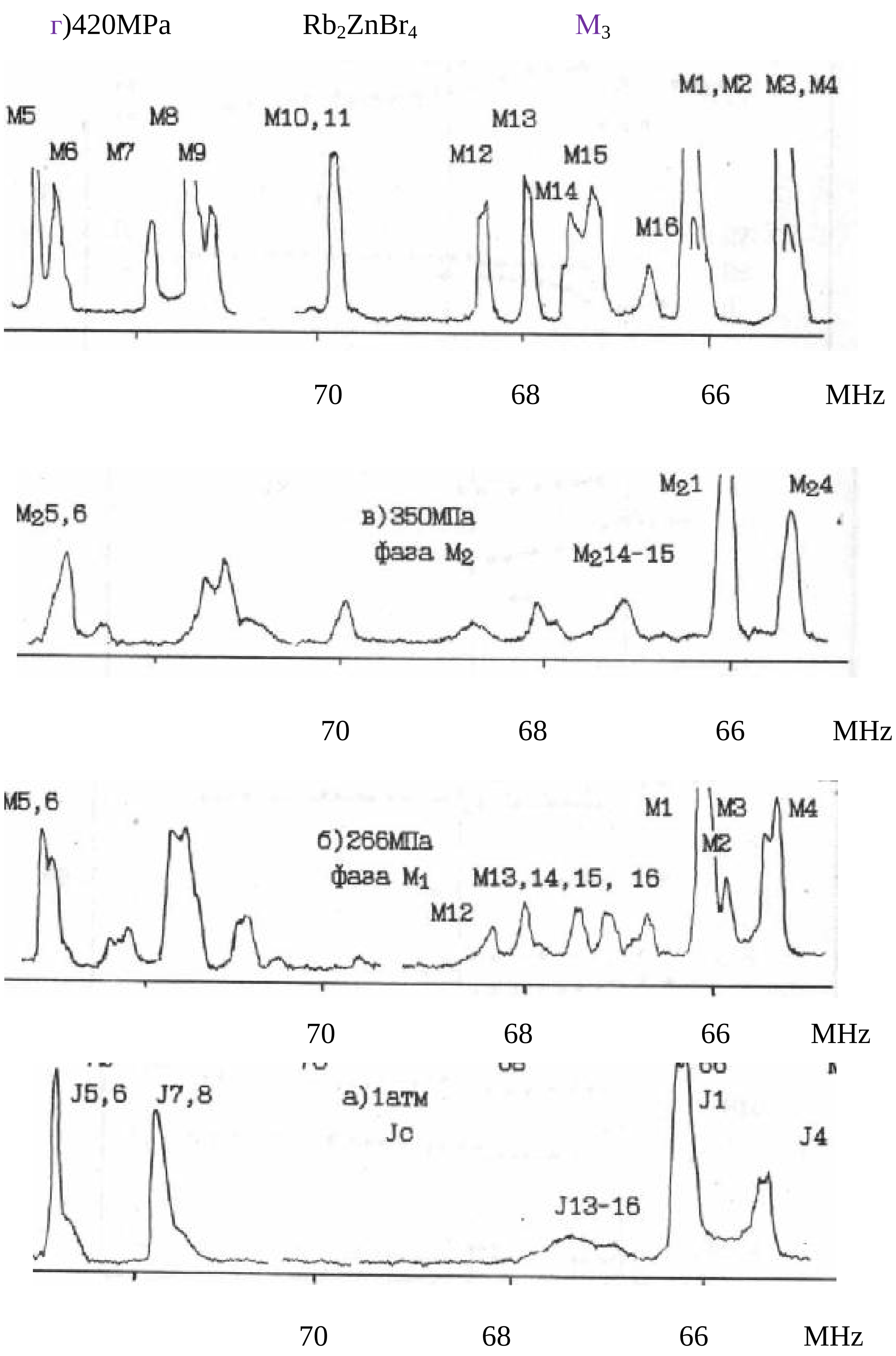

Fig.4.18.Change NQR spectrum at T = 228K

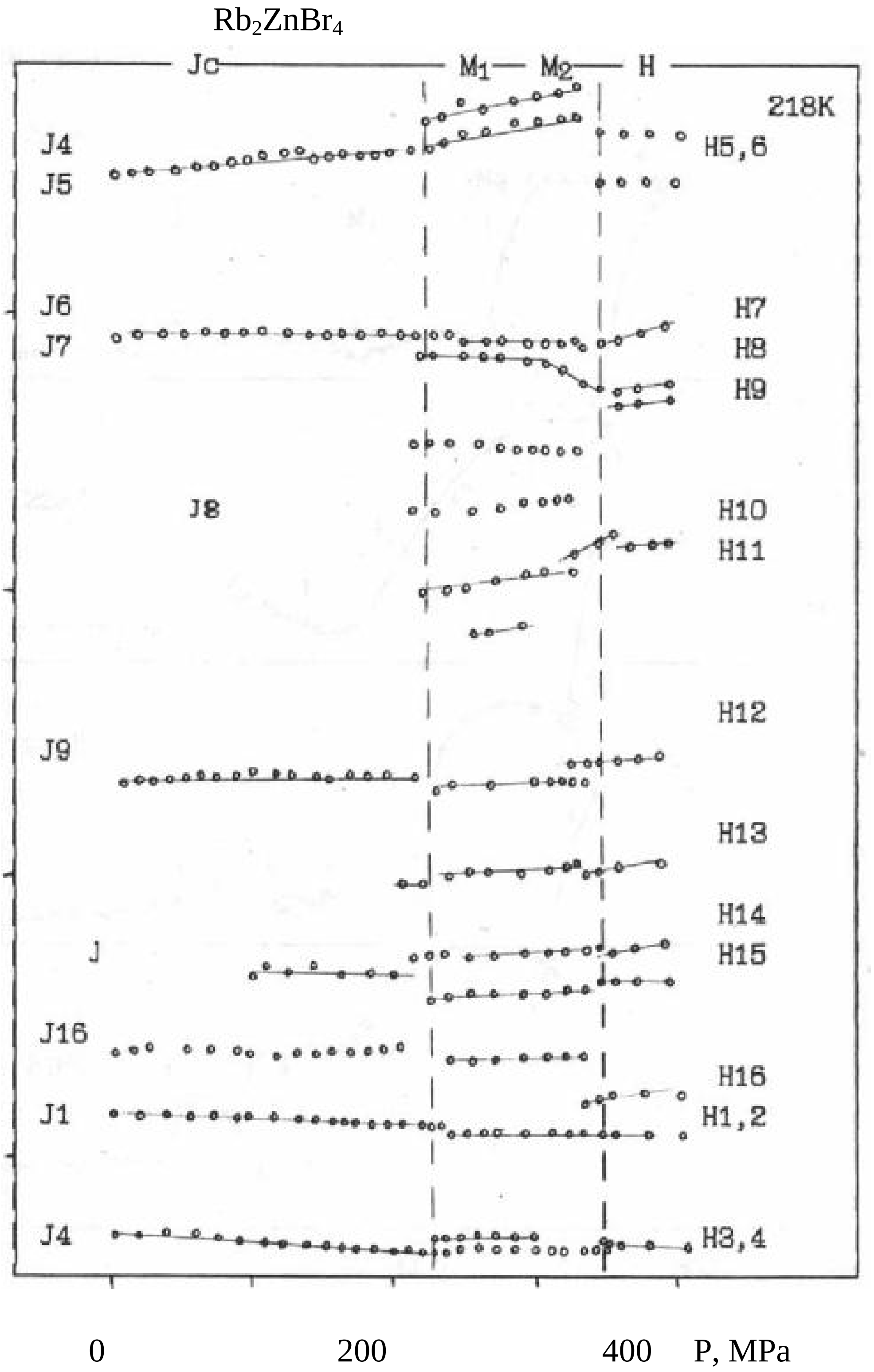

Fig.4.19. Baric move NQR frequencies at T = 218K.

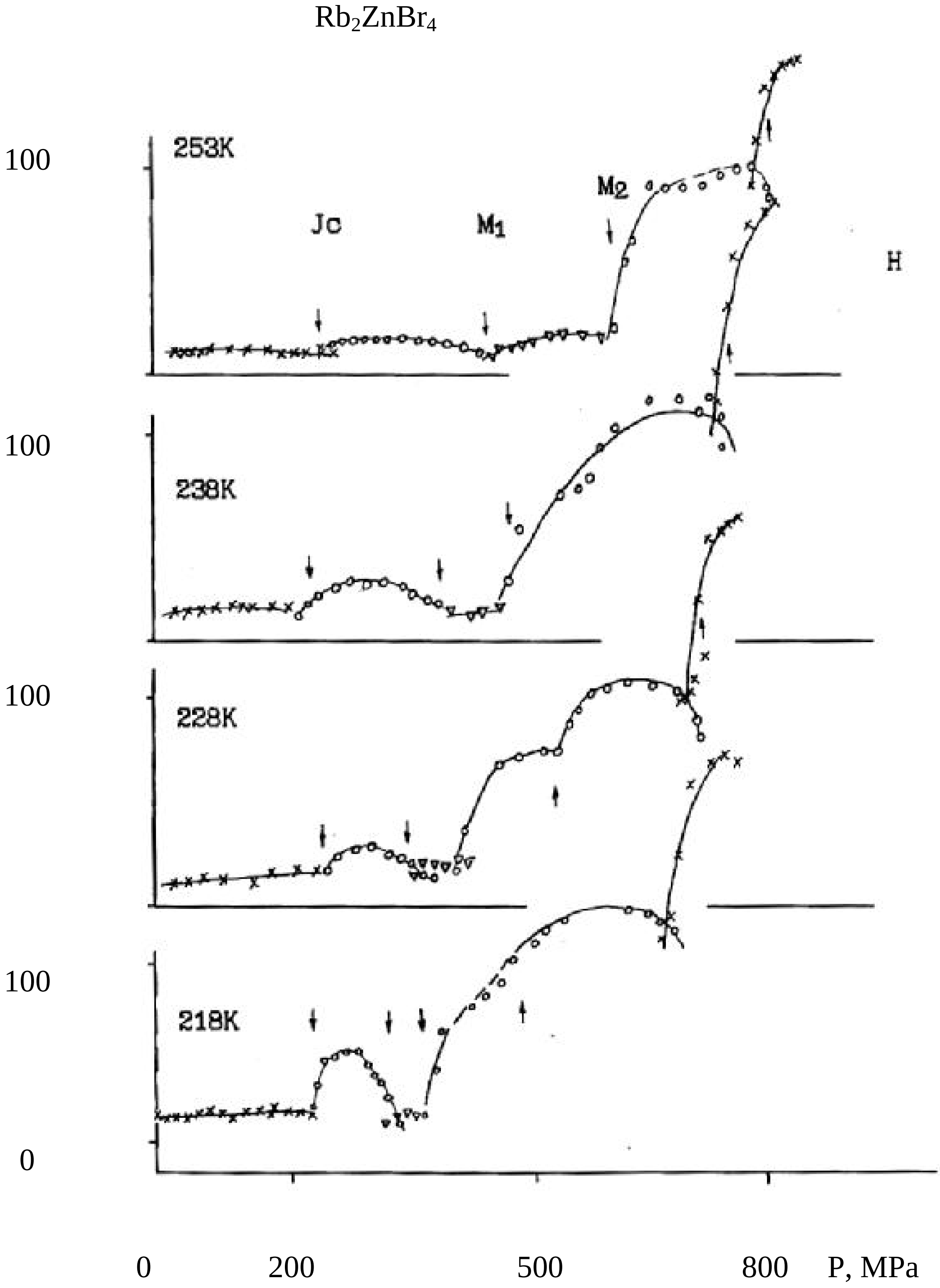

Fig.4.20a-g. Baric change in the intensity of the spectral lines NQR type J4-M14 at different temperatures.

Rb_2ZnBr_4

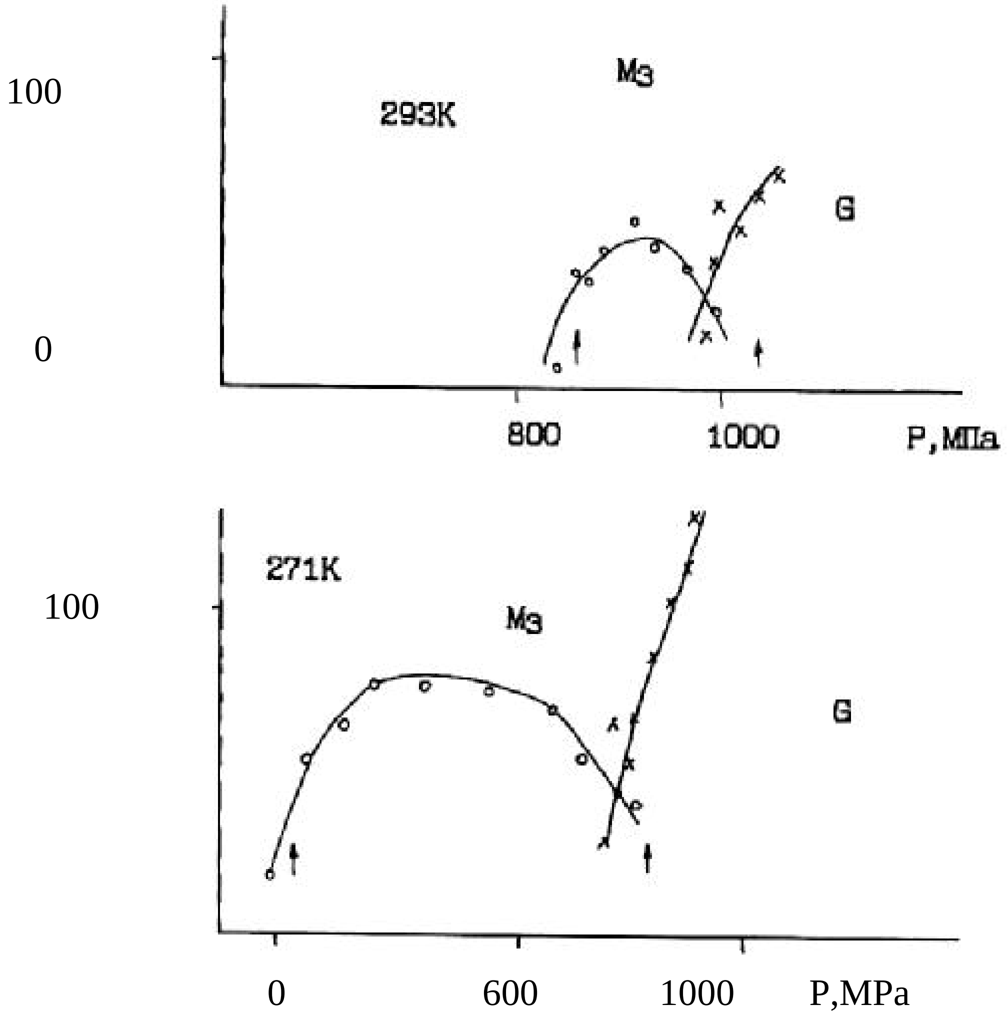

Fig.4.20d th. Baric change in the intensity of the spectral lines NQR type J14-M14 at different temperatures

proceeds to the frequency resolution of the form M1 - M4. Absorption signals at frequencies 70-70,5 MHz observed only above 200MPa, and at high temperatures in all of high pressures.

Also noticeable transformation of the spectrum shape (Fig.4.18a and 4.18b) measured the change in the half-width distributions and their peak intensities (Fig.4.20). Thus, a phase transition from a phase of Jc to a new phase marked by us symbol M1. With increasing temperature recorded overall reduction ratio S/N Features characterizing the anomaly Jc« M1 becoming less distinct and isotherm 250K completely blurred. When the pressure is reduced there is a significant hysteresis of the phase transition Jc« M1 about DP 160MPa. Fig.4.24. Marked change in the slope of the phase transition to negative ¶P/¶T = -75Pa/K.

As the pressure increases in this temperature range by a second anomaly. It is characterized by changes in the forms of spectral distributions (Fig.4.186 and 4.18v), especially during the peak intensities of all lines (Fig.4.go), as well as a notable change in the frequencies of spectral peaks and slopes of the frequency dependencies (Fig.4.19).

Transition into a new phase, which we denote by M$_{2,}$ with increasing temperature isotherm is shifted to higher pressures with a positive slope with respect to the temperature axis ¶P/¶T » 110Pa/K .At temperatures above 260K transition line M$_1$« M$_2$ is not tracked due to the excess of its intended position limit values HPC2 pressure, and in the case HPC1 not sufficient sensitivity of the apparatus. Hysteresis transition M$_2$« measured isotherm 211K is about 50MPa.

When pressure rises above 400MPa width of the spectral distributions decrease at a certain pressure and intensity of the NQR lines increases sharply, then stabilized again (Fig.4.21 and 4.22). There is a new spectral line frequency offset with respect to the spectral lines of phase M$_{2.}$ This spectral anomaly, we compared with the phase transition into the next phase of high pressure M$_3$. Position of the transition points determined from the inflection in the course of baric intensities of the NQR lines M12-M16 (Fig.4.22). At high temperatures, the anomaly in the transition M$_2$« M$_3$ is fixed much clearer. The slope of the transition line between phases M$_2$ and M$_3$ is ¶P/¶T =*8MPa/K. Hysteresis transition DP »40MPa.

Thus, when the pressure in the middle of the incommensurate phase observed sequence of phase transitions J« M$_1$ « M$_2$ M$_2$« M$_3$ The decrease in the width of the spectral lines indicates the ordering of the incommensurate structure with increasing pressure.

With increasing pressure above 500MPa, or with decreasing temperature below 25OK in this P region, the shape of the NQR spectrum continues to change (Fig.4.23) and transformed to characteristic of phase N. Due to the large step measurements (5-10K, 50MPa) in the P-T range, and the vagueness of the anomaly, the proposed line separating phase M$_3$ and H is fixed with a large error.

Rb_2ZnBr_4

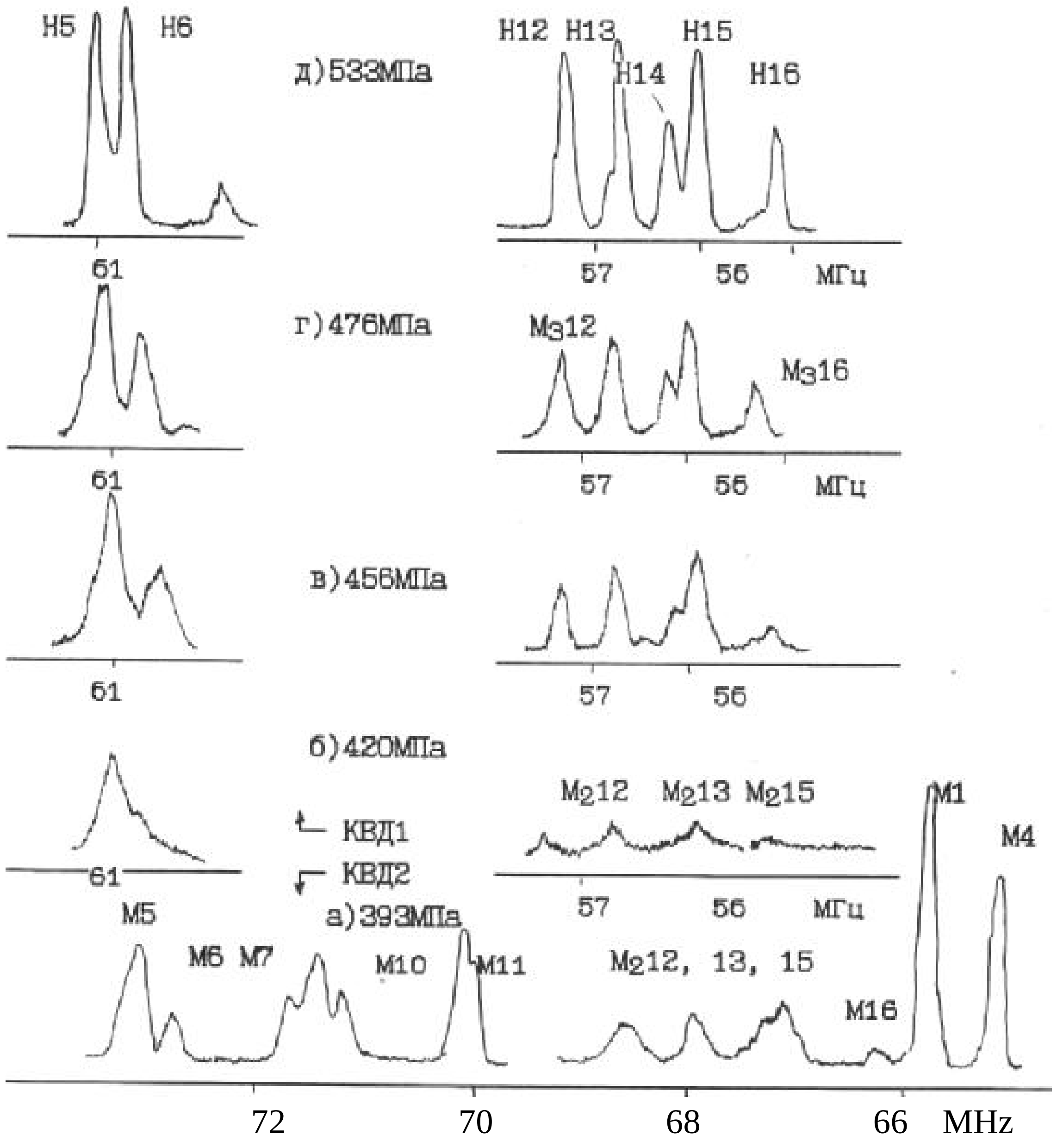

Fig.4.21. Convert NQR spectrum in the phase transition M_2« M_3 M_3« H.

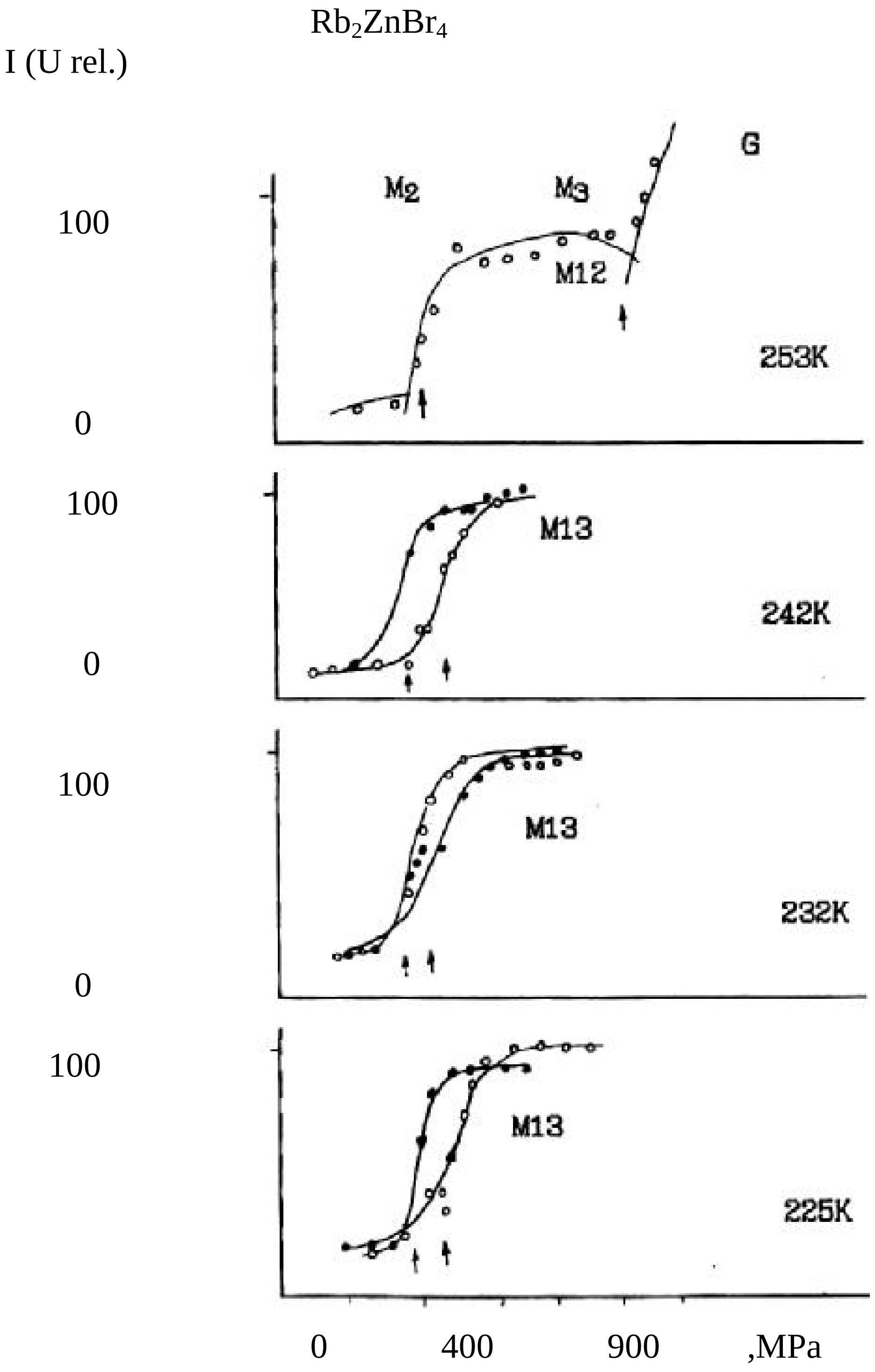

Fig.4.22. Baric of the intensity of spectral lines M13 (M12) in the phase transition M_2 « M_3 at different temperatures.

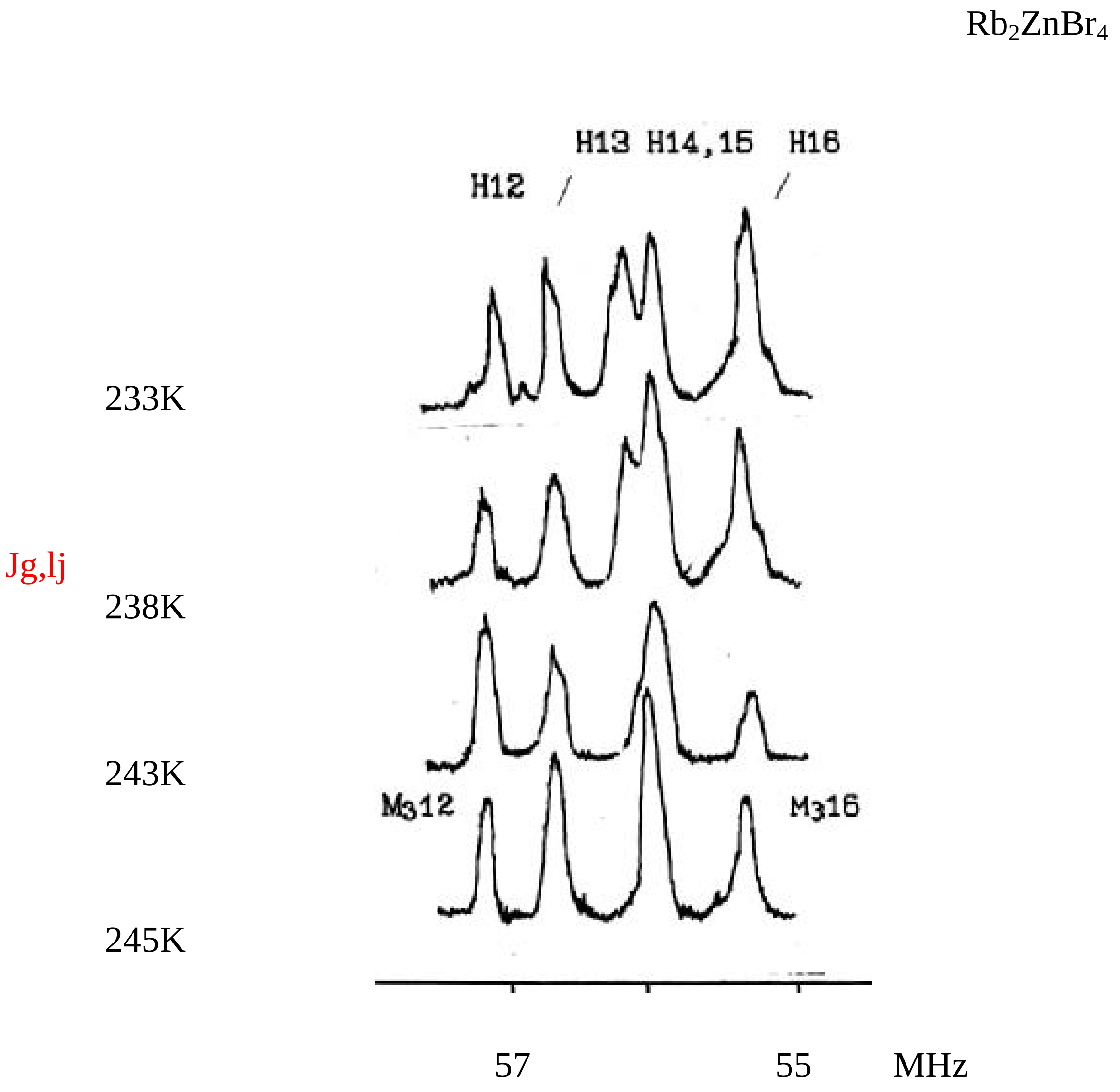

Fig.4.23. Changing of the NQR spectrum in the phase transition M_3 « H at P = 500MPa.

Final step of transforming the structure of Rb_2ZnBr_4 at high pressure is highly symmetric phase **G,** which is characterized by four powerful singlet absorption lines NQR radio nucleus BrI, BrII, BrIII and BrIV (Fig.4.18). Phase transition in phase G is a first-order transition, because, although no hysteresis phenomena (up 5MPa), there is a region of coexistence of phases. End increases with increasing temperature, and this transition is independent of the direction of change of P-T parameters.

Measurements at pressures above the transition to the 6 were not conducted.

P-T phase diagram of Rb_2ZnBr_4 - On Fig.4.24 shows the experimental P-T phase diagram rubidium tetra zinc bromine in the 160-300K at pressures up to 1.0 GPa, built on the results of our data. In addition to the well-studied at atmospheric pressure paraelectric (P), incommensurate (Jc) and ferroelectric (F) phases, it was discovered or suspected the existence of several phases with different structures and symmetries.

By type and nature of changes NQR spectra investigated P-T range can be divided into two areas: 1) the area where the spectrum consists of a small number of intense singlet lines (phase F, G, F and H) and the structure of the phases described by one of the space groups simorfnyh; 2) The second area where the species and the evolution of the spectrum can be associated with the existence of more or less disordered structures (phase N, M and Jc).

Para-electric and the ferroelectric phase are known as spatial symmetry D_2^{16h} (Pnma), and C_2^{9V} ($P2_1/n$), respectively. With this in mind, using the symmetry transformation rules involving data from NQR, we can show that the phase of H must have a rhombic or monoclinic symmetry. Availability 14 NQR lines, two of which have double the intensity allows unequivocally enough to suggest that this phase is described by the point group symmetry $P2_1$ quadruple unit cell volume ($V = 4$, $Z = 16$). Highly symmetric phase G, which is characterized by four nonequivalent positions in structure Br nucleus may have a monoclinic or triclinic symmetry with unit relative to the paraelectric phase, the unit cell volume ($V = l$).

The latter assumption is supported by extensive, approximately 4-fold, increase in the integral intensity of each of the four NQR lines. Reduction of vernix with increasing pressure and temperature indicating the approach to a particular T-P point in the phase diagram. It also indicates the position of the P-T phase line separating Jc and P and P-Jc blur transition with increasing pressure. Based on this and several other reasons, we assumed the existence of the Lifshitz point, which should be located at the intersection of P-T lines separating highly symmetric phase G and P (Ris.4.35).

Region of existence of the disordered structure can also be divided into three parts:

1) low-temperature region N, where there is a well-defined frequency resolution and intense spectral components or groups. In this area, we can assume (with) the existence of long-period nearly commensurate structures;

2) P-T region Jc, where there are blurred spectral shape characteristic of the incommensurate phase (disordered structure of long-period);

3) Field of phases M where NQR spectra have more or less frequency resolution basis. The degree of ordering of the structure is increased when approaching the phase transitions in lines H and G phase. Reduce the blurring and hysteresis transitions between phases M1, M2, M3 with increasing pressure, also indicates the nature of the structural transformations.

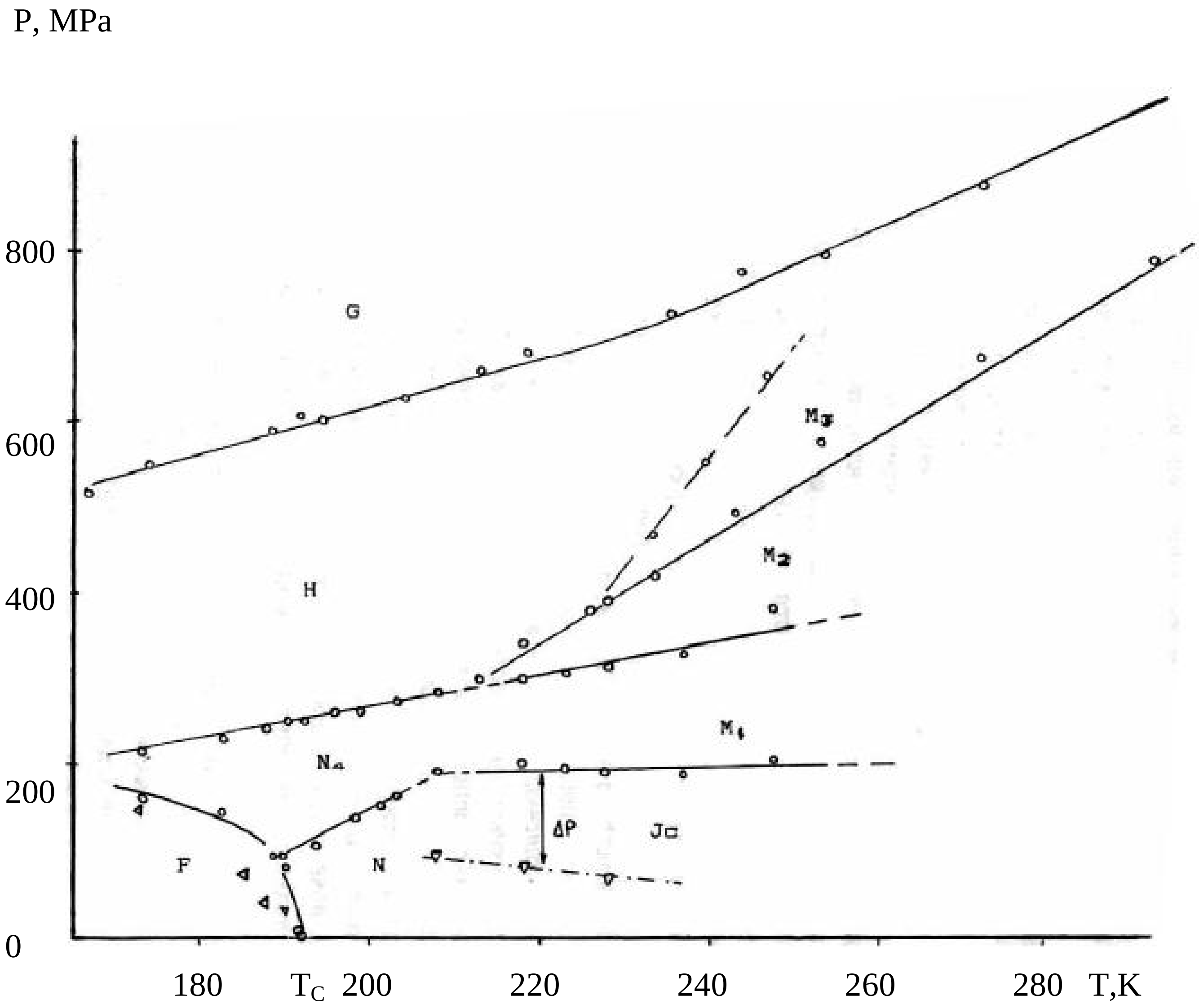

Fig. 4.24. Phase diagram of Rb_2ZnBr_4, obtained by NQR.

As in most of incommensurate phases dielectrics family A_2BX_4 and in compounds with CDW [63,96] hysteresis phenomena are global in nature, and there is a large range of variation of hysteresis phenomena in different surroundings investigated P-T region, from 20 to 160MPa.

Note also feature observed in passing phase transitions F« N« H for different directions of change of P-T parameters (Chapter 4 § 2). This behavior indicates a specific data type conversions, due to the presence of significant non-equilibrium phenomena. Registers significant blurring if the transition phase as it passes along the line, compared with the transverse passage. This is apparently due to a clearer and observation of phase transitions isothermal scan compared with isobaric.

Thus as a result of these studies failed to establish the following:

1) With increasing hydrostatic pressure P-T transition is shifted to higher temperatures;

2) At pressures above 250MPa and temperatures below 220K observed commensurate phase H presumably rhombic symmetry $P2_1$ and quadruple volume;

3) Has a highly symmetrical above 500MPa phase G, with the same, relative to the paraelectric phase, the unit cell volume (V = 1) ;

4) Low-temperature region of the existence of an incommensurate phase increases with increasing pressure up to 250MPa, phase transitions F « N, N « H in isobaric mode significantly eroded;

5) Close T_C observed a special P-T area, increases with increasing pressure and is characterized by the coexistence of different groups of spectral lines;

6) In the middle region of the incommensurate phase in zoom mode pressure observed sequence of phase transitions Jc® M_1® M_2 ® M_3 ® G, Apparent to transform NQR spectra.

Almost simultaneously with our studies were performed measuring the dielectric constant of RZB at different pressures [59]. Although this method is less sensitive than the NQR method, the author managed to watch some anomalies. Position of the phase transition points, tracked in this study was determined from the temperature dependence of the maxima e(T,P), which in most cases were observed strongly blurred.

Comparison of the phase diagram Gezi (Fig.4.11) with our data shows that in the pressure 250MPa near T_C, where we tracked a special area of the phase diagram, the triple point (see details in § 4.3), by e-measurements also assumes the existence of a triple point. There is a clear coincidence P-T lines between II (Jc) and V phases Gezi and P-T line P_3^+ (M2« M3) tracked in this study. However, other data show significant differences. First, there is no phase transition line between phases G « H, « M « N and I « M1 « M2 observed using NQR. Secondly there is the P-T phase line separating Jc in at atmospheric pressure (phase II and II' in the notation Gezi). In this case the author notes that the P-T line between phases II'-II and IV-V are fixed and not very clearly in cooling mode only, and e-peak between II(Jo) and IV phases smeared with increasing pressure. Data differences in our opinion due to the following. First, the significant influence of nonequilibrium processes, as we discovered the character structure transformation depends on the direction and rate of change of external influence. Secondly, impurities. Third, the difference polycrystal-monocrystal. It is therefore possible for a shift of the phase transition lines and their degree of fuzziness for samples of different states and crystallization.

Taking these arguments, we can explain the discrepancy between some of the data as follows. The P-T transitions between phases H« N, I« M_1« M_2 is not recorded in the e-measurements due to their small inclination to the isobaric directions of measurement.

2) Mild line between phases II and II'(Gezi observed in cooling mode only), correlates with the position of P-T line P_1 (M_1« Jc, recorded by us in reducing the pressure mode. The difference in the absolute position PT can be explained along with the above arguments, the difference in the determination of transition criteria.

§ 4.3 Features conversion spectrum near $T_{C.}$ Comparison with the diffraction data.

In this section we consider in detail the change NQR spectra in the low temperature region of the incommensurate phase. As noted in § 4.2 in the P-T region of the absorption spectrum is observed, formed by the overlap of different types of spectral lines Fig.4.25, 4.29, 4.32, 4.34.

Plotting changes in peak intensities with the pressure reveals non-monotonic dependence. Presents data on Fig.4.26 typical changes in the intensities of the spectral lines with the majority of the increase in pressure, and Fig.4.27 as an example - baric moves peak intensities of lines N4, $N4^{+,}$ close in frequency to the line F4. Well tracked fractures in galleries intensities. This behavior confirms the hypothesis based on nonsinglet lines and change their shape due to redistribution of the intensities of the different components.

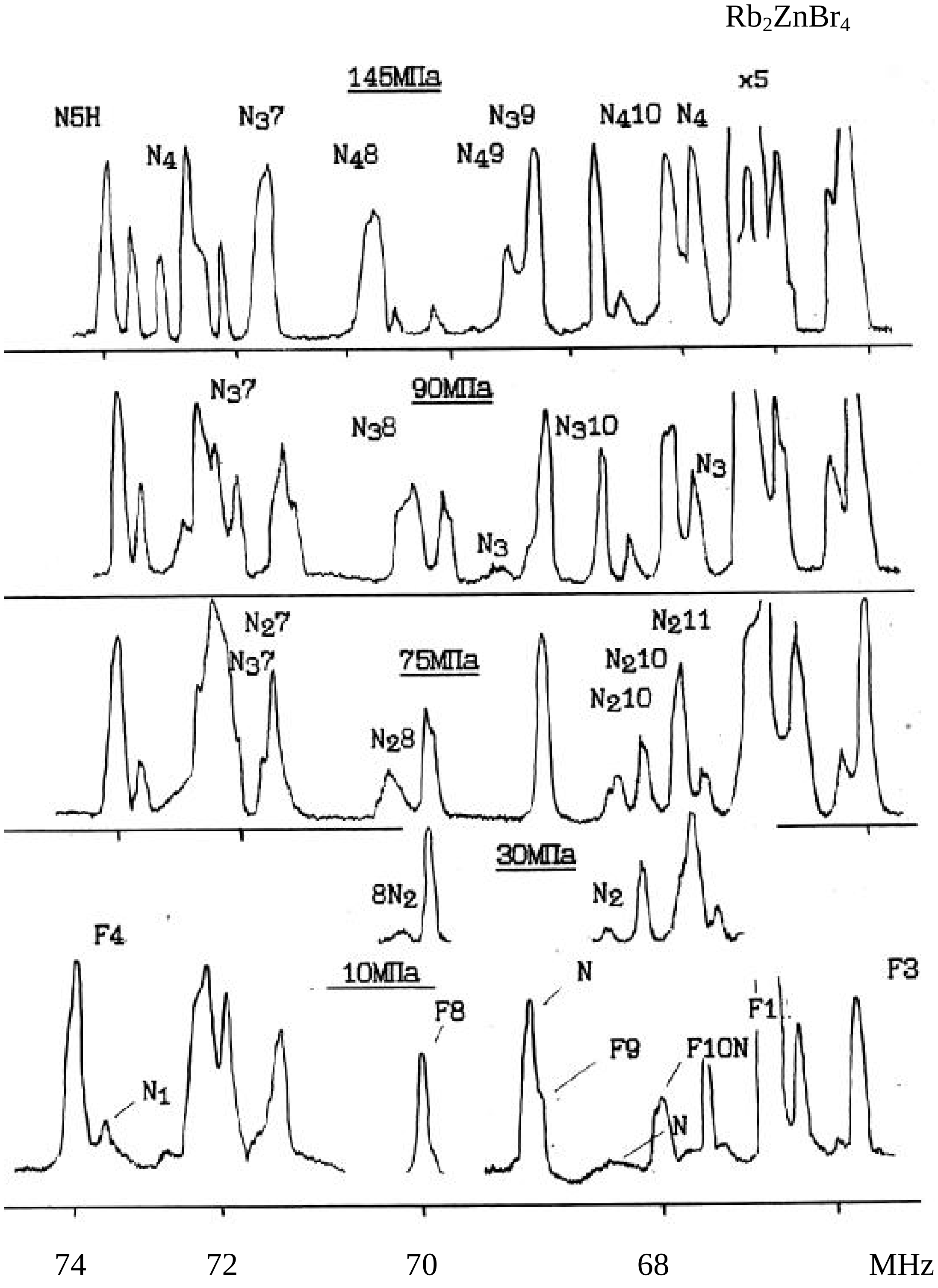

Fig.4.25. Change NQR spectrum with increasing pressure at T = 189K.

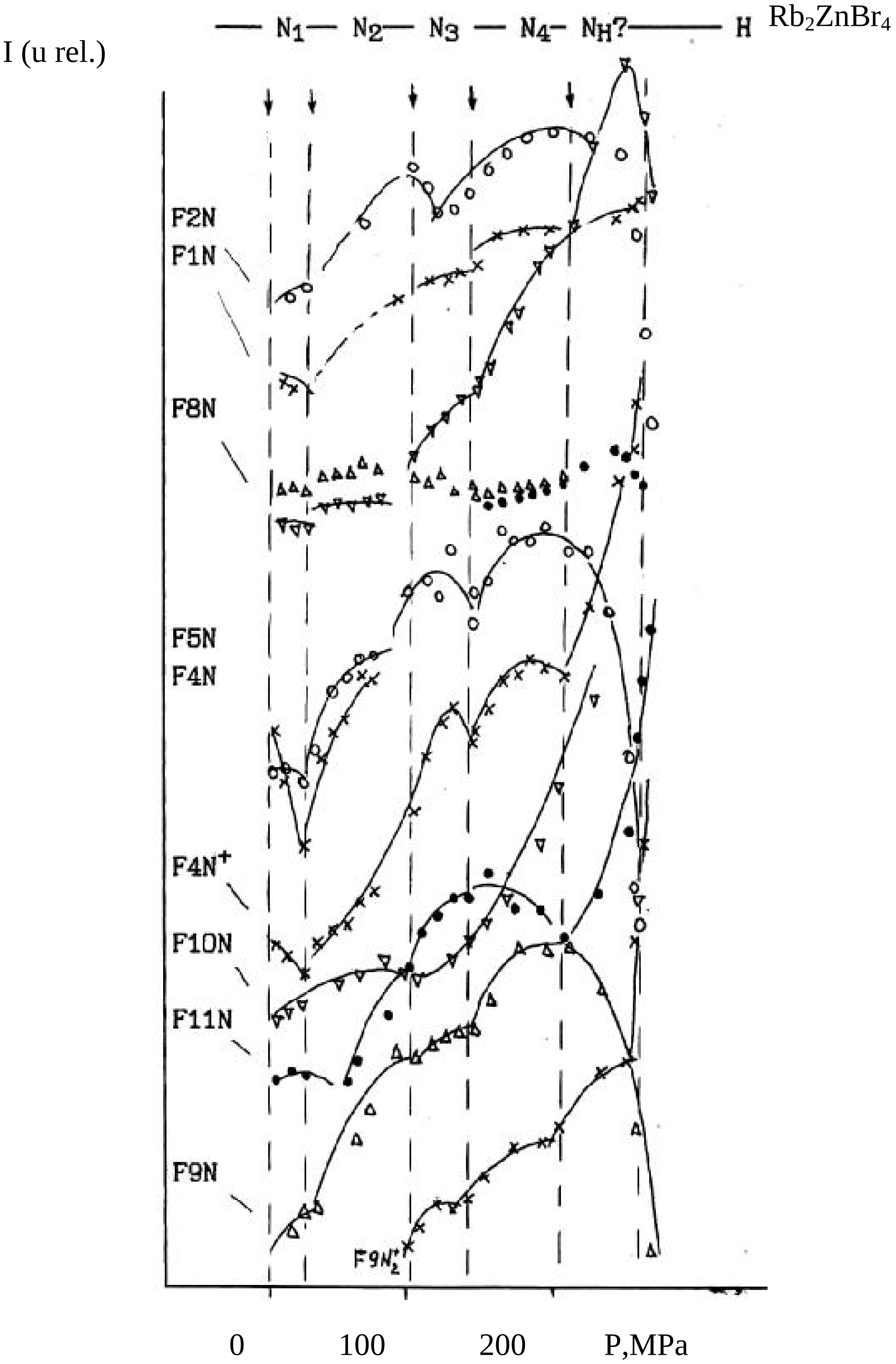

Fig.4.26. Relative change the peak intensities of spectral lines at T = 190K.

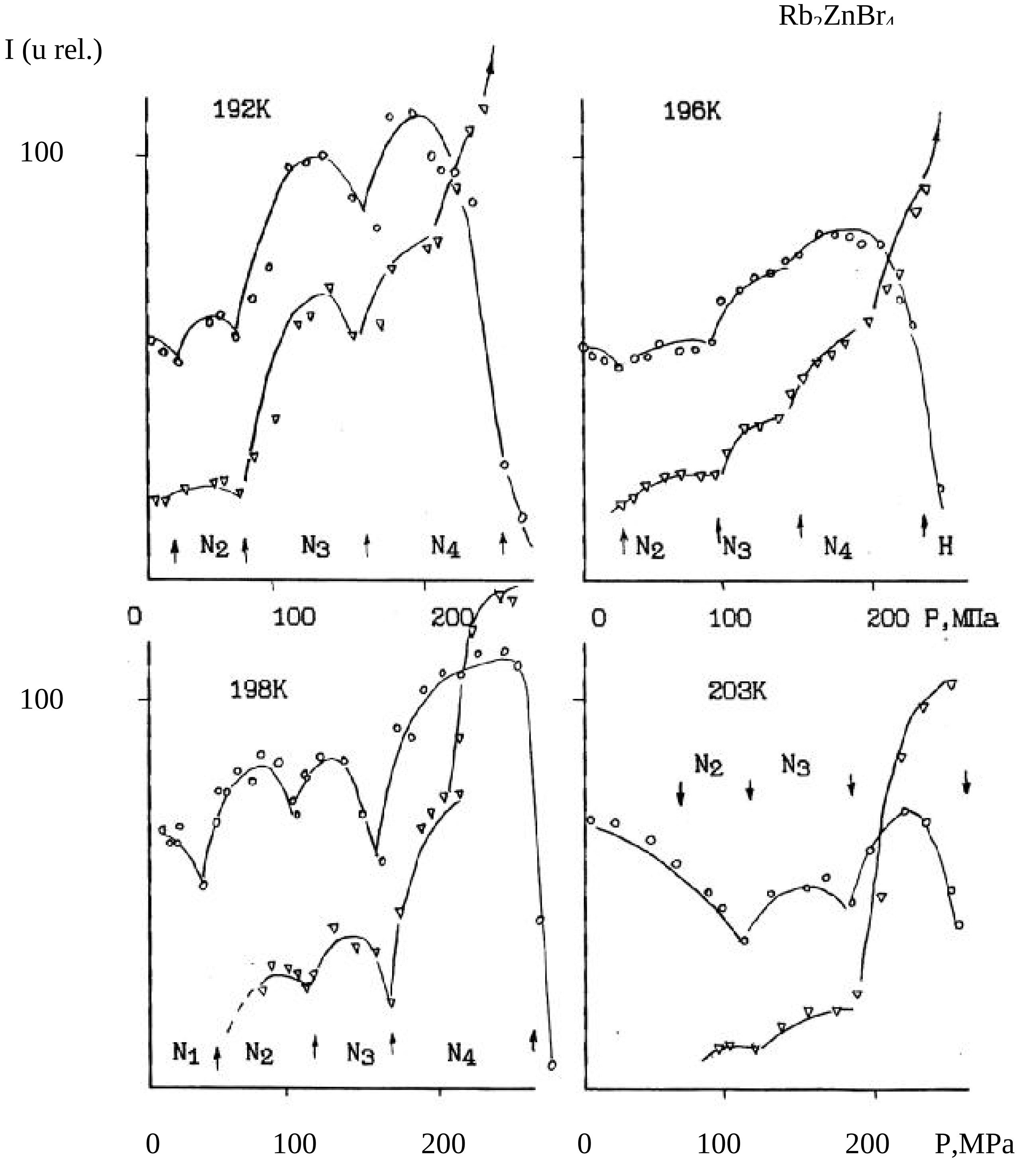

Fig.4.27.Changing the peak intensity of the spectral lines of N4 (o) and 4 N^+ (Ñ) at different temperatures.

Close during the specified behavior was observed intensities and isobaric studies Fig.4-5, Fig.4.12. Although the temperature scanning step was relatively large (~3-5K), but the graphs Fig.4.12, where, in contrast to [115] are all the experimental points, also noted nonmonotonic variation of intensities between Jc and F phases. Besides sensitivity of the isothermal measurements controlled NQR rapper. Therefore, we are quite confident we can assume that celebrated anomalies associated with structural features, rather than instrumental errors.

Noting the arrow (on Fig.4.26 and 4.27) and symbols (for Fig.4.28) P-T conditions of the most distinct breaks and lows in the intensities of the pressure passages, we got the P-T diagram line Fig.4.28.

Turning next to the consideration of changes in the spectra observed in the PT field. With increasing pressure along different temperatures (isotherms 189, 190, 192, 195, 198 К) in the spectrum in the process of conversion to the NQR lines, and H-type F, exhibit a number of features that can be most clearly illustrated by changing the shape of a single line on the N9* 59 MHz frequency and Fig.4.29 Fig.4.30.

On Fig.4.29 shows the change of the line shape N9 in 190¸ 200K from 1 atm to 150MPa. In the upper left part of the figure in the high pressure line N9 has a well-defined asymmetric shape with two maxima of amplitude resolution. In the middle part at lower pressures asymmetry observed on the other side of the line, which is clearly seen in atmospheric changes in a heat chamber at maximum sensitivity (Fig.4.8).

Pressures above 100¸ 150MPa at an asymmetric location wing appears and grows on the new part of the spectrum intensity, so that at higher pressures, there is a doublet, which at the transition to H phase disappears to form a line H12. When the temperature is lowered through the N® F transition distribution N9 is also converted to equal intensity doublet, at a frequency of one component of which is formed ferroelectric line F9, Fig.4.30.

Analysis of the frequency redistribution of intensities within the contour line N9, assuming that it is formed by the overlap of two singlet components of varying intensity, allows present in the form of the frequency dependence of the three components (Fig.4.17).

Position P-T lines constructed by the kinks in the course of baric intensities (Fig.4.28) correlates with P-T lines separating regions of different asymmetry line N9 (Fig.4.30). The line attributed symbol (D) corresponds to the transition to the amplitude resolution of the doublet form N9.

Comparison of changes in forms of individual spectral distributions in various P-T areas also indicates that areas with identical terms of NQR structure arranged along the lines of having positive values ¶P/¶T.

Model analysis of the full range of NQR is beyond the scope of this work. However, we try to make an initial discussion. Isothermal passages in HPC2 at low pressures showed that the phase transition Jc general form of the spectrum in a very narrow neighborhood before T_C (2¸ 3K¸ 3K 60MPa) differs from atmospheric pressure. Along with the NQR lines of type N, recorded at atmospheric pressure (which we assigned here, the index N_1), other-marked line, which we denote the index N_2 Fig.4.32. Changing forms of spectral distributions can be represented by the assumption that near each of the 12 lines of type F, close to the frequencies is a few lines of type N_1 and N_2. With increasing pressure, the intensity of the lines of N_2 increases, and the line intensities of the N_2, within certain limits

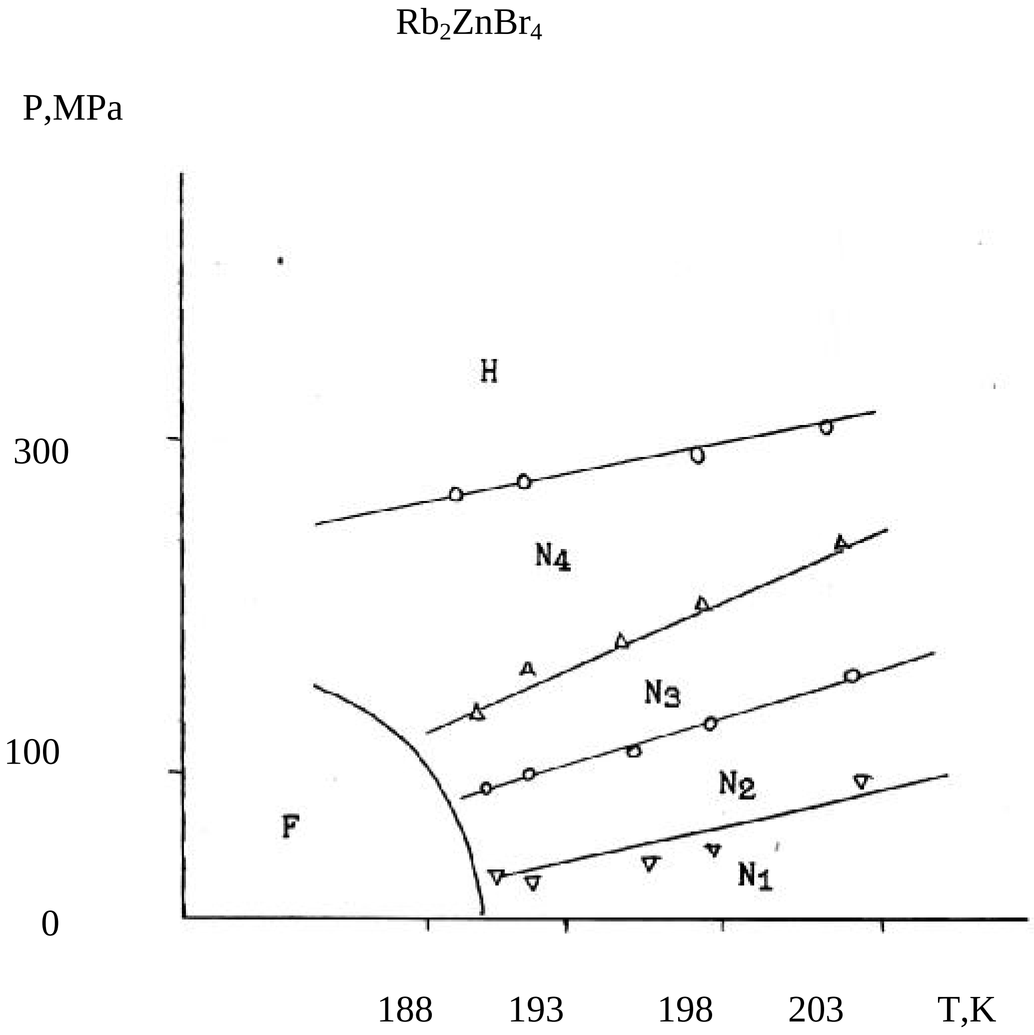

Fig. P-T field Jc phase near T_C marked by anomalous change of the line intensities of the NQR spectrum.

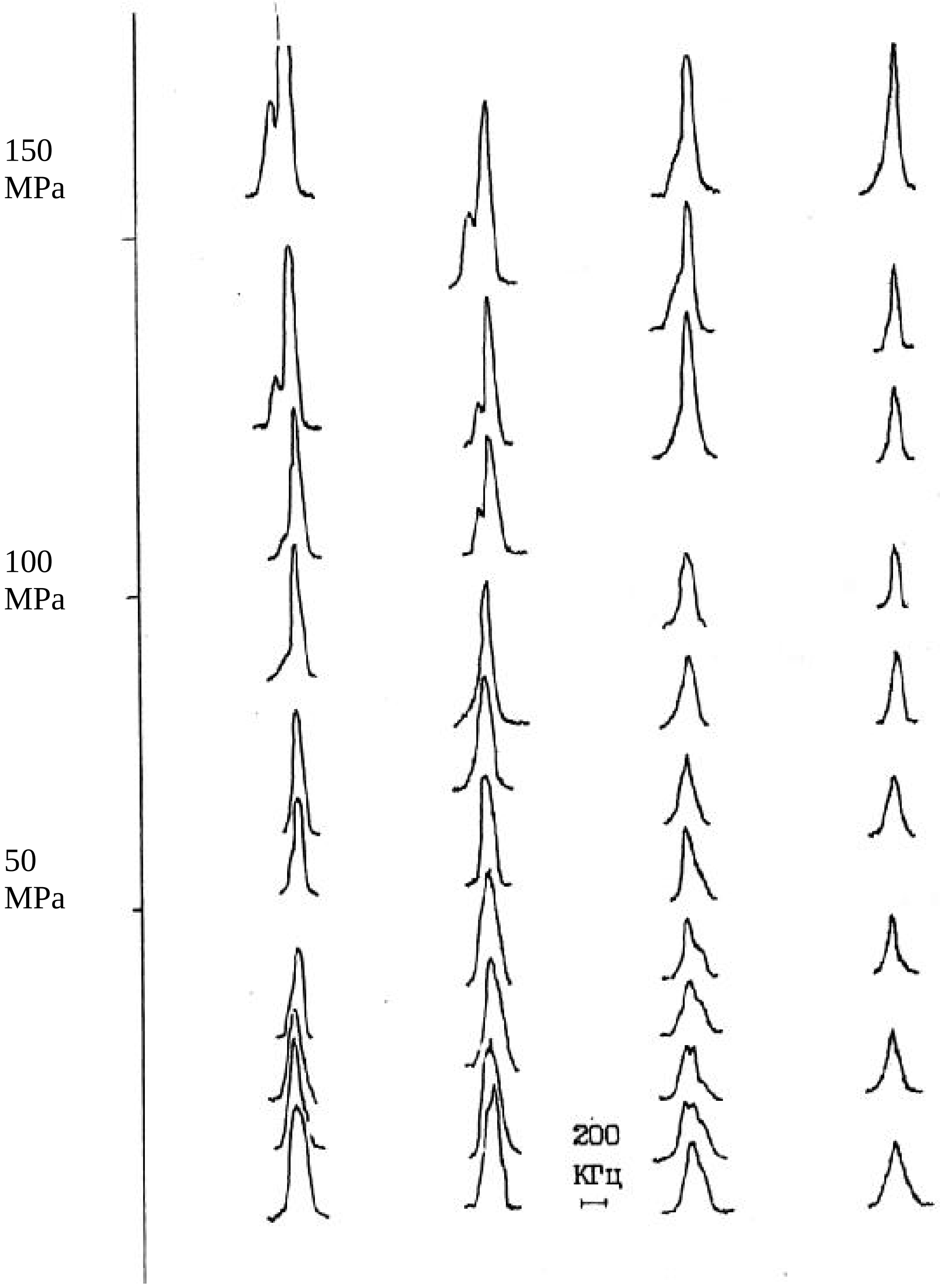

Fig. Variation of the spectral line shapes of type F9-N9 near $T_{C.}$

Rb_2ZnBr_4

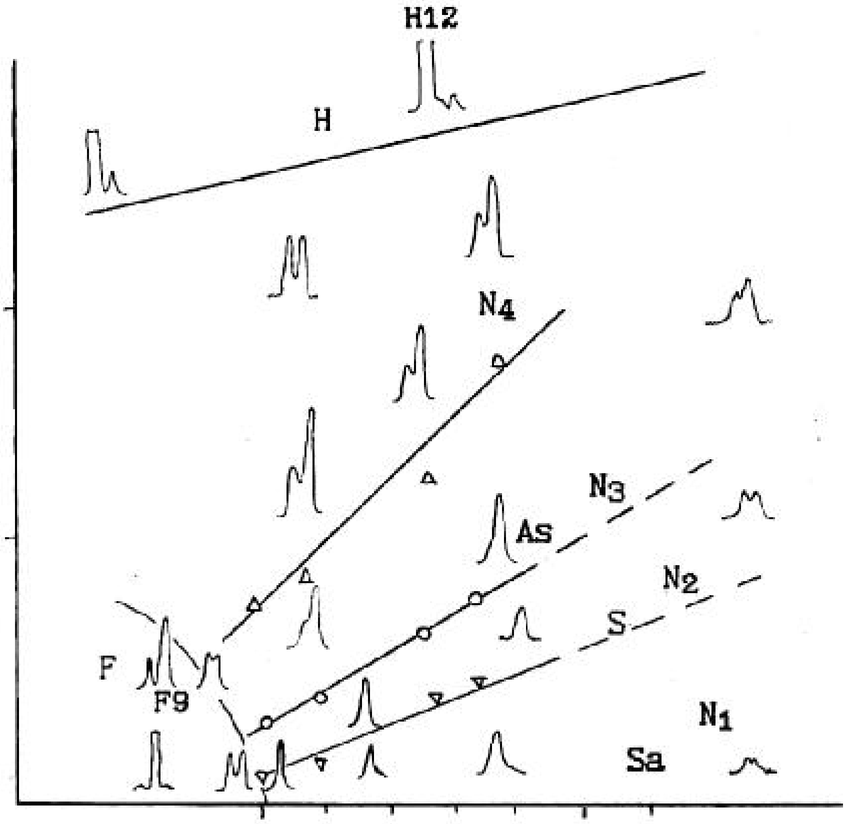

Fig.4.30. P-T field with varying degrees of asymmetry in the line F9-N9-H12.

Rb$_2$ZnBr$_4$

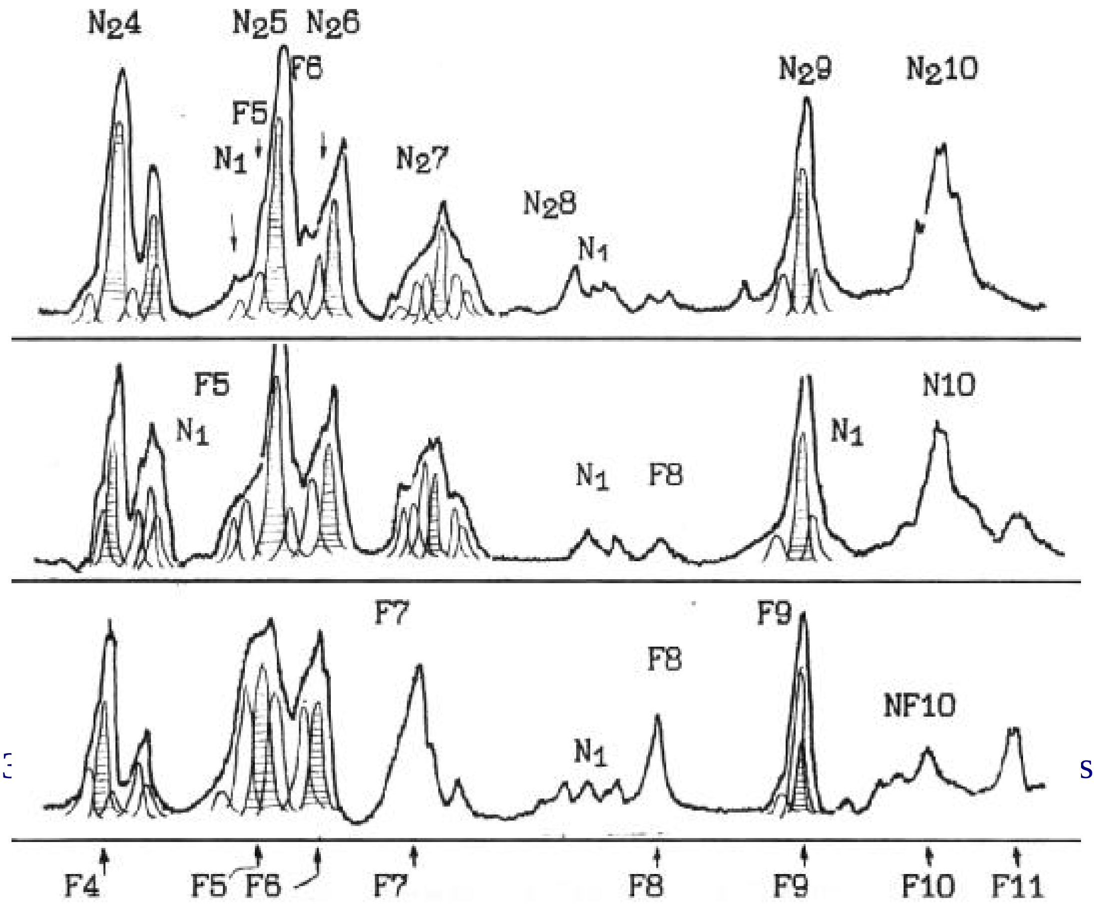

Fig.4. … spheric

Rb_2ZnBr_4

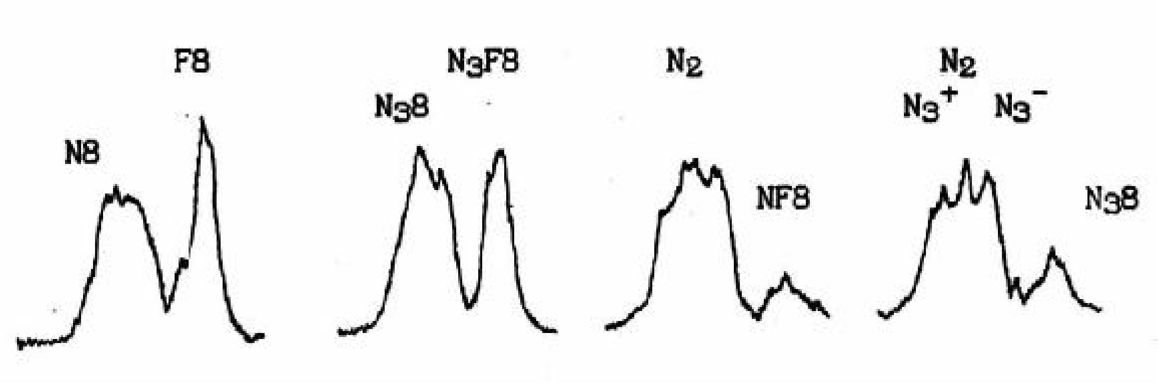

189K	190.3K	191.1K	192K
93MPa	94MPa	94MPa	95MPa

Fig.4.33. Change line NQR spectrum N9-F9 when the temperature changes. P = 100MPa.

vary slightly. Some of the lines are close in frequency, and the peak intensity of the course in this case should be determined by the different contributions.

A similar redistribution of the intensities observed at the transition to the regime of heating in the pressure 100MPa, Fig.4.33. In this case, the change can be represented by overlapping the three groups of spectral lines, as illustrated in Fig.4.33 for the spectral distribution FN8.

At temperatures above $T_{C,}$ where the NQR lines of the phase F is absent, the spectrum at low pressures presented overlapping lines of type N_1 and $N_{2,}$ Fig.4.34 (a-h).

As the pressure increases in N above 80~150MPa range transformed to Fig.4.25d Fig.4.34i-r. His change can be interpreted as the appearance within the contours of spectral distributions of new lines of type $N_{4.}$ Characteristic features of the changes are: a) design of asymmetric line wing N9 (ν=68,98 MHz), b) the emergence of low-intensity lines $N3^+8$, in characteristics redistribution of intensities of lines in the group N5-N7 and N10-N12, etc. Then in the world designated as N_3 shape of the spectrum with respect to stable.

Pressures above 110-200MPa, where there is a third anomaly during the peak intensities, also notes changes in the spectrum. Asymmetric line wing N9 is made in a separate spectral component $N^+{}_{4\ 9er.}$ Change appreciably other spectral distribution (Fig.4.34s-h). The above P-T line separating the region of the $N_{\ 3}$ region designated by us as $N_{\ 4,}$ a broad range of P-T interval is (Fig.4.34s-h).

The slope of the pressure stroke frequency of certain lines (Fig.4.19). Higher pressures (> 250MPa) phase transition is observed in the phase of H (see § 4.2) tracked the fine structure of the NQR spectrum and notes anomalies in its change in the temperature range 190--210K it possible to identify the P-T phase diagram of $N_{1,}$ N_2 , $N_{3,}$ $N_{4,}$ we (in the framework of the "devil" and the stairs in accordance with the data of X-ray diffraction) was interpreted as a manifestation of stages or phases D'Starcase high-order symmetry (HOS) [113,114], and the lines near phase transitions in the area of triple points observed at the coexistence of at least two or three adjacent phases. The magnitude of the coexistence region (shaded region Fig.4.35) and the number of phases is determined by the direction of change of P-T parameters and degree of symmetry.

In $(NH_{4)2}ZnCl_4$ and $(NH_{4)2}ZnJ_4$ where change was observed in the multiplicity of NQR spectra from 16 to 12 absorption lines with narrow temperature intermediate phase, X-ray diffraction at atmospheric pressure are also recorded sequence Jc - 1/4 - 2/7 - 1/3 [47], Figure 1.6, Table 4.1 (p.158).

Interpretation of the data presented NQR was quantitatively tested on samples of Rb_2ZnBr_4 of the same series of crystallization On the basis of the reactor international scientific center of Orsay (France), measurements were made of the position of the wave vector q_d in P-T region of its evolution in F and H phase method by neutron diffraction [119].

Interpretation of neutron data at atmospheric pressure X-ray diffraction data does not contradict the study [110] about the existence of near Jc values $q_{d,}$ which may be

Rb_2ZnBr_4

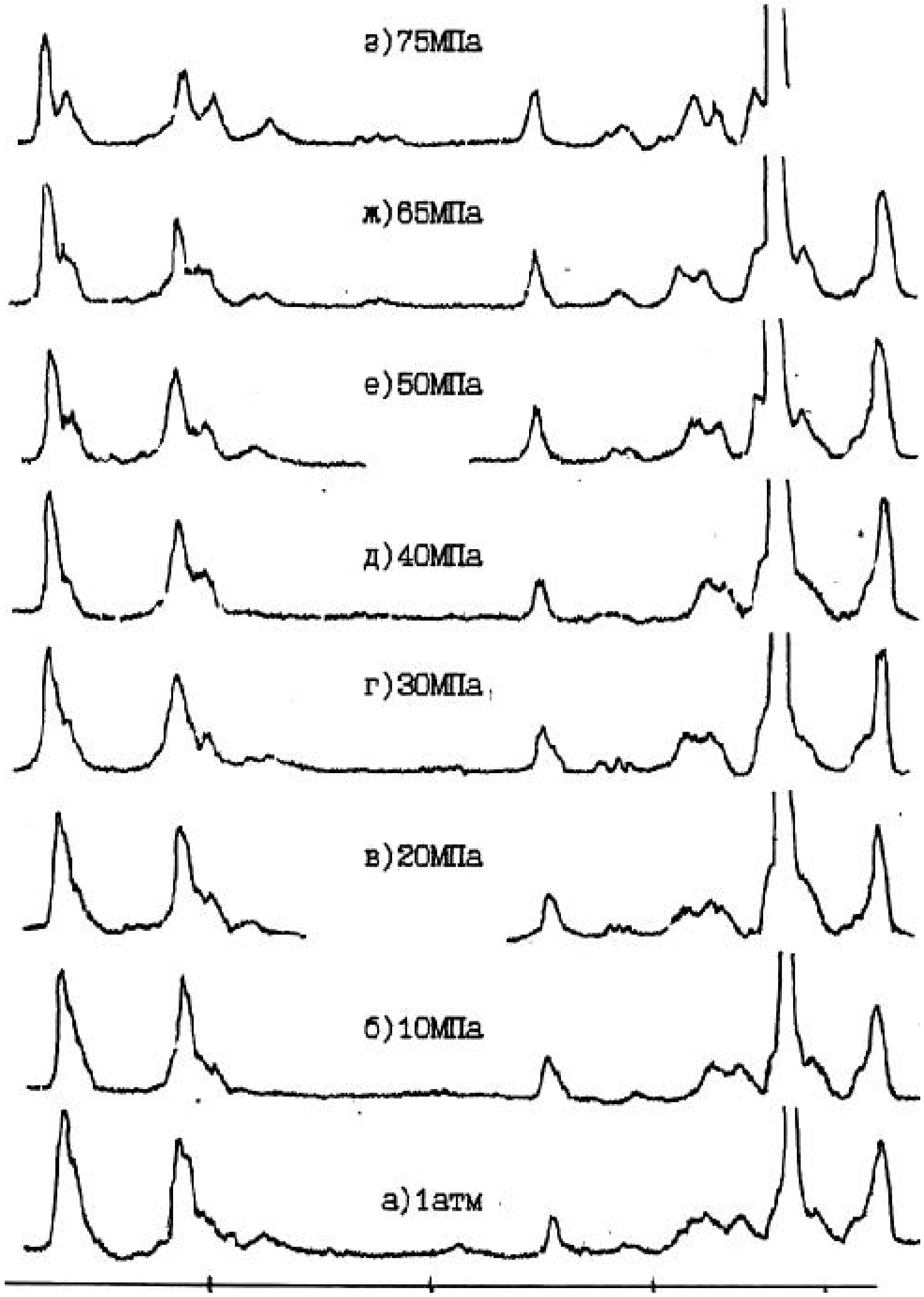

70 68 66 MHz

Fig.4.34. Detailed change in the total NQR spectrum at T = 194K and pressures from 1 atm to 75 MPa.

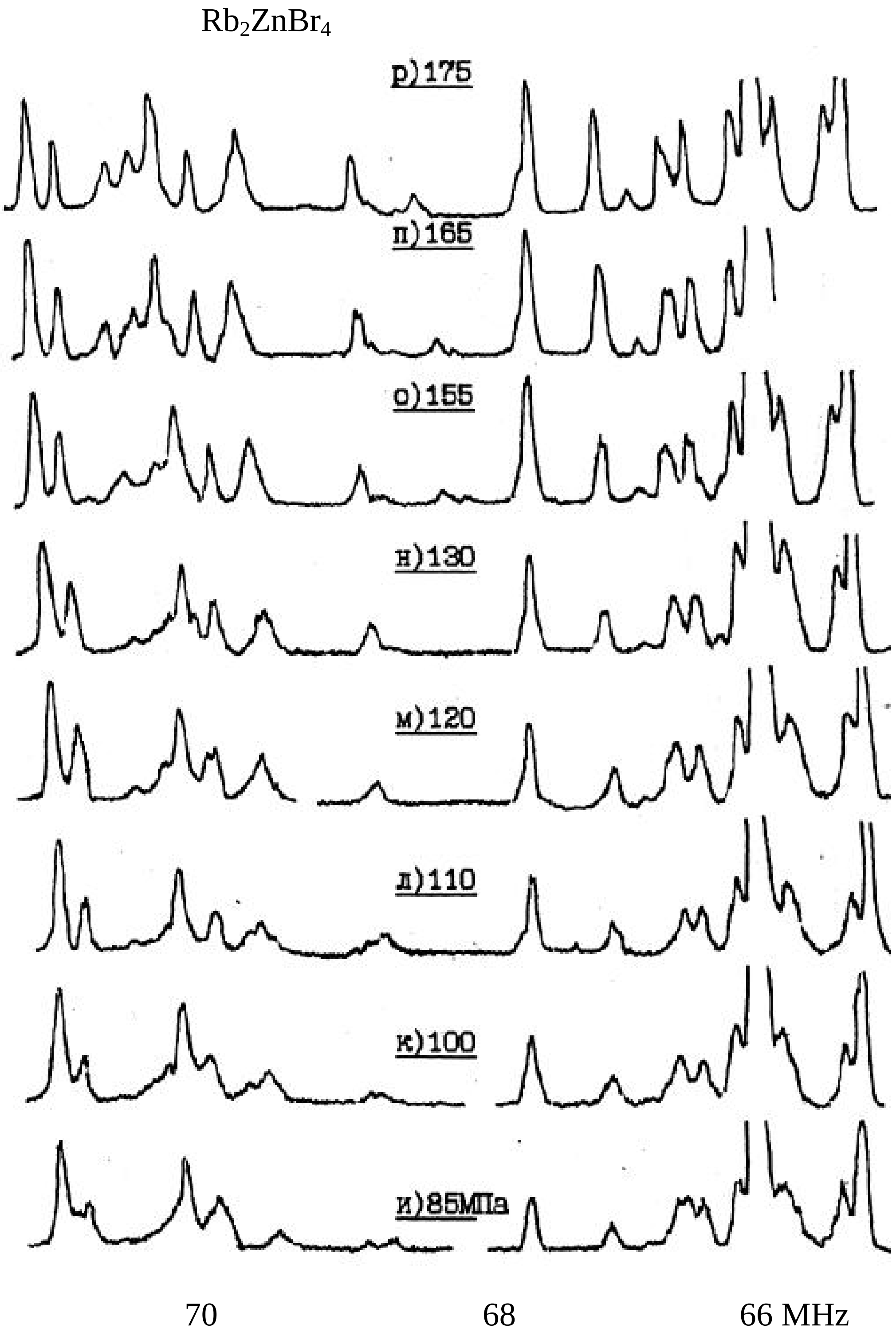

Fig.4.34 (и-р) Detailed change in the total NQR spectrum at T = 194K and pressures from 85 to 175 MPa.

Rb_2ZnBr_4

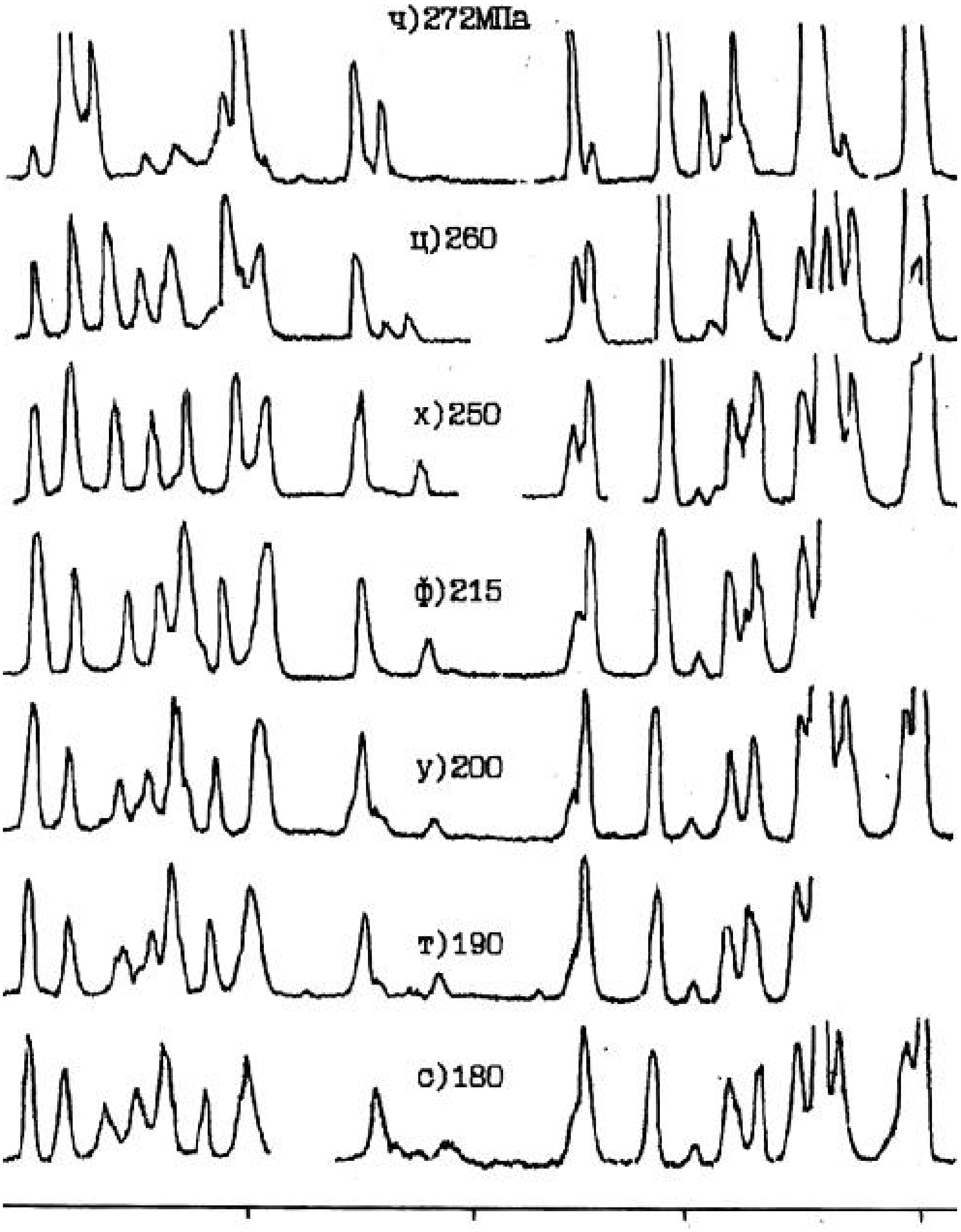

72 70 68 66 MHz

Fig.4.34.Detailed change in the total NQR spectrum at T = 194K and pressures from 185 to 300 MPa

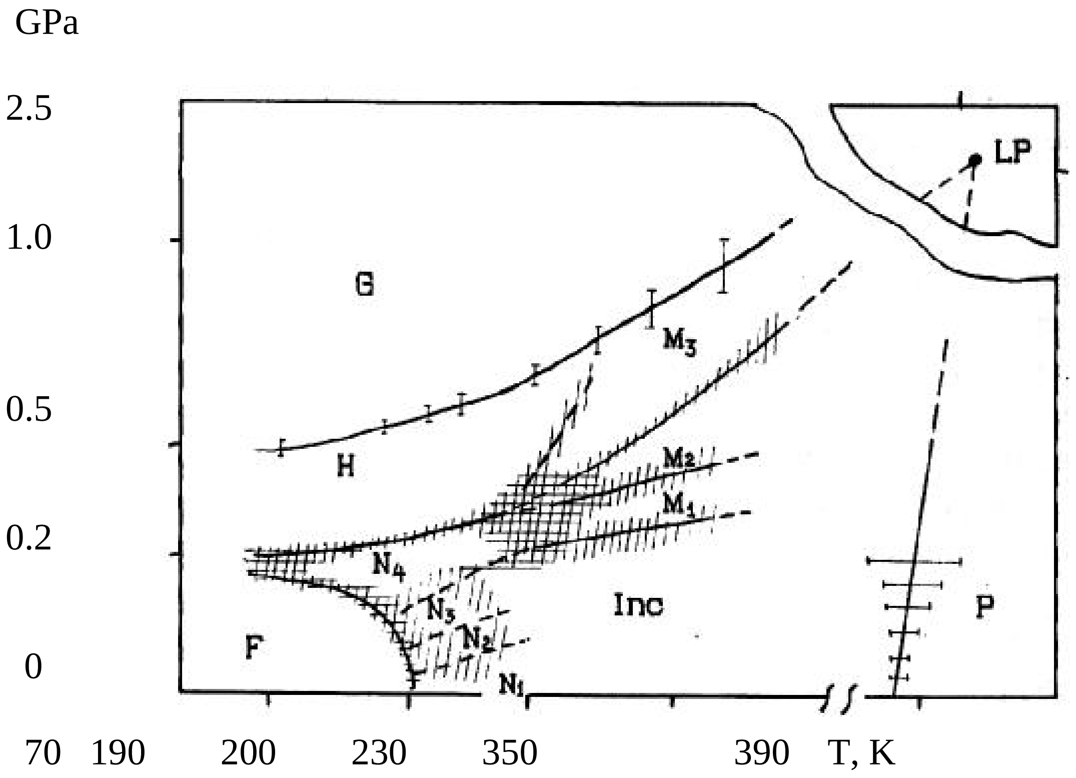

Fig.4.35. General view of the phase diagram of Rb_2ZnBr_4 according NQR Br.

conventionally disposed at steps "going up" ladder: 5/17 ® 3/10 ® 7/23 ® 4/13 ® 5/16 ® 1/3 (in the unit. **a***).

With increasing pressure, has been confirmed, detected previously [115], lock-in the phase transition orthorhombic symmetry $Pn2_1a$, with a cell volume quadrupling (Z = 16) with the value of q_d = l/4 (0.2500). While additionally observed values q_d = 0.296, 0.2917, 0.2857, missing at atmospheric pressure. These values q_d authors of [119], following we [113] compared stairs going down stairs: 3/10, 8/27, 5/17, 7/24, 2/7, 1/4. In this region of the icommensurate phase was marked by the coexistence of two or three satellites in Jc phase diagram. (Satellites 1/3 (0.3329) 5/16 (0.3114) 5/17 (0.2948) 7/23 (0.3043) 7/24 (0.2917), Fig.4.36). At the same time, according to data NQR noted preferential coexistence of three satellites at isobaric aisles near T_C and two satellites under isothermal. Also large widths were fixed caliper with cooling, and the continuous change in the position, especially at low pressures. However, the scattering profiles were slightly different from the X-ray [51], a smaller width and temperature region of coexistence. Slightly different conditions and observations: for neutrons pressure was about 1 kb, and X-rays at atmospheric pressure. According to such an NQR contrast at low pressures from outside the structure indicates difference at atmospheric pressure of 1atm under the atmospheric 1tm at $T_{C.}$ In the middle part of the incommensurate phase observed continuous decrease in the magnitude of the wave vector q_d with increasing pressure (from 0.293 to 0.28 at T = 273K, P <300MPa) and a slight increase in q_d at low temperatures (from 0.2017 (5/17) to 0.300 with P »l.0 MPa, 273 <T <200K). According to the measurement of NQR and neutron diffraction authors [119] was constructed P-T phase diagram (Fig.4.37), which is well distinguished from the proportionate phase wave vectors of 1/3 and 1/4 and the region with the higher order phases. The phase transition between phases 1/3« HOP and HOP« 1/4 exactly coincide with the P-T lines between phases F« N and N« H fixed NQR. In the HOP, where there is a coexistence of satellites, proposed a hypothetical phase diagram presented a set of conventionally separated pseudo incommensurate structures. However, according to another inclination NQR observed, compared with the data NQR P-T lines, separating regions of high phase order.

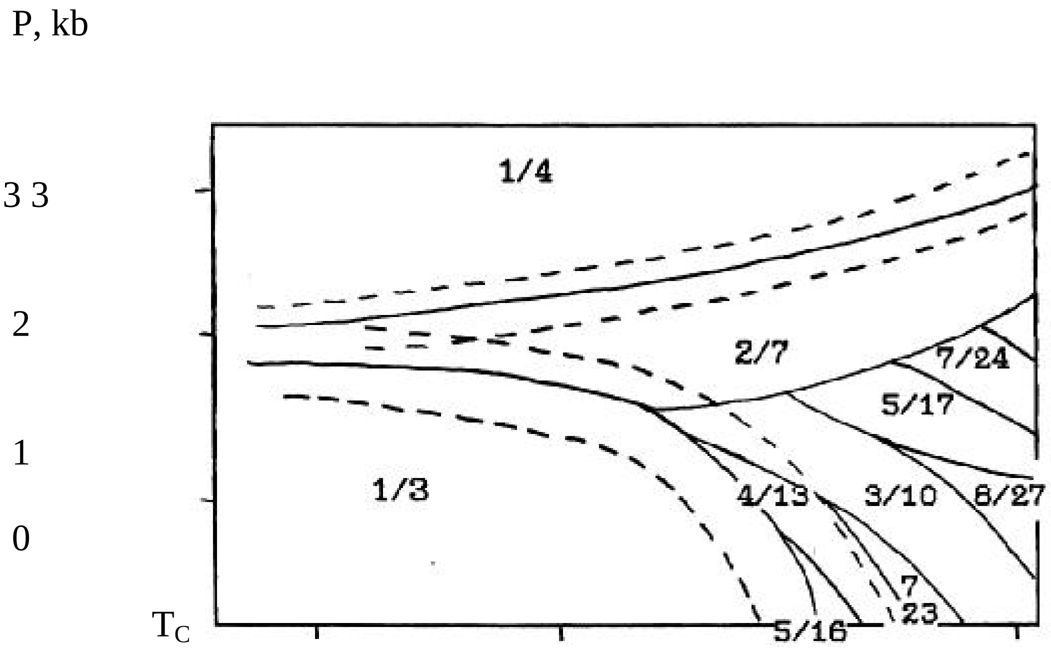

Fig. A phase diagram of Rb_2ZnBr_4 near T_C of analysis neutron diffraction data.

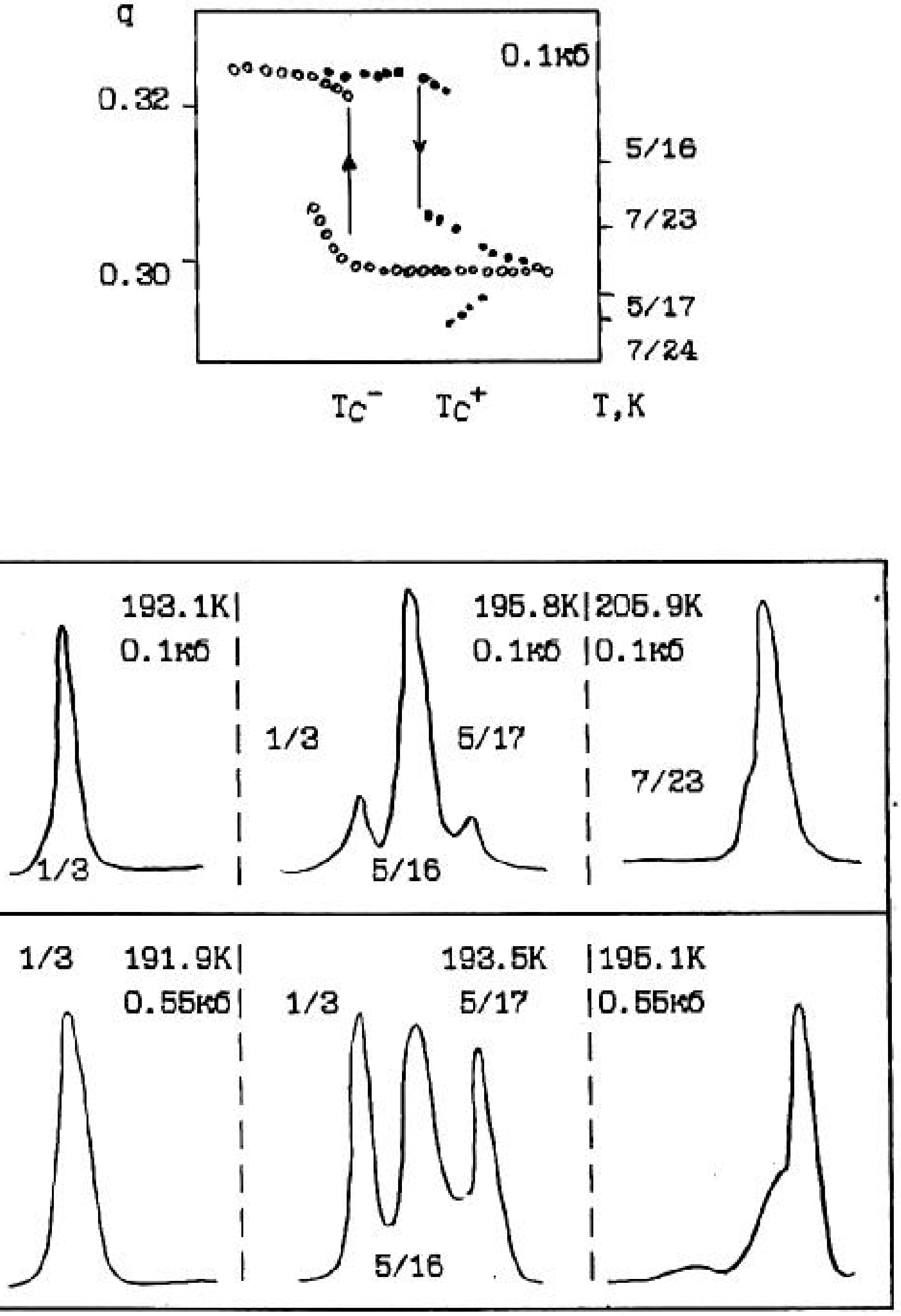

Fig. Scattering profiles and repositioning the satellites according neutron diffraction scattering.

§ 4.4 Discussion of the phase diagrams in the framework of theoretical models "devil's staircase".

In conclusion, we provide a synthesis of the experimental P-T diagram of Rb_2ZnBr_4 according NQR (Fig.4.35) and compare it with the theoretical phase diagrams obtained by numerical methods. Calculations performed in [15,12,121] are based on the anisotropic Ising model with the interaction up to three neighbors. We are interested in that part of the phase diagram, where realized structure with a period close to 1/3 and 1/4 Fig.4.38a. In this diagram, the value of q_d = l/3 corresponds to the configuration of spins <12> (one up, two down), q_d = l/4- <121>, q_d = 5/17- <1121212 (12) 2>; 2>; q_d = 3/10- <112 (12) 2>; etc. If this diagram spend dashed line, as shown on Fig.4.38a, and relate it to the experimental scale temperature at atmospheric pressure, is located above this line, the phase diagram [121], would be enough comparable to the experimental P-T diagram obtained world. In this case the transition to the modification of this model in the framework of the pseudo-spin variables [12], the region of existence of structures with different configurations can be changed (Fig.4.38b).

A somewhat different approach developed in recent years [12]. Its foundations were laid by a modification of the parabolic model of Frenkel-Cantor and put nesimorfny symmetry element, which acts as a nonlinear part of the polarization of communication between sublattices. With the increase of the contribution of the nonlinear polarization P_{NL} , in a structure with symmetry series Pnma, phase fractions of 1/3 and 1/4 respectively decrease and increase, appear between lower-order symmetry structures (Fig.4.39). Inset on a larger part of the diagram shows Fig.4.39 Aubrey, which can be compared with our P-T phase diagram.

When considering the field of existence of the phase 2/7, located between phases 1/3", 1/4" phase diagram Aubrey and lines separating phases 1/3", 1/3 and 5/17, we can imagine that in our case there a fine structure of these regions (as shown in Fig.4.39b) as intermediate steps between 1/3 and 5/17, and between 5/17 and 2/7.In this case, the phase diagram obtained RZB NQR based on the values of the wave vectors of the measured diffraction neutron diffraction well compared with the theoretical phase diagram in the model Aubrey [12].

As follows from numerous data on the experimental study of the phase diagrams of various systems with frustrating interactions diagrams complication occurs not only in the case of registration of more distant neighbors across the anisotropy axis of the system, but with the introduction of structural disorder (random field). The latter may be due to impurities, H_2 bonds, nuclear isotopes, as well as presence in the crystal layers or surface phases of another structure. Omitting, however, the discussion neutron diffraction [124, 21] and scaling [123] type of behavior that can be observed in this case, we dwell on the reasons leading to the stochastic regime celebrated applications of three-dimensional and two-ANNNI models [13]. If, for example, the energy of the system is close to the case of a tripling of the unit cell (or j $\approx\pi/3$), the average structure is a topological articulation solitons, antisolitons and their random combination. Depending on the interaction, some combinations will be energetically more favorable. Such chaotic phase will be metastable, and the degree of metastability depends on the communication parameter disproportion to the elastic energy. Infinite (or finite) number of stable states of a set of "devil staircase"

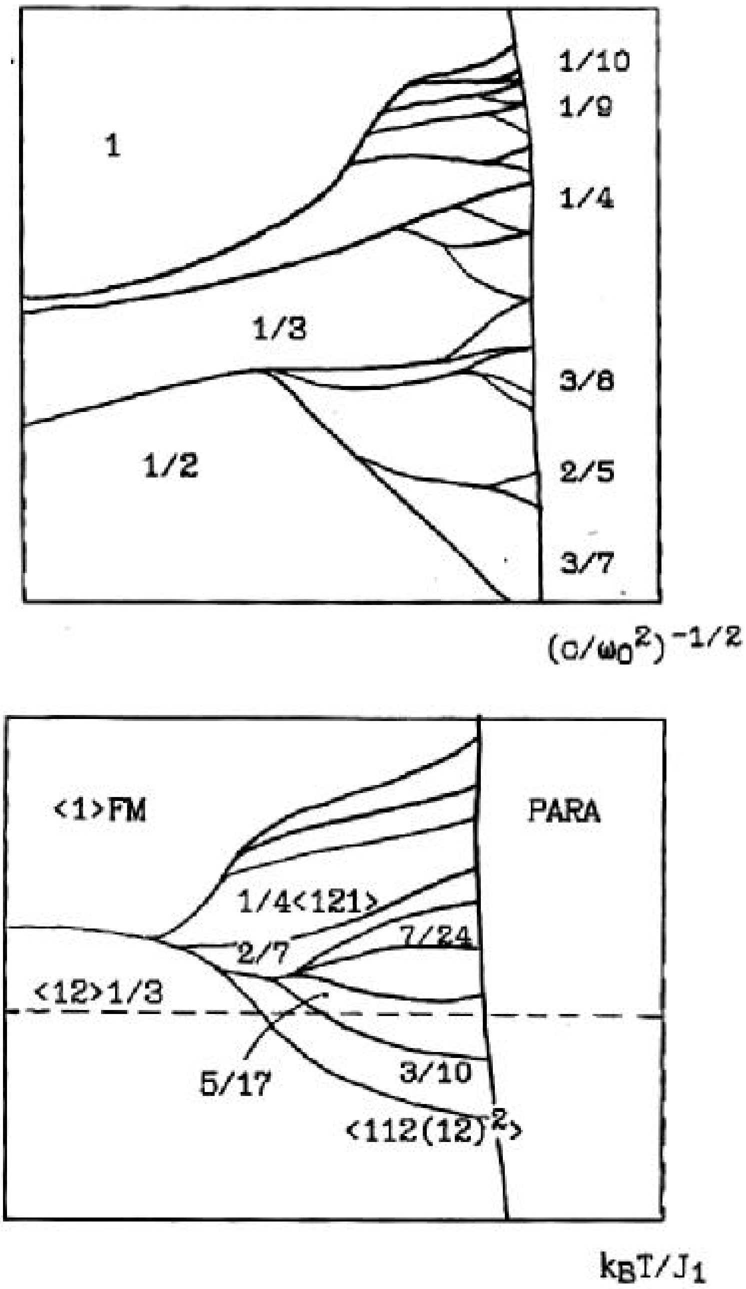

Fig.4.38.
a) theoretical diagram Celka [121];
b) phase diagram Aubrey [5].

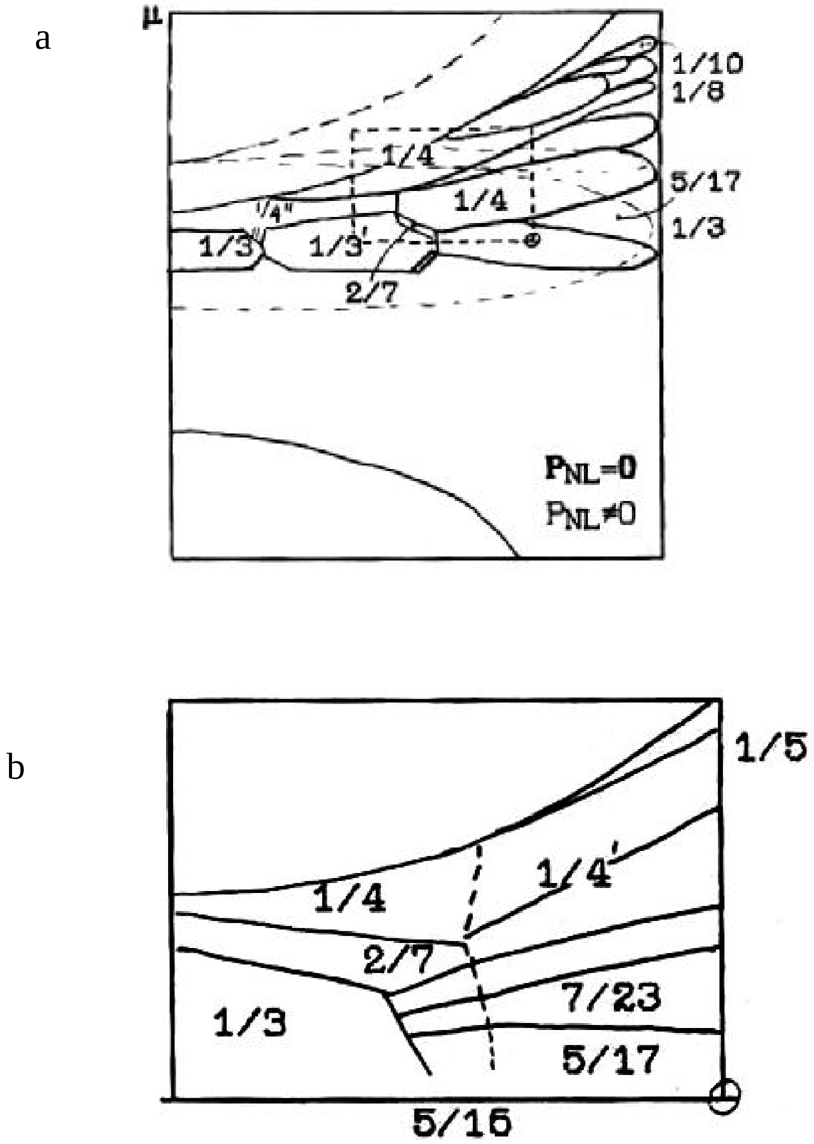

Fig.4.39. Theoretical phase diagram of the polarization model Aubry [12].

can be separated by energy barriers and the real system can not relax to the ground state in a finite time.

In this mode, there are two cases: weak and strong interaction potential [13,120]. In this case, when the distance between solitons small incommensurate phase is stable. When the distance between the solitons, repulsive interaction between them can not overcome the pinning lattice and observed soft chaotic regime. With significant excess disproportionate period compared with the lattice period, high-temperature phase is stabilized. Here it is possible to conduct a similar cluster pretransition ordering.

At strengthening ties between the sublattices ANNNI model (strong potential), the width of the chaotic regime can greatly increase and the incommensurate phase will be able to include some long-period phases. For example, instead of the phase $q = 2p/4*(l-q_d)$ in the range of wave vector $q \pm Dq$ four possible modulation states $q = 3/16 = 1/4*(1-1/4)$. The phases will differ phase shift value $j = j_0 \pm Dj$ close to p/4. When these four long-period would be two chaotic phase. When reducing the magnitude of the wave vector number energetically close phase will increase. Each incommensurate phase is represented by a set of long-period and chaotic phases. In this case, should be observed smoothed (incomplete) mode «Devil's starcase», as opposed to purely chaotic regime, where the wave vector varies according to the classical (smooth) mode Devil's starcase'. In this case (for large values of the period disparity) is true incommensurate phase is not realized.

To analyze this possibility in our case, we, on the [120], should appeal to the structure of Pnma. As is known, the structure of A_2BX_4 type β-K_2SO_4 in a certain layer ab-plane of the two centers of gravity BX_4 tetrahedra are located at the same level as the ion A (Fig.3.14). Between coats z = l/4 and z = 3/4 **A** ions are remaining. When considering the structure within a single layer, it can be assumed that the electrostatic force acting within the layer is not stable, whereby there is the rotational mode, which each tetrahedron rotates so that the other two in this tetrahedron unit cell are rotated in opposite directions. Structure should stabilize spatial redistribution of the charge between the ion A and one of the X atoms of the tetrahedron. Potential energy within the layer can be represented by a double pit: a polynomial of fourth degree of j. Interaction between the layers appear in the repulsion between the top and the base of the tetrahedron tetrahedron lying in another layer, and through A ions. When along the **c** direction has two layers on the lattice constant (such as in Rb_2ZnBr_4), the potential energy of interaction of ions can be characterized by the rotation of the pyramid in the n-th layer at an angle $j_{\mathbf{n}}$ and is represented in form similar to $j^{\mathbf{4}}$ discrete tasks ANNNI model [120]:

$$V=\mathring{a}\,|\,A/2\times\varphi_n^2+1/4\times\varphi_n^4+B\times\varphi_n\varphi_{n-1}+D\times\varphi_n\varphi_{n-2}|$$

As is known, in this case there are non-linear solutions (Eg "solitons"). For the calculation of the parameters ***A, B*** and ***D*** need to know the specifics of the interatomic interactions and the structure of the chemical bond. However, some solutions $j^{\mathbf{4}}$ models have a chaotic regime. As shown in [120,122], in particular cases, for small values of width **1** "solitons" relative lattice constant (narrow solitons), there are several states with high-order proportionality little distance between solitons $\mathbf{l_o}$. With an increase $\mathbf{l_o}$ and reaching its value a certain critical value $\mathbf{l_{cr}}$, a mixed state becomes chaotic behavior with randomly pinned (anti) solitons.

Trying to satisfy neutron diffraction data, X-ray scattering data and RF, we can represent the structure of the incommensurate phase of an infinite set of fragments with a long period, which differ in the non-equivalence of the chemical bond in subfragment located in the structural cell in a certain way. For example, assuming that $\mathbf{N_4}$ phase, Rb_2ZnBr_4 crystal cell 14 has a size of the lattice constant, the substructure it can be composed of two fragments with a length $\mathbf{3a}_0$ and $\mathbf{4a}_0$ of the **t**wo in the lattice constants relative to each other spaced randomly (mixed nonlinear solutions). In the primitive description limited fourteen tetrahedra (in their double-well Librational position), we can make a subcell $\mathbf{3a}_0$, for example, one of the tetrahedron in the left and two in the right position, and $4\mathbf{a}_0$ subcell of the two left and two right successive tetrahedra. Then cell $14\mathbf{a}_0$ can be represented on five ways (basic solutions) consistent position two nested cells $3\mathbf{a_0}$ and $4\mathbf{a}_0$ two cells. One of these methods may be more favorable. In the full sense of the overall structure is determined by the specific nonlinear solution.

Spreading such structuring on the high temperature region of $Rb_2ZnBr_{4,}$ one can try to describe the transition structure of the 5/17 to 1/3 or 1/4 for each halogen atom tetrahedron through a small redistribution of electron density in a group of neighboring atoms (flash polarization). In implementing such a process cell size is reduced through a series of steps to $3a_0$ or $4\mathbf{a}_{0.}$ Modulation does not seem continuous displacement of nucleus from state to state, and the redistribution of the electron density of the two ranked energetically close structures $3a_\mathbf{0}$ and $4a_\mathbf{0.}$

According to this concept, according to NQR Rb_2ZnBr_4 under pressure in a wide temperature range from $T_\mathbf{i}$ to 230K near atmospheric pressure observed mixed mode and a long-chaotic behavior. This is evident from a comparison of the observed shape of the spectrum, which is directly after annealing presented blurred frequency distributions. In this case, the diffraction data, where there is a blurred satellite in the same position (≈5/17), see only the periodicity of the structure. At $T_\mathbf{c}$ phase transition to a long-F behavior prevails over chaotic And with increasing pressure to phase H, the chaotic behavior is almost completely disappears and "satanic staircase" seen more clearly (complete). In this phase 2/7 structure is dependent on the prehistory combination phases ≈1/3 and" ≈1/4. N-phase is a mixture of long-period phase with a small admixture of chaotic. As the pressure increases in J_C and M phases, the number of energetically equivalent sets of long-period and chaotic phases, according to [13], may increase. The phase transition in this case represent the areas where change is carried out medium wave vector. We can assume that the phase transition $\mathbf{M_1}$« $\mathbf{M_2}$ is a change of the wave vector q_S chaotic structure of 1/4 to 1/5 or 1/6 through the intermediate value type $q_S \approx 0.222 \approx 1/4$-d. Therefore, diffraction techniques can be observed here another narrow phase, as predicted by the model Aubrey [12] and have been reported in $(NH_4)_2ZnCl_4$ [47,50] and $(NH_4)_2ZnBr_4$ (Figure 1.6).

Shape of the resonance lines in the incommensurate phase may reflect a certain type of mixed between states q_d ≈l/4 and q_d ≈l/3 of the nonlinear solutions.

Thus, the comparison of the theoretical phase diagrams with P-T diagram of the NQR data and taking into account the data neutron diffraction scattering, suggesting that an increase in pressure in the RZB should be observed structure type 1/5, 1/6, 1/8 and etc., approaching the Lifshitz point. As for structural changes in phase modulated, one can assume the presence of a substantial Rb_2ZnBr_4 interactions frustrating crystal spatial symmetry. Framework for describing transformation of the structure and evolution of the NQR spectra, from this point of view, should be sought in the implementation of competition electrical interaction between the sublattices of the structure and its connection with the phonon spectrum. Availability the nonlinear polarization in this class of compounds has long been established. It is due to significant distortion and rotation groups BX_4 and inhomogeneous polarization of the electrons in the atomic core In this connection there are substantial electric dipole moments of atomic groups, the values of which differ for each group in both magnitude and direction. Accounting for such a spatially inhomogeneous nonlinear electrical deposits can significantly change the way in the shape description resonance spectra in the compounds of the family A_2BX_4. Cause of heterogeneity to be found in the intricacies of the nature of the chemical bond.

Finally, we can also make a comparison of theoretical phase diagram Aubrey with experimental data on change in the magnitude of the wave vector q_d in other compounds A_2BX_4 (Table 4.1).

From the point of view of crystal chemistry, the relative magnitude of the radius of the cation A compound A_2BX_4 can be divided into two groups. In the first group, with a large cation Cs**,** the following sequence transforming structures:

113K
CS_2ZnJ_4: Pnma Jc, q-(l+d)a*/2P2_1/n $\bar{P}1$
d=0.15 Z=8 Z=4

Cs_eCdJ_4: Pnma Jc, $q < 0,25a^*$ P2_1/n
Z=4 Z=8

In Cs_2CdJ_4, Cs_2CdBr_4 sequence transformation structures and size q_d in Jc close to those for Cs_2CdJ_4. In the second group, with medium and small radius of the cation, there is a different sequence of transformations of the structure, characterized by low-temperature phase with the space group Pn2_1 a, but with different multiplicity of the unit cell volume relatively high. So for Rb_2ZnBr_4 under pressure, we have:

Table 4.1. Modulation Character and evolution of the family structure in crystals A_2BX_4 -type structure b-K_2S0_4.

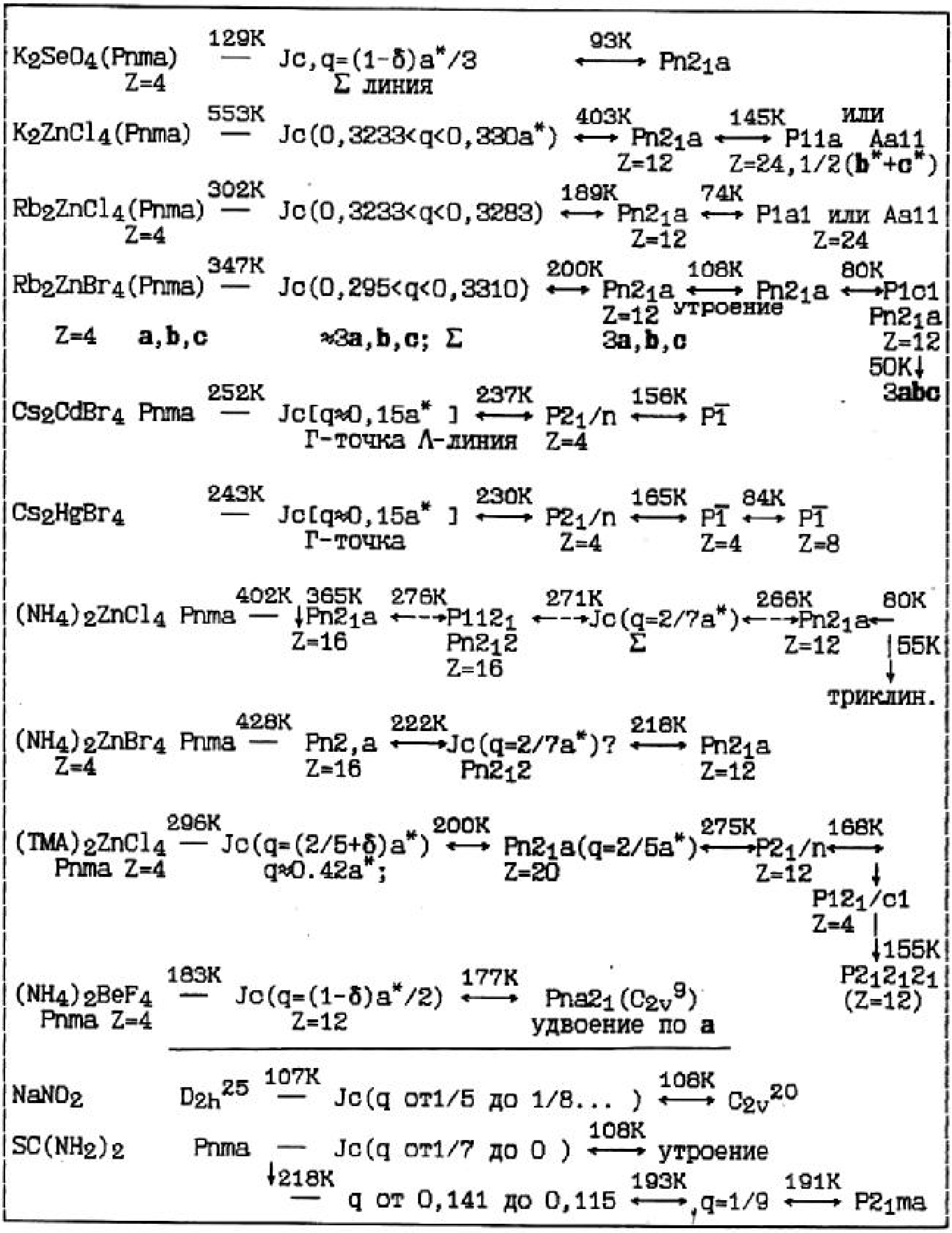

K_2SeO_4(Pnma) Z=4 $\overset{129K}{—}$ Jc, $q=(1-\delta)a^*/3$ Σ линия $\xleftrightarrow{93K}$ $Pn2_1a$

K_2ZnCl_4(Pnma) $\overset{553K}{—}$ Jc($0,3233<q<0,330a^*$) $\xleftrightarrow{403K}$ $Pn2_1a$ Z=12 $\xleftrightarrow{145K}$ P11a или Aa11 Z=24, $1/2(\mathbf{b}^*+\mathbf{c}^*)$

Rb_2ZnCl_4(Pnma) Z=4 $\overset{302K}{—}$ Jc($0,3233<q<0,3283$) $\xleftrightarrow{189K}$ $Pn2_1a$ Z=12 $\xleftrightarrow{74K}$ P1a1 или Aa11 Z=24

Rb_2ZnBr_4(Pnma) Z=4 **a, b, c** $\overset{347K}{—}$ Jc($0,295<q<0,3310$) ≈**3a, b, c**; Σ $\xleftrightarrow{200K}$ $Pn2_1a$ Z=12 **3a, b, c** $\xleftrightarrow{108K}$ утроение $Pn2_1a$ $\xleftrightarrow{80K}$ P1c1 $Pn2_1a$ Z=12 50K↓ **3abc**

Cs_2CdBr_4 Pnma $\overset{252K}{—}$ Jc[$q\approx0,15a^*$] Г-точка Λ-линия $\xleftrightarrow{237K}$ $P2_1/n$ Z=4 $\xleftrightarrow{156K}$ $P\bar{1}$

Cs_2HgBr_4 $\overset{243K}{—}$ Jc[$q\approx0,15a^*$] Г-точка $\xleftrightarrow{230K}$ $P2_1/n$ Z=4 $\xleftrightarrow{165K}$ $P\bar{1}$ Z=4 $\xleftrightarrow{84K}$ $P\bar{1}$ Z=8

$(NH_4)_2ZnCl_4$ Pnma $\overset{402K}{—}$ $\overset{365K}{\downarrow}$ $Pn2_1a$ Z=16 $\xleftrightarrow{276K}$ $P112_1$ $Pn2_12$ Z=16 $\xleftrightarrow{271K}$ Jc($q=2/7a^*$) Σ $\xleftrightarrow{266K}$ $Pn2_1a$ Z=12 $\xleftarrow{80K}$ |55K ↓ триклин.

$(NH_4)_2ZnBr_4$ Pnma Z=4 $\overset{428K}{—}$ Pn2,a Z=16 $\xleftrightarrow{222K}$ Jc($q=2/7a^*$)? $Pn2_12$ $\xleftrightarrow{218K}$ $Pn2_1a$ Z=12

$(TMA)_2ZnCl_4$ Pnma Z=4 $\overset{296K}{—}$ Jc($q=(2/5+\delta)a^*$) $q\approx0.42a^*$; $\xleftrightarrow{200K}$ $Pn2_1a(q=2/5a^*)$ Z=20 $\xleftrightarrow{275K}$ $P2_1/n$ Z=12 $\xleftrightarrow{168K}$ ↓ $P12_1/c1$ Z=4 ↓155K $P2_12_12_1$ (Z=12)

$(NH_4)_2BeF_4$ Pnma Z=4 $\overset{183K}{—}$ Jc($q=(1-\delta)a^*/2$) Z=12 $\xleftrightarrow{177K}$ $Pna2_1(C_{2v}^9)$ удвоение по **a**

$NaNO_2$ D_{2h}^{25} $\overset{107K}{—}$ Jc(q от1/5 до 1/8...) $\xleftrightarrow{108K}$ C_{2v}^{20}

$SC(NH_2)_2$ Pnma — Jc(q от1/7 до 0) $\xleftrightarrow{108K}$ утроение

↓218K — q от 0,141 до 0,115 $\xleftrightarrow{193K}$, q=1/9 $\xleftrightarrow{191K}$ $P2_1ma$

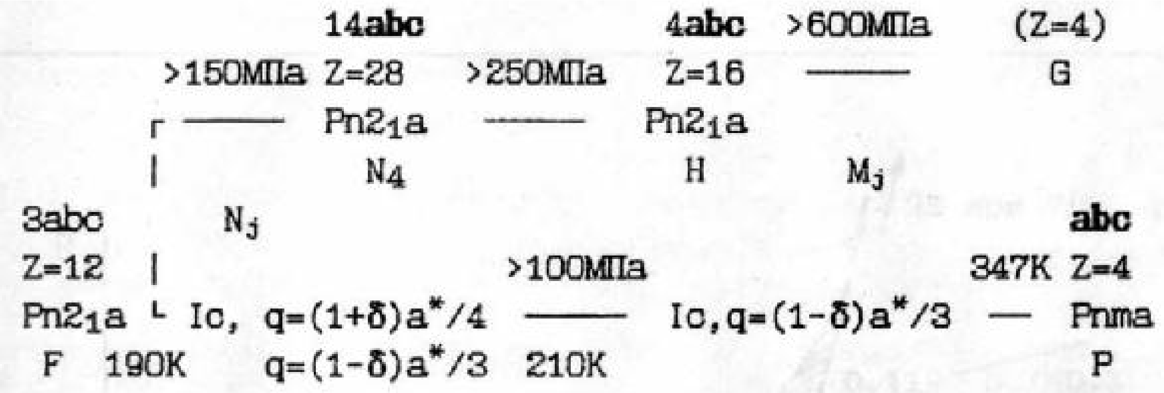

From a comparison of the amount of change of the wave vector q_d within the incommensurate phase at atmospheric pressure (Table 4.1) compounds A_2BX_4 and taking into account the data for Cs_2CdJ_4, Cs_2ZnJ_4 and Rb_2ZnBr_4 under pressure, we can put isobaric line atmospheric temperature change of each compound from Table. 4.1 the theoretical phase diagram and Aubrey Buck. As a result, we obtain the circuit (Fig.4.40), where through the line marked by the particular compound A_2BX_4 are isobaric atmospheric line q_d experimental measurements in this compound, and the oval area outlined by dashed lines represent stylized model Aubrey polyhedra [12], where the period of the structure does not change, but changes the phase shift between the sublattices model.

As can be seen from the presented scheme, despite unconfirmed some experimental data or their limitations, there is sufficient correlation between the known experimental P-T phase diagrams of the generalized phase diagram of Scheme Fig.4.40. Please keep in mind that the cesium compound was isolated as a subclass, characterized by a specific sequence of symmetry transformations associated with the softening of the phonon spectrum near the **T** point of the Brillouin zone, and the rest - in the subclass - along S line.

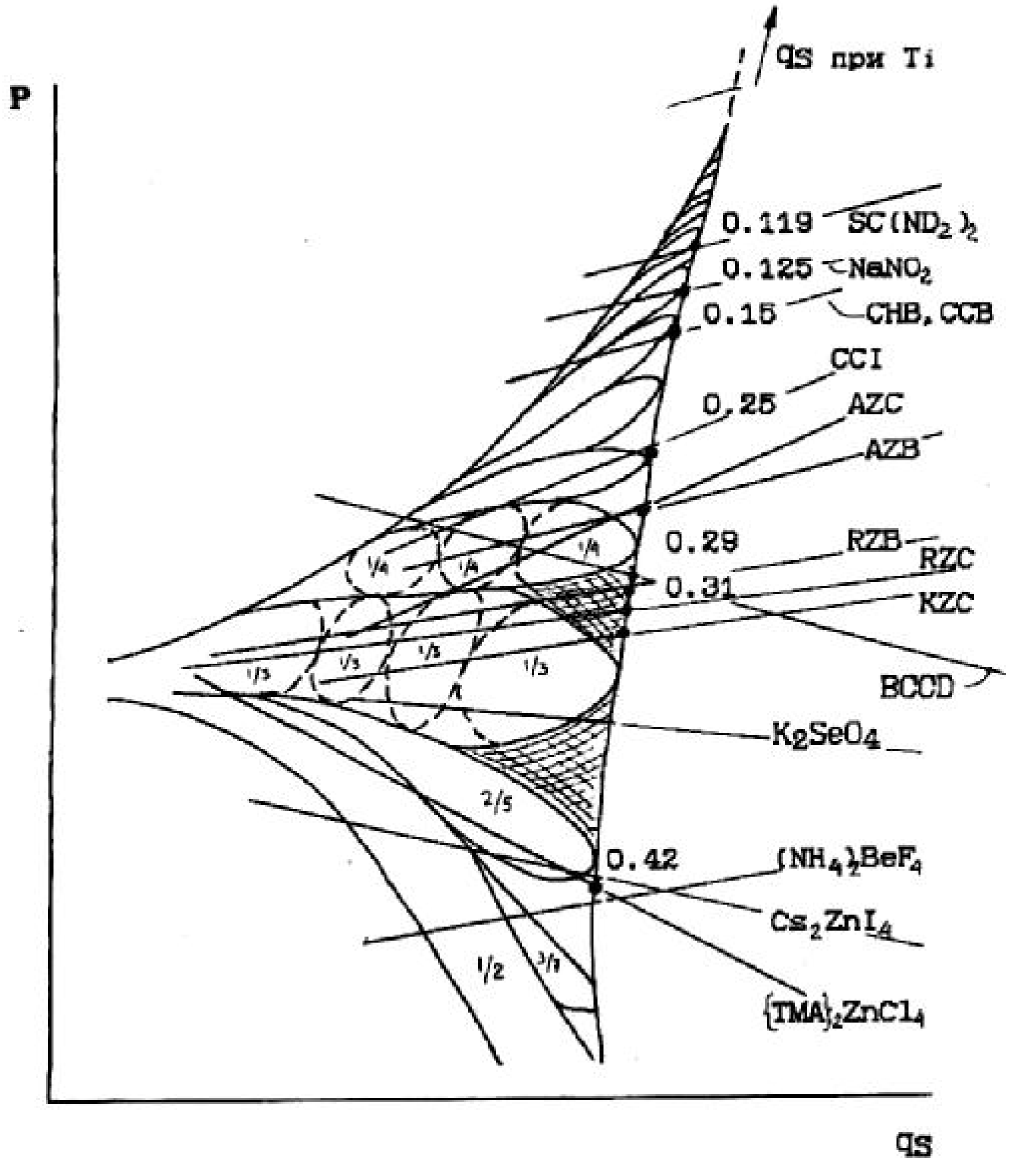

Fig.4.40. Comparison of experimental data on the change of the wave vector q_d in various compounds such β-K_2SO_{d4} with the theoretical phase diagram [12].

MAIN RESULTS.

1. NQR for precision studies of phase transitions created Gradientless thermal consoles and high-pressure chamber having an optimal agreement with the receiving part of the standard quadrupole resonance spectrometer.
2. Studied the sequence of phase transitions in $Cs_2CdJ_{4.}$ First detected NQR incommensurate phase in this crystal modification β. Complementary experimental methods built circuit symmetry changes. X-ray diffraction analysis confirmed the presence of the incommensurate phase.
3. The sequence of phase transitions in the crystal $Cs_2ZnJ_{4.}$ NQR ^{127}J registered incommensurate phase, found a wide temperature range subtransient ordering. The assumption is made and confirmed the change of symmetry in phase transitions in this compound.
4. The author synthesized and studied by NQR compound $(NH_{4)2}ZnJ_{4.}$ According to transition 1/2« 3/2 ^{127}J found three phase transitions. The line shape and features of the temperature dependence of the frequencies suggest that the intermediate phase in the crystal of $NH_{4)2}ZnJ_4$ are disproportionate.
5. Held temperature measuring the T_{Q1} and T_{Q2} nuclear spin relaxation ^{127}J. A substantial effect of the spin-spin relaxation of halogen correctness registration form of the resonance line in the incommensurate phase. Two-scalefixed nature of the nuclear dynamics in $Cs_2ZnJ_{4.}$
6. Polymorphic modifications crystal Rb_2ZnBr_4 and Cs_2CdJ_4 α« β Found that β - modification in compounds Cs_2CdJ_4 and Rb_2ZnBr_4 is metastable. The conditions for the implementation of transition.
7. NQR constructed and investigated P-T phase diagram of Rb_2ZnBr_4 in the incommensurate phase to pressures greater than 1.0GPa. Detected sequence highly symmetric and disproportionate disordered high-pressure phases. Interpretation of experimental data NQR in the "devil's staircase" is not contrary to the diffraction measurements and theoretical models pseudospin-ANNNI incommensurate phases.

Conclusion

The investigations demonstrate the pulse NQR method in studying disordered structures, including at high hydrostatic pressure.

On the basis of the developed equipment for temperature and high-pressure measurements investigated the sequence of phase transitions in a number of compounds with incommensurate phases.

On the basis of data on the degree of structural ordering and dynamic nucleus used compounds studied can be developed transformation model of atomic structure.

The author is grateful supervisor candidate physical and mathematical sciences A.K. Moskalev for help with the manuscript and helpful suggestions. Thanks Soros Foundation for financial support.

REFERENCES.

1. P. Anderson, Proc.: Physics of Dielectrics, edited by G. Skanavi, Izd. USSR Academy of Sciences, I960.

2. Iizumi M., Axe JD, Shirane G., Shimaoka K., Physic Review., 1977, B15, 9, p.4392-4411, Structural Phase Transformation in K_2SeO_4.

3. Yarnada N., Ikeda T., Ono Y., Incommensurately modulated structure of K_2SeO_4, J.Physic.Soc.Jap., 1984, v.53, 8, R.2555-2574.

4. Frenkel Frenkel, Cantor T. Lett, 1938, vol.8, str.1340-1352 The interaction of atoms with the crystal surface.

5. Aubry S., Solitons and Condensed Matter Physics, ed. Bishop AR and Schneider T., Berlin, Springer-Verlag, 1979, p.264.

6. Axel F. and Aubry S., J.Phys C.: Solid. St.Phys., 1981, vl4, p.5433.

7. McMillan WL, Theory of discommensuration and commensurate-incommensurate CDW phase transitron, Phys.Rev., 1976, B14, p.1496-1504.

8. Jassen T., Tjon JA, Microscopic model for incommensurate crystal phases, Phys.Rev., 1982, B26, N6, p.3767-85.

9. Frank FC, Vander Merwe TN 1949, Proc.R.Soc., 198, p.205-216; A ground states of the 1D Ising model for sine potentiale.

10. Currie JF, Trullinger SE, Bishop. AR.Krumhansl JA, Numerical Simulation of Sine-Gordon dynamics in the presence of perturbation.

11. Yamada Y.. Fujii Y., Hatta I., J.Phys.Soc. Japan, 1968, v.24, p.1053-1058.

12. Aubry S., Axel F., Vallet F., Devil's staircase and Manhaten profile in an exact model for an incommensurate structure in an electric field, J.Phys C.: Sol.St.Phys., 1985,018, p .753-788.

13. Bak P., Commensurate phases, incommensurate phases and devil's staircase, Rep.Prog.Phys., 1982, v.45, p.587-629.

14. Bak P., J.von Boehm, Ising model with solitons, phasons and "devil's staircase", Phys.Rev., 1980, VB21, 11, p.5297-5308.

15. Kovalev OV, Irreducible and induced representations and co-representations Fedorov groups., Nauka, 19V6, 386 p.

16. Wolf PM de; Jansson T., Janner A., Crystal Structure with a One-Dimensional Modulation, ActaCryst., 1981, A31, p. 625-63.

17. Grim H., Neutron scattering studies of improper ferroelectric and incommensurate phase transitions, Ferroelectrics, 1980, 24, p.229-236.

18. Muralt P., Arend H., Altermatt D., Chopuis G., Ferroelectrisity in organic-inorganic double halides, Ferroelectrics, 1984, v.56, pp.7-12,

19. A. Bruce, R. Pauli, Structural phase transitions., V., Mir, 1984.

20. Armstrong R.L., Displacive order-disorder crossover in perovskite and antifluorite crystals undergoing rotational phase transitions, Progress in NMR spectroscopy, 1989, v.21, p.151-173.

21. Blinc R., Dolinsek, Zalar B., NMR Determination of the Order Parameter in proton and deuteron glasses., 17th Congress Ampere, Novosibirsk.

22. Bersuker IB Theory of vibronic interactions, M., ed. Science, 1984.

23. Semin G.K. some foreign magazine.

24. Grechishkin BC Nuclear quadrupole interactions in solids., MA. Nauka, 1973.

25. L.D.Landau Liftits EM, Theory of Fields., MA. Nauka, 1970

26. Safin I.A. Osokin D.Y., nuclear quadrupole resonance in nitrogen compounds, 1977, Moscow. Science.

27. Borsa F., Higamonti A., Quadrupole effects in higt magnetic fields and static and dynamic oritioal phemenona at structural phase transitions, J. of Magn. Resonance, 1975, 20, p. 232-58.

28. Toyama M., Relative Intensities of Zeeman Components in NQR Spectrum, J.Phys.Soc. Jap., 1956. V. 14, 12, p. 1727-1738.

29. Lenovenko, Studies of transfer functions and regenerative superregeyaerativnyh NQR detectors, PhD thesis, Lviv, 1979.

30. Aybinder M.E., Grechishkin BC, in coll. "Spectroscopy", N 5, Perm, PSU, 1969, pp. 109-115, 0 influence on the asymmetry parameter quadrupole spin echo.

31. Mims W.B., Envelope Modulation in Spin-Echo Experiments, Phys.Rev., 1972, v.5, 7, p.2409-2419.

32. Sapozhnikov Y.E. GZP tensor asymmetry study on nucleus with spin 1 = 3/2 pulse NQR PhD thesis, Ufa, 1982.

33. Blinc R., Magnetic resonance and relaxation in structurally incommensurate system, Phys.Reports, 1981, v.79, 5, p.331-398.

34. Blinc R., Aleksandrova I.P., Chaves AS, Milia F. Rutar V., Seleger J., Topic B., Zummer S., NMR Lineshape and-phase solition effects in incommensurate Rb_2ZnCl_4, J.Phys.C .: Sol.St.Phys., 1982, 15, p.547-563.

35. Blinc R., Seleger J., Zummer S., NMR in incommensurate systems: non-local effects, J.Phys.C.: Sol. State phys., 1985, v.18, p.2313-2330.

36. Moskaliev A.K., I.A. Belobrova Aleksandrova I.P., Application of the method in the study of NQR incommensurate superstructure on the example of phase transitions in Rb_2ZnCl_4, FTT, v.20, 1978, pp. 3288-93 ..

37. Milia F., Kind R., Slak J., Phys Rev., 1983, B27, p.6622-6668, The Phase Transitions in $K_2Zn\ Cl_4$.

38. Belobrova IA, Aleksandrova I.P. Moskalev A.K., Br NQR in the incommensurate phase of Rb_2ZnBr_4, Phys Stat.Sol. (A), 1981, v.66, P.K17-20.

39. Aleksandrova I.P., Moskalev A.K., Belobrova I.A., NQR Investigation of the commensurate-incommensurate phase transitions in Rb and $(NH_{4)2}ZnCl_4$, J.Phys. Soc. Japan, 198S, v.49, Suppl.B, p.86-89.

40. Beznosikov B.V. Aleksandrov K.S., Crystal structures and prediction of compounds A_2BX_4, Krasnoyarsk, 1983, Institute of Physics, preprint N 243.

41. ItonK., Hinasada A., Matsunaga M., Nakamura E., Disordered Structure of Rb_2ZnCl_4 in the Normal Phase, J.Phys. Soc. Jap., V.52, 4, p.664-70.

42. Vtyurin A.H., Shkuryaev P.G., features of the lattice dynamics of incommensurate oegnetoelektrikov type A_2BX_4, Math. USSR Academy of Sciences, Ser.fiz., 1983, 47, 4.

43. Semin G.K, Grandma T.A., Jacobs GG, Application NQR in Chemistry, L., Izd.Himiya, 1972.

44. Scaife D.E., Halogen NQR in Tetrahedral Halogen Complexes of Zinc, Aust.J.Chem., 1971, v.24, p :1315-23.

45. Asker W.J., Scaife D.E., Watts J.A., Halogen NQR and Structural Relationships in some complex halides of zink and cooper, Aust. J.Chem., 1972, v.25, p.2301-9.

46.Semin G.K. Alymov I.M. Burbelo I.M. Pakhomov V.I. Fedorov P.M., NQR study of phase transitions and features of the crystal structure of Cs_2HgBr_4. AN SSSR, Ser. nat., 1978, v.42, 10, str.2095.

47. Makita Y., Sato T., Ichikawa M., Osaka T.. J.Phys.Soc.Jap., 982, v.51, p.3409; J.Phys.Soc.Jap., 1983, v.52, p.3297; Jc-Com Rhase Transition in $(NH_4)_2ZnY_4$ (Y = Cl, Br). {X-gay}

48. Plesko S., Kind R., Arend H., A new structural phase sequence with incommensurate phases in A_2BX_4 Halides, Phys. St. Sol. (A), 1980, v.61, p.87.

49. Moskalev A.K., Belobrova I.A., Zherebtsova L.I., lAleksandrova I.P., Ferroelectric Phase Transition in $(NH_4)_2ZnBr_4$, IPhys. stat.sol. (a), 1980, v.72, p.K19-21.

50.Toshio 0 ,.. Masuru K.. Yasukary; J.Phys.Soc.Jap., 1982, v.55, 11, p.3409-12, Phase Transitions In $(NH_4)_2ZnCl_4$ and $(NH_4)_2$ $ZnBr_4$.

51. Veda T., Iida S., Terauchi H., X-ray study on the successive phase transition in Rb_2ZnBr_4, J. of Phys Jap., 1982, v. 61,12, p.3953-57.

52. Blinc R., Dolinsek J., Prelovsek P., Hamano K., Phason Qap in Substitutionaly Disordered Incommensurate Systems, 1982 (preprint).

53. Denoyer F., Moudden A.M. Currat R., Vettier C, Bellamy A., Lambert M., Effect of hydrostatic pressure on modulated structures in thiourea, Phys.Rev., 1982, B25, 3, p.1697-1702.

54. Hornreich R.M., Luban, Stritman S., Phys.Rev. Lett., 1975, v. 35, p.1678.

55. Marion G., Almairac , Ribet M., Steigcnberger V., Vettier C, Temperature-pressure phase diagram of deuterated tetramethylammonium tetrachlorozincate, J.Physique, 1984, v.45, p.929-938.

56. Baisa D., Bondar A., Gordon A., Maltsev S., Phys.Stat.Sol., 1979, v.93. Phase Diagram of Ar3AsSe3 by NQR Method.

57. Maltsev S.V Study of lattice dynamics and structural phase transitions in crystals and halogenates halkogenatov NQR, 1979, Lviv, PhD thesis.

58. Kudo S., Ikeda T.; J.Phys.Soc.Jap., 1981, v.50, Hydrostatic Pressure Effect on the dielectric properties of K_2SeO_4; Press W., Phys.Rev., 1980, B22, p.332-334.

59. Gesi K., Effect of hydrostatic pressure on the normal-incommensurate-ferroelectric transitions in Rb_2ZnCl_4, Rb_2ZnBr_4, K_2ZnCl_4, Ferroelectrics, 1985, v.63, p.413-421.

Unruh H.-G., Pinning effects in incommensurately modulated structures, J.Phys. Sol. St. Phys., 1983, v.16. p.3245-3255.

Jamet J.P. and Lederer P., Observation of new memory effect in a modulated structure, J.Physique letters, 1983, V.44, p.L257-64.

62. Nattermann T., Nucleating, pinning and hysteresisis effects at the IC transitions, J.Phys.C: Solid Stat.Phys., 1985, 18, p.5683-5696.

63. Prelovsek D., Rice T.M., Nucleation processes in the. Charge density wave state of 2H-2 TaSe, J.Sol id Stat.Phys., 1983, v.16, p.6513-6530.

64. T. Farrar, E. Becker, Pulse Fourier NMR spectroscopy, Wiley, New York, 1973.

65. Batygin V.V. Bruin I.M., Collection of problems in electrodynamics, Nauka, Moscow, 1970.

66. Nemtsov M.V. , Shamaev Y.M., Manual calculation of inductors, M. Energoizdat, 1981, p.106.

67. Zeitlin L.A., inductance of wires and circuits, L.-M. 68. Kaden G., Electromagnetic screens vycokochasotnoy communications technology, Leningrad. Gooenergoizdat, 1957.

69. Quilichini M., Compared Ramanstudy of phase transitions in Rb_2ZnCl_4, Rb_2ZnCU, Rb_2ZnBr_4 and K_2SeO_4 J.Physique, 1982, v.43, p.787-793.

70. Sekine T., Takayma M., Raman-scatering study of Successive Phase Transitions in K_2ZnCl_4, J.Phys.Soc.Jap., 1986, V.ll, p.3903-3917.

71. International tables for X-ray Crystallography, edited by NFM Henry and K.Lonsdal, Birmingham, 1969, Kynoch Press.

72. Hamano K., Ema K., Hirotsu S., Ferroeleotrics, 1981, v.36. p.343.

73. Sawada S. Yamaguchi T., Syiroishi Y.Yamamoto;J. Jap., 1981, v.50, p.3677, The dependence of phase transition

74. Structural phase transitions in crystals under high pressure, Novosibirsk, Nauka, 1982, ed. Aleksandrov K.S.

75. Serebrenniko v V.L., Moskaliev A.K. High-pressure chamber for measurement of NQR spectrometer ISSH-1, PTE, 1977, N4, p.183-185

76. Skripichnikova V.V., search and study of phase transitions in crystals of β-K_2SO_4, Krasnoyarsk, 1984, thesis

77. Flerov I.N., Gorev, L., Cote, V.A.Grankina Calorimetric study of phase transitions in the orthorhombic and monoclinic Cs_2CdJ_4, FTT, 1988, volume 30, page 7, p.1948-51.

78. Aleksandrov K.S., Flerov I.N., Kokov I.T., Kruglik A.I., Melnlkova S.V., Shemetov E.V., Successive phase transitions in Cs_2 $CClJ_4$ crystal, Ferroelectrics, 1988, v.79, p. 137-140.

79. Shemetov E.V., Aleksandrov K.S., Aleksandrova I.P., Primak S.V. ^{127}J NQR study of the phase transition sequence In Cs_2CdJ_4, Phys.Stat.Sol. (A), 1987, v.104, p.K89-92.

80. Aleksandrova I.P., Primak S.V., Shemetov E.V., Krugiik A.I., Elizaryev Yu. G., Successive phase transitions in Cs_2CdJ_2 and Cs_4ZnJ_4. Ferroelectrics, 1990, v.105, p.177-181.

81. Shemetov E.V., Aleksandrov K.S., Aleksandrova I.P., Primak SV, The ^{127}J NQR study of the phase transition in Cs_2CdJ_4., Xth Ampere summer school, Abstracts, Novosibirsk, 1987, p.247.

82. Shemetov E.V., Aleksandrova I.P., Primak S.V., J-127 NQR Study of Phase Transition in ; Xth International Symposium on NQR, Takayma, Japan, 1989, Abstracts.

83. Aleksandrova I.P., Shemetov E.V., Primak S.V., Krugiik A.I., Sucoesive phase transitions in Cs_2CdJ_4 and Cs_2ZnJ_4, 12th European Crystallographies meeting, Moscow, 1989, vl, p.526.

84. Aleksandrova I.P., Shemetov E.V., Primak S.V., Kruglic A.I., Study of phase transitions in Cs_2ZnJ_4 and Cs_2CdJ_4, XII All-Union Conference on the Physics of Ferroelectrics, Rostov / Don, 1989 , Vol.1, p.122.

85. Aleksandrova I.P., Primak N.E., Shemetov E.V., Kruglic A.I., sequence of phase transitions in Cs_2ZnJ_4, FTT, 1991, v.33, 5, str.1344-1349.

86. Arend N., Muralt, Plesko S., Altermatt, Halide Ferroelectics, Ferroelectric, 1980, v.24, p. 297-3037.

87. Boguslavsky A.A., Zagorsky D.L., Semin S.K., ^{127}J NQR Phase Transition Study in Cs_2ZnJ_4 and Rb_2ZnJ_4, Xth International Symposium on NQR Spectroscopy, Tokayama, Japan, 1989, Abstracts, IIIP4,

88. Boguslavskiy A.A., Zagorski D.L., Lotfulin R.Sh., Pakhomov V.I., Kirilenko V.V., Semin G.K. Study Cs_2HgJ_4 NQR ^{127}J., Zh.Neorganicheskoy Chemistry, 1989, v.34, 7, S.108B-1087.

Raman scattering study of the phase sequence in A$_2$BX$_4$ halides., Solid State Coinmun., 1984, v.60, 11, p. 3535-36.

90. Gesi K.. Jap., 1981, v.50, 11, p.3535-36,.

91. Aleksandrova I.P. Primak N.E., Elivarev Y.G., Denovue F. Kruglic A.I., Shemetov E.V., Incommensurate phase in the crystal Cs$_2$ZnJ$_{4,}$ Soviet-Polish seminar on ferroelectricity, LVIV, 1990, Proceedings, pp. 219-220.

92. Semin G.K., Shemetov E.V., Moskalev A.K., ^{127}J NQR Study of phase Transitions in (NH$_4$)aZnJ$_4$, XII th International Symposiym on NQR Spectroscopy, Zurich, Shwezerland, 1993, Abstracts.

93. Perez-Mato JM, Gaztelua F.. Madariga G., Tello MJ, J.Phys.C: Solid Stat.Phys., 1986, v.19, p.1923-35, Symmetry-mode analysis of the ferroelectric phase in K$_2$SeO$_{4.}$

94. Heine V., McConnell JDC, J.Phys.C: Solid Stat.Phys., 1984, v.17, p.1199-220, The origin of incommensurate structures in insulator.

95. Pfeffer L., Walstedt RE, Bell, Temperature dependence of orthorhombic CDW parameters in 2M-TaSe$_2$ by ^{77}Se NMR, Phys. Rev Lett., 1982, v. 49, p. 1162-65.

96. McWhan D.V., Fleming RM, in "Physics of solids under High Pressure", ed.

97. Kadaba P.K., O"Relly D.E., J.Chem.Phys., 1971, v.55, 12, p.5833; NQR frequencies and critical broadening of iodine in thermochromlc Ag$_2$HgJ$_4$ and Cs$_2$HgJ$_{4.}$

98. Nechtschein M., Devreux F., One Dimensional Spin diffusion in poliatetylene (CH)$_{X,}$ Phys.Rev.Lett., 1980, v.44, 5, p.356.

99. Heritier M., Lederer P., Quantum Crystals of fermions (^{3}He), Phys.Rev.Lett., 1979, v.41, p.1068.

100. Rong A.O., Gernot Lingg, Schaack, Zoller M., Ferroelectrios, 1990, v.105, p.391, pT phase dlaiT.am of partially brominated betaine calciumchloride dihydrate {(CH$_{3)3}$NCH$_2$ $^+$ OOOCaCl$_{2*}$ 2H$_2$0 - BCCD}.

10l.Tentrup T., Siems R., Ferroelectrics, 1990, V.105, p.379, Interprltation of the DCCD-phase diagram within the frame of an ANNNI model with pseudo-spin-phonon-ooupling.

102. Reynolds RW, Boather LA, Dynamic, intermediate and static Jahn-Teller effect in the spectra of E ^{g} orbital states, Phys.Rev., 197B, BIZ, 11, p. 473B-4754

Cooper AV Riabchenko CM., Hahlan LB, Relaxation studies NQR Jo phases of Rb$_2$ZnBr$_4$ and Cs$_2$HgBr$_4$ <IT, 1988, v.30, 8, p.79-85

104. Janssen T., Tjon JA, Bifurcation of Lattice structures, J.Phys. A: Math. Gen., 1983, v.16, p.673-696.

105. Rutar V., Milia F., Topic B., Rasing, ^{87}Rb Nuclear MagnetJc Resonance evidence for solitions and pasons in Rb$_2$ZnBr$_4$,, Phys.Rev., 1982 Vyb, 1, p.281

106. Chekmaryov V.P., Petrov M.P., Nonresonant ereeonansnoe excitation of nuclear spins in crystals with a large dynamic NMR frequency shift, Lett, 1976, t.71, 1, str.377.

107. Sokolov A.I., Renormalization group, critical phenomena and phase diagram of the anisotropic systems, Moscow, 1983, doctoral dissertation

108. Aleksandrova I.P., Shemetov E.V., Serebrennikov V.L., Research proportionate and incommensurate phases of Rb$_2$ZnBr$_4$ NQR under pressure, XII All-Union Conference on the Physics of Ferroelectrics, Rostov-Don, 1989, v.1 , p.122.

109. Shemetov E.V., Measurements of the spin-spin relaxation of ^{81}Br Rb$_2$ZnBr$_4$ in the incommensurate phase, 1985, unpublished

110. Iizumi M., Gesi K., Incommensurate-commensurate phase thansition in Rb_2ZnBr_4, J.Phys.Soc. Jap. , 1983, v.52, 7, p.2526-2533

111. Shemetov E.V., Moskalev A.K., Semin G.K., Pressure-Temperature Phase Diagram of Rb_2ZnBr_4 by ^{79,81}Br NQR Method, Xllth International Symposium in Nuclear Qudrupole Resonans. Spectroscopy, Zurich, Swizerland, 1993, Abstracts

112. Aleksandrova I.P., lth American-Soviet Symposium on Ferroeiectricity, LISA, 1990, (printed in Ferroelectrios)

113. Aleksandrova I.P., Transformation of structure in the incommensurate phase Rb_2ZnBr_4 under pressure, 23 Congress Ampere Summer School Novosibirsk Shushenskoe, 1987

114. Aleksandrova I.P., in Magnetic Resonance and Related Phenomenona, 24th Ampere congress, Poznan, Poland, 1988, p.21-33, NMR and NQR of Modulated systems Incommensurate phase? in the real crystals.

115. Aleksandrova I.P., Shemetov E.V., Serebrennikov V.L., neighborhood study ferroelectric phase transition in Rb_2ZnBr_4 voedeystviem NQR under high pressure, Phys, 1987, v.29, 9, 2661-57 .

116. Aleksandrova I.P., Shemetov E.V., Br-79, 81 NQR Study of the Pressure-Temperarure phase diagram of Rb_2ZnBr_4, Xth International symposium on NQR spectroscopy, Takayma, Japan, 1989, Abstracts, IIIP2.

117. Aleksandrova I.P., Shemetov E.V., Serebrennikov V.L., Pressure-Temperature Phase Diagram of Incommensurate Rb_2ZnBr_4, XII-th European Crystallografisal Meeting, Moscow, 1989, Abstracts.

118. Aleksandrova I.P., Shemetov E.V., Serebrennikov V.L., High Pressuren Sience and Technology, Procedings XI AIRAPT International Conference, Kiev, Naukovs Dumka, 1989, vi, A Study of Phase PT Diagram of Rb_2ZnBr_4 by NQR Mettod.

119. Parlinski K., Aleksandrova I., Cura R., Neutron difraction investigation of Rb_2ZnBr_4 in around T_c linder pressure.

120. Janssen T., Jap.J.of Appl.Phys., 1985, v.Z4, Suppl. .

121. Selke W., Ising model with completing interactions, Jap. J. of Appl. Physics, 1986, v. 24. Supplement, p.24-2

122. Bak P.and Pokrovsky V.L., Rev.Lett., 1981, v.47, p.958 Excitations in a discrete anharmonic lattice model.

123. Kosterlitz J.M., Nelsen D.R., Fisher M.E., Bicritical and tet racrltical points in anisotropic systems, Phys.Rev.B, 1976, v.13, N24 p.412-432.

Edwards S.F., Anderson P.W., J.Phys.Rev 'Letters, 1975, v.35, p.1972

125. Shemetov E.V., Polymorphism in K_2ZnBr_4 and others (unpublishedData), 1991

126.Thieret T.E., McNaiiy J., Kraft K., J.of Magnetic ,distortions from pulsed NMR experiment with lock-In amplifier or boxcar integrator detection.

127. Moskaliev A.K., Krieger A.I., Seryukova I.V., V.I. Pakhomov, Research tetrabrommerkurata cesium ^{133}Cs NMR in a strong magnetic field, Journal of Inorganic Chemistry, 1991, t.36 in. 11 s.2860 66.

128. Pakhomov V.I., Fedorov P.M. Alymov I.M., Ivanova-Corfinium K.N., Semin G.K., Ivv.AN ser.fiv USSR., V.39, N12, str.2519-2522, 1975, (about yodomerkuratah and structural distortions).

129. Boguslavskiy A.A., Lotfulin R.S., Peresh E.J., Research Cs_2CdBr_4 NQR $^{79-81}$Br, FTT, 1988, .5, s.1558.

130. Boiko F.A., Equlibrium and metastable phases formed at successive ordering of Jahn-Teller distortions in $Cu(H_2O)_6SiF_6$ crystals., Ferroelectrics, 1987, v.75, p.431-447.

131. Boguslavskiy A.D., Lotfulin R.SH., Simonov M., Kirilenko V.V., V.I. Pakhomov, A.Y. Mikhailov, Temperature dependence of the NQR frequencies in Cs_2HfCl_4, FTT, 1985, v. 2, N2, 523-4.

132. Gesi K. Phase transitions in monoclinic rubidium tetraiodozinoate Rb_2ZnJ_4, J.of Phys.Soc.Japan, 1984, v.53, N11, pp.3850-54.

133.Pakhomov V.I., Fedorov P.M., Crystallography, v.17, 1972, VB, str.942-946, the structure Cs_2CdJ_4.

134. Fuminao, Shimizu, Toshihisa Yamaguohi, H.Suzuki, M.Takashige, S.Sawada, Suppercooling effect in K_2ZnBr_4 and K_2CoBr_4, J. Phys.Japan, 1992.

135. Burstein Semendyaev, Physical Kinetics, lectures and 2, 1976., Publishing KRU.

136. Aleksandrova I.P., Shemetov E.V., Serebrennikov V.L., Primak S.V., Pressure-Temperature Phase Diagram of Rb_2ZnBr_4; IV Japan-Soviet symposium on ferroelectricity, 1988, Abstracts.

137. Serebrennikov V.L., Shemetov E.V., Belobrova I.A., Investigation NQR disproportionate and proportionate phage in Rb_2ZnCl_4 and Rb_2ZnBr_4 under pressure; Union Conference on Magnetic Resonance in Condensed cpedah, Kazan, Abstracts, Part 1, 1984.

138.Aleksandrova I.P, Prlmak S.V., Shemetov E.V., Krusrlik P.M. Successive phase transition in Cs_2CdJ_4 and Cs_2ZnJ_4.

139. Aleksandrov K.S., Flerov I.N., Kruglik A.I., Melmkova S., Shemetov E.V., Phase transitions in Cs_2CdJ_4 crystal.